CHARACTERIZATION OF BENZOYL-SUBSTITUTED GROUP 8 METALLOCENES AS PHOTOCHEMICAL INITIATORS FOR THE ANIONIC POLYMERIZATION OF VINYLIC MONOMERS

by

CYNTHIA T. SANDERSON

(Under the Direction of Charles Kutal)

ABSTRACT

This thesis demonstrates that ferrocene, ruthenocene, and their benzoyl-substituted analogs are photoinitiators for the anionic polymerization of ethyl 2-cyanoacrylate and evaluates the effectiveness of these photoinitiators based on the rates of polymerization as determined by attenuated-total-reflectance Fourier-transform infrared spectroscopy (ATR-FTIR). While all of these compounds are effective photoinitiators, the mechanism of photoinitiation depends on which metal is present and whether or not the compound contains electron-withdrawing benzoyl groups. The parent compounds exhibit solvent insensitive ligand field transitions in the visible/near UV region of the spectrum, and resist photoinduced ring loss. Photoinitiation is thereby shown to occur via a photoactive charge-transfer-to-solvent complex between the metallocene and the cyanoacrylate monomer which results in the oxidation of the unsubstituted metallocene and reduction of the electrophilic monomer. In contrast, addition of one or more benzoyl groups to the cyclopentadienyl rings of the metallocene causes the mixing of charge-transfer character (metal-to-ligand) into the ligand field transitions of the parent compound. This charge-transfer character is manifested by an increase in the intensity of the electronic transition, which is accompanied by a shift to lower energy as compared to the transitions of the parent compounds. The nature of this charge transfer character has been studied using resonance Raman spectroscopy, and it is shown that the assignment of metal-to-ligand charge transfer is accurate for all of the benzoyl-substituted metallocenes studied. In the case of 1,1'-dibenzoylferrocene, this metal-to-ligand charge transfer character is responsible for photoinduced ring loss which occurs upon irradiation into the low-energy electronic transition. This photoreaction has been studied using an on-line photolysis procedure which allows the identification of short-lived photoproducts by mass spectrometry. For the ruthenium containing compounds, addition of a benzoyl group to one or both of the cyclopentadienyl rings causes similar spectral changes as those seen in the case of the iron

analogs; however, there is no indication that the primary photochemical reaction is ring loss. Rather, photoinitiation occurs via the same charge-transfer-to-solvent mechanism as seen for the unsubstituted metallocenes. Finally, this manuscript attempts to expand the use of these photoinitiators to another vinylic monomer, methyl methacrylate, which is also susceptible to anionic attack.

INDEX WORDS: ferrocene, ruthenocene, 1,1'-dibenzoylferrocene, benzoylruthenocene, 1,1'-dibenzoylruthenocene, cyanoacrylate, methyl methacrylate, group transfer polymerization, mass spectrometry, resonance Raman spectroscopy, photoinitiated anionic polymerization, attenuated-total-reflectance Fourier-transform infrared spectroscopy

CHARACTERIZATION OF BENZOYL-SUBSTITUTED GROUP 8 METALLOCENES AS PHOTOCHEMICAL INITIATORS FOR THE ANIONIC POLYMERIZATION OF VINYLIC MONOMERS

by

CYNTHIA T. SANDERSON

B. S., Northern Illinois University, 1999

A Dissertation Submitted to the Graduate Faculty of The University of Georgia in Partial Fulfillment of the Requirements for the Degree

DOCTOR OF PHILOSOPHY

ATHENS, GEORGIA

2004

CHARACTERIZATION OF BENZOYL-SUBSTITUTED GROUP 8 METALLOCENES AS PHOTOCHEMICAL INITIATORS FOR THE ANIONIC POLYMERIZATION OF VINYLIC MONOMERS

by

CYNTHIA T. SANDERSON

Major Professor: Charles Kutal

Committee: I. Jon Amster
Michael K. Johnson
R. Bruce King

Electronic Version Approved:

Maureen Grasso
Dean of the Graduate School
The University of Georgia
August 2004

DEDICATION

In loving memory of Nicole Marie Gradowski and Grandma (Dottie) Burbrink; without either of you, I would not be the woman I am today. You are both loved and missed by all who knew you.

ACKNOWLEDGEMENTS

There are so any people to thank that it's hard to know where to begin. Firstly, there is Dr. Kutal, my research advisor. Throughout my tenure as a graduate student you have been a constant source of inspiration and strength. I have learned so much from you about what it means to be a good scientist, teacher, and person. I would also like to thank the members of my committee, Dr. Amster, Dr. Johnson, and Dr. King. During my graduate career each of you has gone out of your way to help me through the process. I have always felt that if I needed help or had any questions that each of your office doors was open. Thank you. I would also like to thank Dr. Dluhy for allowing me to use his instrumentation, and Dr. Mike Murphy for showing me how to use the instrument and software. Also, a special thanks to Dr. Rick Conover for all of his help with the resonance Raman experiments and discussions about life. In addition, I would like to thank Dr. Duncan for his support throughout my stay here at UGA.

I have made so many friends here at UGA, that I find it hard to express my gratitude to all of you. If I forget anyone, please forgive me. First, I would like to thank my fellow group members: Matt Morgan for supplying me with laughs during the (often painful) writing process, Jessica Quinlan for the whole experience of having you as a student, mentee, and finally friend. You, along with my little sister, Christie, kept me grounded, and made me strive to be a role model. I cannot express my level of gratitude towards Dr. Wei Ding for his help

and support in each possible way. You are one of the kindest, smartest, and most patient people I know. You were a hard act to follow through this group, but you always said that I could do it, even when I wasn't so sure.

I would also like to thank 'The Round Table': Brion Berman, Bryan Parks, and Joe Emerson for allowing me to be myself. I would like to express my gratitude to Brian Knapp-Melkowits and Amanda Knapp-Melkowits (the 'Melkonapps') for being there whenever I needed anything. I can't tell you how much it helped that you were willing to care for Tramp so that I could have hours of uninterrupted time to complete my writing. Also, I want to thank you for reminding me that it's important to take time away from science (and writing) to have fun and relax. Nicole Brinkmann, thank you for your many talks, laughs, and helping me to learn about myself, density functional theory, and life in general.

I would also like to thank my family. Together, we went through some very rough times while I was in graduate school, and yet we managed to stand united in the face of adversity. Without your love and support, I would not be here. Memaw and Gramps, thank you for understanding that I could not spend nearly as much time in Savannah as we both wanted, and thanks for the lunches. I enjoyed our time together immensely. And to my parents, thank you for the emotional, physical, and financial support you have given me throughout my life.

Finally, I would like to thank God. Despite everything I have been through, I have constantly felt your presence in my life. Without You, I would have no hope and this world would be a dark, dreadful place.

TABLE OF CONTENTS

LIST OF TABLES

Page

LIST OF FIGURES

Page

CHAPTER 1

INTRODUCTION

1.1 The Polymerization Process

Polymerization is the process whereby many smaller molecules, called monomers, combine chemically to form a larger molecule, called a polymer. Polymers can be made by many different methods which can be divided into two general categories: step-wise growth and chain growth, also called condensation and addition polymerization, respectively. Step-wise, or condensation polymerization is the combination of monomer units to form a new bond with the expulsion of a small molecule such as water. There are many examples of these kinds of polymers; the most well known are peptides (which are biological polymers) and nylon. In chain growth, or addition polymerization, some reactive species, called an initiator, is added to or formed in the presence of the monomer. In the initiation step, the initiator reacts with the monomer breaking an internal bond of the monomer and transferring the reactive site from the initiator to the monomer. In the next step, called propagation, this new species then attacks a second monomer and begins growing a polymer chain; this can continue until all of the monomer is consumed. The final step in polymerization is termination. In this process, the growing polymer chain reacts with another species to terminate the reaction, resulting in a dormant species. These reactions are illustrated in Figure 1.1 for styrene, where ‡ indicates a reactive site. There are many examples of chain growth polymers, some of the most popular are polystyrene, poly(vinyl chloride), and polytetrafluoroethylene (Teflon®).

The initiating species (IN) can be added directly to the reaction mixture, or it can be generated in situ, by either a thermal or photochemical process. If the

Figure 1.1: Initiation, Propagation, and Termination in Addition Polymerization

Shown in this figure are the initiation (a), propagation (b), and termination (c) steps in a chain-growth polymerization for a sample monomer, styrene, where ‡ denotes a reactive site, and T indicates any species capable of terminating the polymerization reaction.

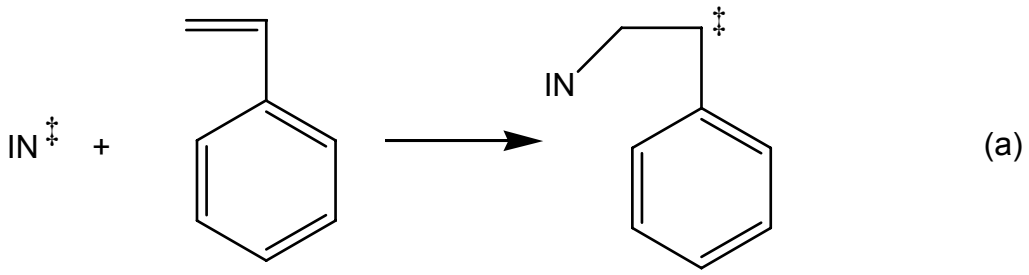

(a)

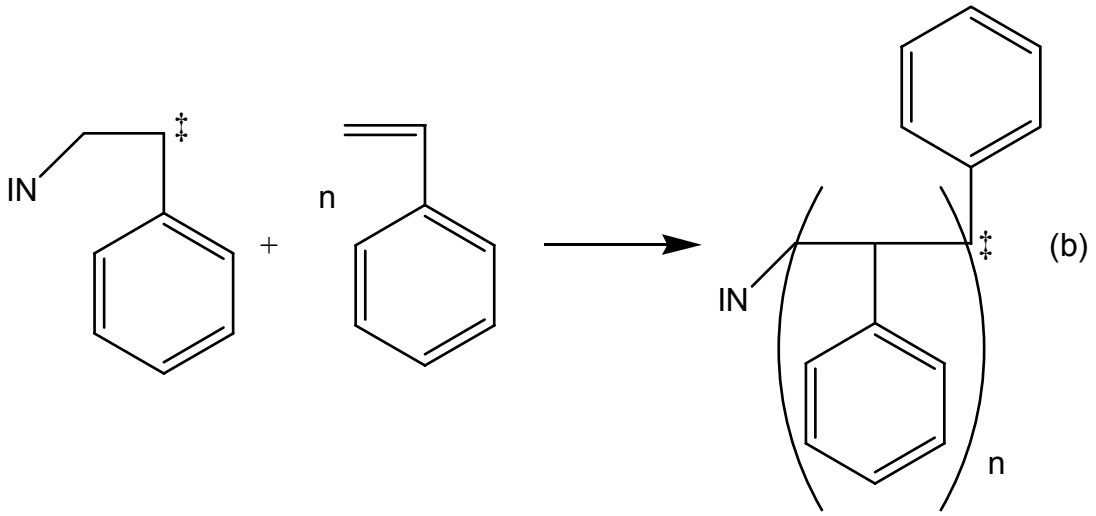

(b)

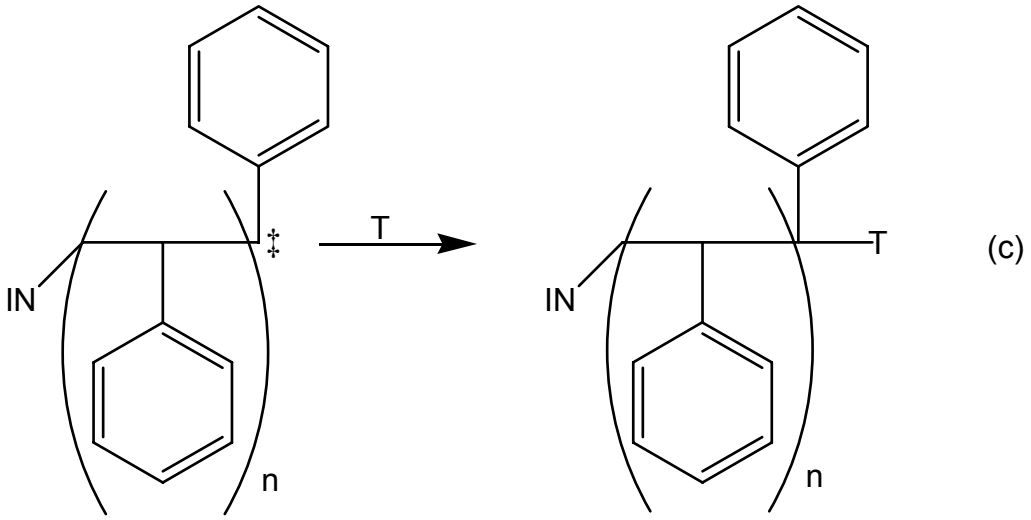

(c)

initiator is to be generated photochemically, then a stable precursor molecule called a photoinitiator (PI) must be added to the reaction mixture. Upon photolysis, the photoinitiator undergoes a reaction to release the actual initiating species, IN, which has a reactive site, denoted by ‡. Once the initiating species is present, polymerization commences. These steps are illustrated in equations 1.1 and 1.2, where 'M' is monomer. The initiating species may have any reactive site capable of reacting with the monomer of interest. Examples of radical, cationic, and anionic initiating species are known.

$$PI \xrightarrow{h\nu} IN^{\ddagger} \qquad (1.1)$$

$$IN^{\ddagger} \xrightarrow{nM} IN\text{-}[M]_n^{\ddagger} \qquad (1.2)$$

Photochemical initiation has found many industrial applications, particularly in the paints, inks, adhesives, and coatings industries.[1,2] Due to its industrial applications, photoinitiated polymerization is an area of active research. From a practical standpoint, photochemical polymerization reactions are very similar to their thermal analogs, with some advantages. First, photochemical polymerizations can be done at ambient temperatures, increasing the types of monomers that can be polymerized using these methods since one is not worried about thermally decomposing the monomer. Another advantage of photochemical initiation is that polymerization only occurs where the sample is exposed to light.[1,2] This allows for great spatial resolution, and has been employed in printing plates, microcircuits and optical disks. As well,

photochemical initiation has many solvent free applications which help to minimize the environmental impact of waste solvents.[1,2] One final advantage photoinitiated polymerization reactions have over their thermal counterparts is that by using an intense light source, one can generate a lot of the initiator at one time, which allows very high polymerization rates to be obtained.[2]

By far, the most popular type of polymerization reactions are radical polymerizations. Most monomers, specifically vinylic monomers, are susceptible to radical attack. While vinyl typically refers to the CH_2=CH– group attached to some substituent, in polymer chemistry, the term vinyl (or vinylic) monomer refers to any molecule which can be viewed as a substituted ethylene, including acrylates, alkenes, and styrene;[3] this convention will be used throughout this text.

While radicals and ionic species can be used in chain growth polymerizations, the use of one type of initiator over another is not a matter of whim. Not all types of initiators are suitable for all monomers. Most monomers will undergo radical polymerization (since almost all substituents can stabilize a radical through delocalization), but the rate of this reaction varies. With respect to ionic initiators, monomers are only susceptible to attack by certain ions, and the rate of polymerization also depends on the ionic initiator used.[3] The reason for this selectivity is that substituents on the carbon-carbon double bond have a large inductive effect on the propagating species. Electron donating groups, such as alkyl, alkoxy, and aryl groups, increase the electron density on the carbon-carbon double bond, thereby favoring attack by cations or other electrophiles. In

contrast, electron withdrawing groups, such as cyano and carbonyl groups, decrease the electron density on the carbon-carbon double bond, making the monomer more susceptible to attack by anions or other nucleophiles. These inductive effects may be complemented by resonance stability lent to the ionic propagating end by these same substituents. Examples of this resonance stability are illustrated in Figure 1.2. Table 1.1 lists some typical monomers, and their susceptibility to radical, cationic, or anionic attack.[3]

1.2 Polymerization of Ethyl 2-Cyanoacrylate

Alkyl 2-cyanoacrylates (the active monomer in Krazy Glue®) are a class of monomers that are extremely susceptible to anionic polymerization.[4] Cyanoacrylate monomers have found wide use in the adhesives industry owing to their unsurpassed ability to bond a variety of substrates together. Additionally, cyanoacrylates are widely used in the automotive, electronics, and home repair sectors,[5] cyanoacrylates are also used in forensic science to isolate latent fingerprints from crime scenes.[6] In addition to these various applications, cyanoacrylates are also used in a large number of medical applications such as being used as alternatives to staples or sutures after surgery, to seal the cranium after a craniotomy, some sutureless cardiac and ophthalmology techniques, and possibly as drug-delivery carriers.[7-13]

Along with these practical applications of cyanoacrylate polymerization, there are many chemical characteristics which make cyanoacrylates very interesting to study. For example, cyanoacrylates are among the most reactive

Figure 1.2: Resonance Stability from Substituents on Vinylic Monomers

Shown here are examples of how an alkoxy group can lend resonance stability to a cationic propagating end (a) and an ester group can lend resonance stability to an anionic propagating end (b).

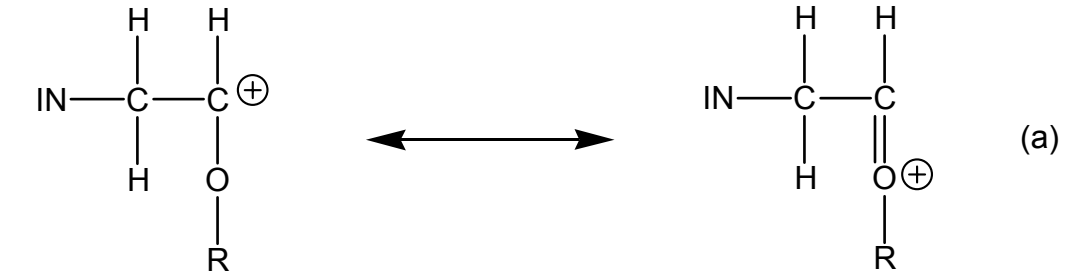
H
H
IN
C
C
H
O
R
(a)

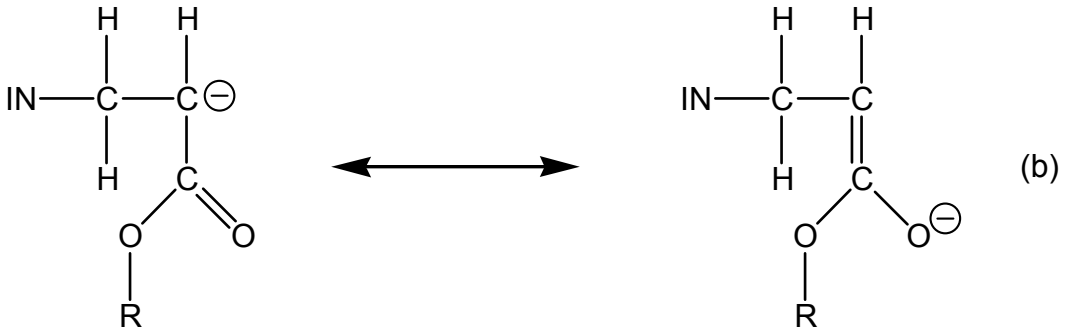
H
H
IN
C
C
H
C
O
O
R
(b)

Table 1.1: The Susceptibility of Various Monomers to Radical, Cationic, and Anionic Polymerization

Monomer	Type of Initiator[a]		
	Radical	Cationic	Anionic
Ethylene	+	−	+
1-Alkyl olefins (α-olefins)	−	+	−
1,1-Dialkyl Olefins	−	+	−
1,3-Dienes	+	+	+
Styrene, α-methyl styrene	+	+	+
Halogenated olefins	+	−	−
Vinyl esters (CH_2=CHOCOR)	+	−	−
Acrylates, methacrylates	+	−	+
Acrylonitrile, methacrylonitrile	+	−	+
Acrylamide, methacrylamide	+	−	+
Vinyl ethers	−	+	−
N-Vinyl carbazole	+	+	−
N-Vinyl pyrrolidine	+	+	−
Aldehydes, ketones	−	+	+

[a] + and – refer to whether or not a particular type of initiator is capable of producing a high molecular weight polymer from the given type of monomer.[3]

monomers towards anionic polymerization (defined here as any polymerization reaction in which propagation proceeds via attack of an anion on the carbon-carbon double bond of the monomer).[4] As well, the propagating carbanion is very stable towards termination reactions with adventitious impurities. Finally, despite the extreme reactivity and considerable stability of the propagating anion, poly(cyanoacrylates) are relatively unstable, especially in solution.[4,14-17]

These properties have led many people to study the anionic polymerization of such an interesting class of monomers. Cyanoacrylates are susceptible to attack by simple inorganic anions such as I^-, Br^-, OH^-, CH_3COO^- and NCS^- [4,18] as well as neutral bases such as amines and phosphines.[4,19,20] If we consider the classical anionic polymerization mechanism shown in equation 1.3:

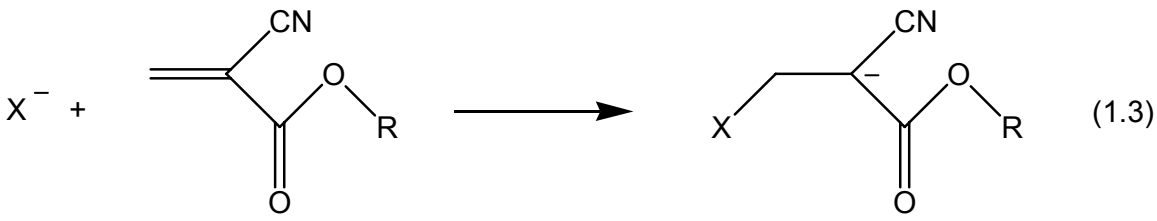

(1.3)

an anion (X^-) attacks a monomer molecule to form the carbanion shown, which can be considered a resonance stabilized ester enolate anion. The resulting carbanion is very stable when compared to the carbanions formed in other anionic polymerization reactions. This is due to the resonance stability lent to the carbanion by both the ester and cyano moieties. In fact, these carbanions are so stable that that addition of small (up to ~200 ppm) amounts of O_2, CO_2, H_2O, and methanol have been shown to have little effect on the rate of polymerization of

cyanoacrylate monomers, whereas these species are known to inhibit other anionic polymerization reactions even in these small concentrations.[4,20,21]

The rate of polymerization of cyanoacrylates is, as expected, dependent on the reaction conditions as well as the propagating species. Pepper coined the term slow-initiation no termination (SINT) to describe the kinetics of cyanoacrylate polymerization.[22-24] Pepper proposed the SINT scheme to describe the zwitterionic polymerization of cyanoacrylates when initiated by uncharged Lewis bases, but it was later shown that the same mechanism is operational in 'classical' anionic polymerization reactions of cyanoacrylates as well as other monomers;[25] for this reason, it is appropriate to discuss the SINT mechanism as applicable to cyanoacrylate polymerization by anions as well as the Lewis bases originally intended.

As the name (SINT) suggests, in the anionic polymerization of cyanoacrylates, the initiation is slow. This means that there are few active propagating centers. This accounts for the higher than expected molecular weights typically seen in the polymer product, especially when high concentrations of initiator are used. The SINT theory evaluates the number of chains initiated during the polymerization, which can then be used to predict the number-average molecular weight (M_n). We define M_n, on a per liter basis, for the case where no termination and no chain transfer reactions occur as shown in equation 1.4:

$$M_n = \frac{M_m[M]_o}{n_i} \quad (1.4)$$

where M_m is the monomer molecular weight, $[M]_0$ is the initial monomer concentration, and n_i is the number of polymer chains initiated in the reaction. Any deviation from the theoretical number average molecular weight is accounted for by an inefficiency of the initiator. Equation 1.5 describes the efficiency of an initiator. While equation 1.5 is helpful from a theoretical standpoint, in practice the initiator efficiency is typically determined by assuming that initiation is quantitative and calculating a predicted value for M_n. The actual M_n is then determined experimentally, and the values are compared after solving for n_i as shown in equation 1.4.

$$\text{Efficiency} = \frac{\text{Number of Reactive Species which Initiate Polymerization}}{\text{Number of Reactive Species Formed}} \qquad (1.5)$$

One might be tempted to surmise that slow initiation (or initiator inefficiency) means that the polymerization reaction does not proceed very fast, and that therefore the polymer yield is low; however, this is not the case since the rate of propagation can be very large. This fast propagation rate overcomes the inconvenience of low initiator efficiency to give high molecular weight product. In addition to the large propagation rate, the carbanion at the propagating end of a poly(cyanoacrylate) chain is very stable. This stability means that there is little to no premature termination: in fact, these carbanions are so stable that these are the only anionic polymerizations which proceed in an open container.

As mentioned previously, despite the stability of the propagating carbanion, poly(cyanoacrylates) are unstable both in solution and (to a much

lesser extent) in the solid form.[4,14-16] Ryan and McCann originally proposed that the mechanism of degradation in the presence of added base was via the 'unzipping' of the polymer chain which resulted in the formation of daughter polymer chains, of much lower molecular weight than the parent chains. Robello and co-worker's[14] results are in general agreement with those of Ryan and McCann, as far as the mechanism of degradation; however, Robello and co-workers demonstrated that the degradation of the parent polymer chain occurs without the addition of base. The mechanism proposed by both groups, Figure 1.3, indicates that the polymer chain is a stabilized carbanion in equilibrium with the free monomer. The chain end may then be protonated by water or an acid (shown as H^+) to form the dormant polymer, or parent chains. Since the two electron-withdrawing groups adjacent to the C—H make the proton acidic; the proton can therefore be removed by adventitious bases in the solution, including unreacted initiator. This instability makes the accurate determination of the molecular weight of poly(cyanoacrylates) difficult. This inherent instability may be circumvented by the addition of acid to the solution, which suppresses the back reaction by either protonating the base so that it cannot take the proton off of the dormant polymer chain, or simply by having an excess of protons around to ensure that the equilibrium between the active and dormant polymer chains favors the dormant chain.

Figure 1.3: Unzipping Mechanism for the Degradation of poly(Cyanoacrylates)

Shown here is a schematic drawing of the unzipping mechanism for the degradation of poly(cyanoacrylates).[4,14-16]

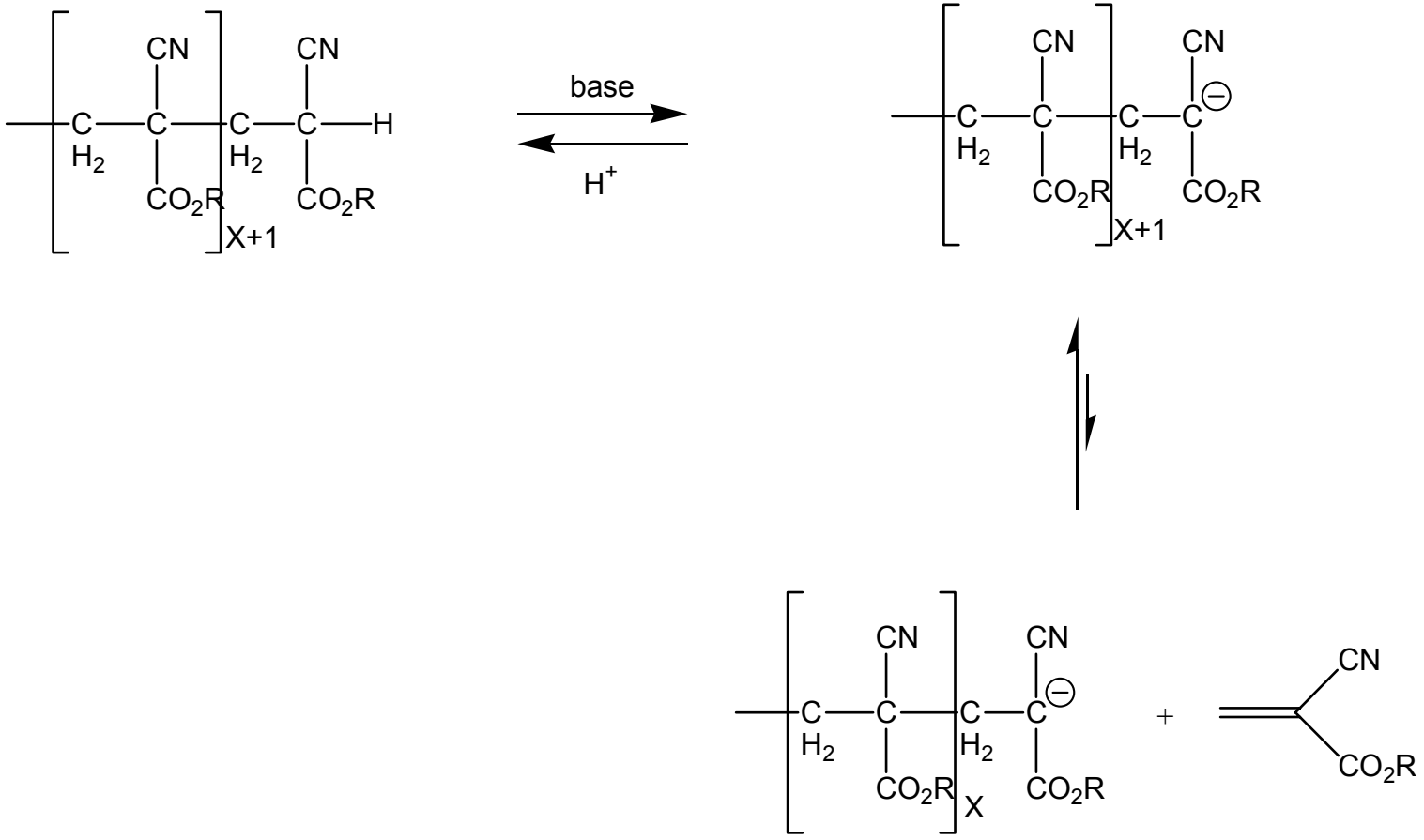
CN
CN
C
C
C
C
H
H2
H2
CO2R
CO2R
X+1
base
H+
CN
CN
C
C
C
C
H2
H2
CO2R
CO2R
X+1
CN
CN
C
C
C
C
H2
H2
CO2R
CO2R
X
+
CN
CO2R

1.3 Photochemical Initiators for Anionic Polymerization

As early as the 1960's photoinitiated polymerization was being investigated, but most of the research was focused on developing new photoinitiators for radical and cationic polymerizations. However, in 1972, Irie and coworkers reported the photoinitiated anionic polymerization of a solution containing nitroethylene in tetrahydrofuran (THF).[26] Upon mixing nitroethylene and THF, the absorption band of nitroethylene was extended farther into the visible region. Since THF is an electron donor, and nitroethylene (NE) has a high electron affinity, the new feature in the electronic absorption spectrum was assigned as charge transfer from THF to nitroethylene (THF→NE). Irradiation into this band caused the oxidation of THF and the reduction of nitroethylene to its radical anion (equation 1.6). The nitroethylene radical anion then initiated polymerization via an anionic mechanism (equation 1.7).

$$\mathrm{THF} + \mathrm{NE} \rightleftharpoons \{\mathrm{THF, NE}\} \xrightarrow{h\nu} \mathrm{THF}^{\bullet+} + \mathrm{NE}^{\bullet-} \qquad (1.6)$$

$$\mathrm{NE}^{\bullet-} \xrightarrow{\mathrm{NE}} \mathrm{poly(NE)} \qquad (1.7)$$

Since the initial reports by Irie and coworkers, several new classes of photoinitiators for anionic polymerization have been developed and exploited. The new model monomers for anionic polymerizations are cyanoacrylates. The reason for their use are their extreme susceptibility to anionic polymerization, the considerable stability of the propagating anion, and their relative thermal stability compared to nitrated monomers.

One system developed for the anionic polymerization of cyanoacrylates is the anthracene photosensitized decomposition of N-alkoxy pyridinium ions (Figure 1.4a).[28] In this reaction, anthracene absorbs a photon of light, and the photoexcited anthracene then reacts with an N-alkoxy substituted pyridinium compound to form the anthracene radical cation, the alkoxy radical, and pyridine. The pyridine is the active initiating species for the anionic polymerization of cyanoacrylates. In a second system, a phosphonium salt reacts photochemically either by heterolytic cleavage to form triphenylphosphine directly, or by homolytic cleavage to give the triphenylphosphonium radical cation, which can then form triphenylphosphine in a secondary thermal reaction. The triphenylphosphine is the active initiating species for the anionic polymerization of cyanoacrylates (Figure 1.4b).[29] The macromolecules produced in these two examples are technically zwitterions since they are formed by the reaction of an uncharged Lewis base with the monomer; however, the active propagating species is an anion, and the mechanism is therefore considered anionic.

A third class of organic photoinitiators for the anionic polymerization of cyanoacrylates are leuco dyes.[30] In this example, the photolability of a leaving group from the dye is exploited. In this class of photoinitiators, a leuconitrile is irradiated to release the cyanide anion. The photoreleased cyanide then attacks the monomer and the anionic polymerization of cyanoacrylate commences, while the color of the dye develops at the same time (Figure 1.4c).

While these examples show the utility of organic compounds in photoinitiated anionic polymerization, there have also been strides taken to

expand this chemistry to include transition metal coordination compounds. In 1991, Kutal and co-workers reported the photoinitiated anionic polymerization of cyanoacrylates using Reinecke's Salt ($K[Cr(NH_3)_2(NCS)_4]$, abbreviated K^+R^-).[18] Upon irradiation into a ligand field absorption band of the compound, the Reineckate anion undergoes efficient ligand substitution to release a thiocyanate anion (equation 1.8).[31] The thiocyanate anion then attacks the cyanoacrylate monomer and anionic polymerization commences (equation 1.9).

$$K[Cr(NH_3)_2(SCN)_4] \xrightarrow[S]{h\nu} K^+ + Cr(NH_3)_2(SCN)_3S + SCN^- \qquad (1.8)$$

$$SCN^{\ominus} \xrightarrow{CA} \text{poly(CA)} \qquad (1.9)$$

In 1997, Kutal and co-workers also reported that the coordination compound $Pt(acac)_2$ (acac is the acetylacetonate anion) can be used as a photoinitiator for the anionic polymerization of an alkyl 2-cyanoacrylate.[32] This study demonstrated that irradiation into the ligand field band of $Pt(acac)_2$ causes efficient photosubstitution of one acetylacetonate ligand (equation 1.10). This reaction occurs via a monodentate intermediate, and by using acidified solvent, the oxygen is then protonated and recoordination to the metal is inhibited. In cyanoacrylate, the oxygen on the free end of acetylacetonate in the intermediate may or may not be protonated owing to acid added to stabilize the commercial monomer. However, either the oxygen from the monodentate intermediate or the free ligand can attack the CA monomer and initiate polymerization.

$$Pt(acac)_2 \xrightarrow[CH_3CN]{h\nu,\ H^+} Pt(acac)(CH_3CN)_2^+ + H(acac) \qquad (1.10)$$

Figure 1.4: Photoinitiators for the Anionic Polymerization of Cyanoacrylates

Shown are the anthracene-sensitized, N-alkoxy pyridinium (a), phosphonium salts (b), and leuco dye (c) systems for the photoinitiated anionic polymerization of cyanoacrylates. Each of these classes of organic compounds reacts photochemically to release either an anion or an uncharged Lewis base which then attacks the monomer to initiate polymerization.

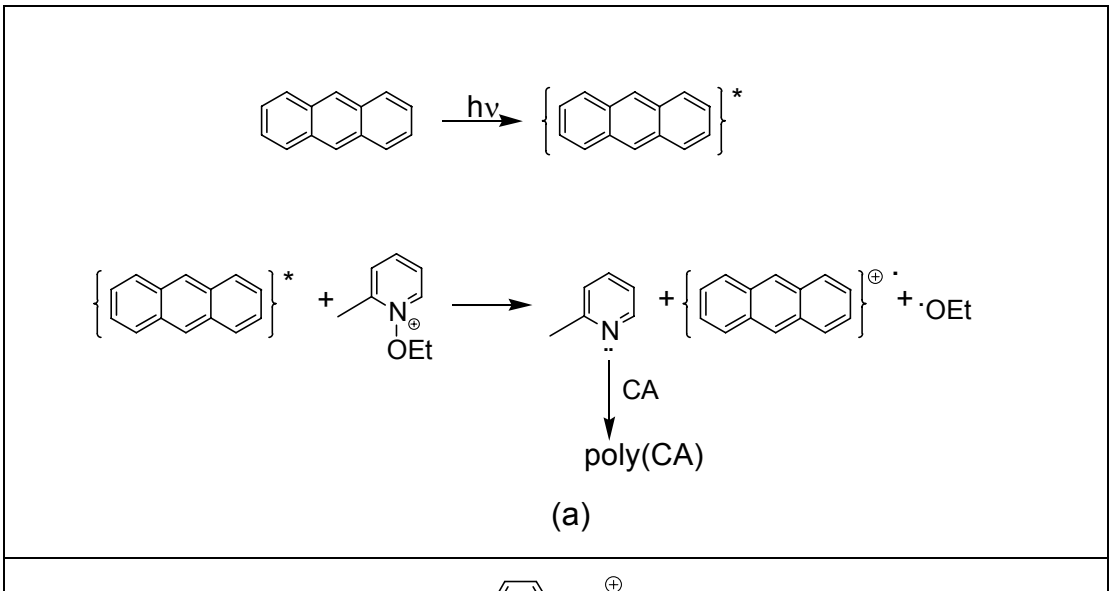
hν
OEt
CA
poly(CA)

(a)

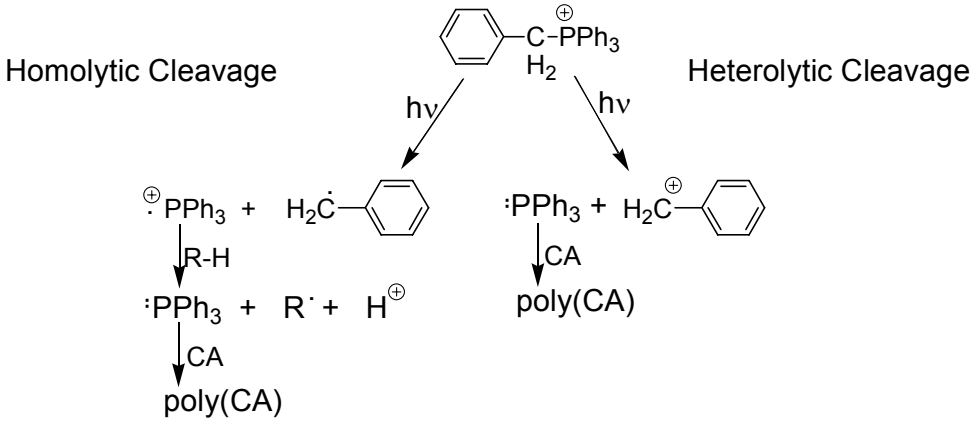
Homolytic Cleavage
Heterolytic Cleavage
hν
hν
R-H
CA
CA
poly(CA)
poly(CA)

(b)

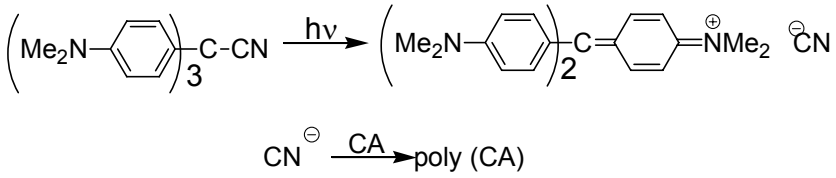
hν
CA
poly (CA)

(c)

A later report by Paul and coworkers[19] indicated the use of tungsten or chromium pentacarbonyl amine complexes as photoinitiators for the anionic polymerization of cyanoacrylates. Irradiation into the ligand field absorption band of these compounds results in release of the amine. In the particular compounds looked at, the amines were pyridine and its ring substituted analogs, which are known initiators for the anionic polymerization of CA. The nitrogen atom of the amine attacks the carbon-carbon double bond, and polymerization commences via the same type of zwitterionic species as indicated in Figure 1.4a for the N-alkoxy pyridinium compounds.

In addition to the photoinitiators mentioned above, Kutal and co-workers have also reported that benzoyl-substituted ferrocenes are capable of photoinitiating the anionic polymerization of cyanoacrylates. A portion of this project will be devoted to determining whether or not a series of substituted Group 8 metallocenes photointiate the anionic polymerization of a cyanoacrylate monomer. If these metallocenes do photoinitiate the anionic polymerization of the cyanoacrylate, then I will undertake studies to determine the mechanism of photoinitiation and the rate of polymerization. Since a significant portion of this manuscript is devoted to the characterization of these substituted metallocenes as photoinitiators for the anionic polymerization of cyanoacrylates, let us take a closer look at them, beginning with the unsubstituted parent compounds.

1.4 Group 8 Metallocenes

Ferrocene (bis(η^5-cyclopentadienyl iron(II)), discovered in 1951, became the first known example of a class of compounds called metallocenes, or sandwich compounds. The discovery of this new compound led to many studies directed at the elucidation of the bonding, electronic structure, chemical properties and reactivity of this new class of compounds. In addition to these studies on ferrocene, other studies were directed at the synthesis of ferrocene-type compounds with various substituents on the cyclopentadienyl rings and/or containing different metals.

When the structure of ferrocene was determined by Wilkinson et. al. in 1952, it appeared that two cyclopentadienyl (Cp) ligands were centrally bonded in a symmetric fashion.[33] Thus, in this new molecule, all carbons on the two Cp rings were equidistant from the metal center. This structure was inconsistent with the current models of bonding in the early 1950's, and as such, a new wave of research was directed at explaining and understanding this new type of bonding. It was later shown that the two cyclopentadienyl rings in ferrocene adopt a staggered conformation in the solid state. The staggering of the rings confers upon the ferrocene molecule symmetry consistent with the D_{5d} point group; the structure of ruthenocene is very similar to that of ferrocene, except that the rings tend to adopt an eclipsed conformation in the solid state making the symmetry of the ruthenocene compound effectively D_{5h}[34]. The structures of these two metallocenes are shown in Figure 1.5.

Figure 1.5: Solid State Structures of Group 8 Metallocenes

Shown here are the solid state structures depicting the staggered structure of the cyclopentadienyl rings in ferrocene and the eclipsed structure of the cyclopentadienyl rings in ruthenocene.

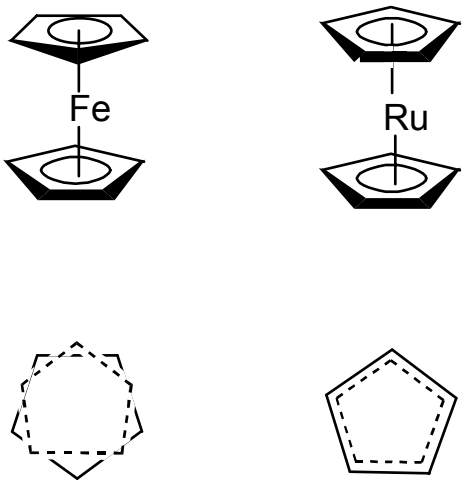
Fe
Ru

In order to facilitate a discussion of the electronic absorption spectra of these two metallocenes, a qualitative molecular orbital (MO) diagram of the group 8 metallocenes is shown in Figure 1.6.[35-38] In the case of ferrocene (D_{5d} symmetry) the 10 π electrons in the p orbitals of the cyclopentadienyl rings form the symmetry adapted linear combinations designated a_{1g}, a_{2u}, e_{1g}, e_{1u}, e_{2g}, and e_{2u}. Interactions of these ligand orbitals with the metal 3d, 4s, and 4p orbitals form the molecular orbitals depicted in the MO diagram. In the case of ruthenocene, the symmetry is different, but this has little to no effect on the ordering of the molecular orbitals or on the electronic properties.[35,36,38] If we consider the z axis to be the metal-ligand axis, then the filled a_{1g}, e_{1g}, and e_{2g} orbitals are situated so they can interact with d orbitals on the metal and donate electron density. The overlap between the d_z^2 metal orbital and the a_{1g} ligand orbital is essentially zero; therefore, the resulting $2a_{1g}$ molecular orbital is non-bonding and almost entirely metal in character. Overlap between the ligand e_{1g} orbitals and the metal d_{xz} and d_{yz} orbitals result in the strongly bonding $1e_{1g}$ molecular orbital which is mostly ligand in character and the anti-bonding $2e_{1g}^*$ molecular orbital, which is mostly metal in character. Poor overlap between the $d_{x^2-y^2}$ and d_{xy} orbitals on the metal and the e_{2g} orbitals on the ligands results in a weak bonding interaction, and the $1e_{2g}$ molecular orbitals are therefore also mostly metal in character. This gives ferrocene a ground state molecular orbital occupation of $(1a_{1g})^2(1a_{2u})^2(1e_{1g})^4(1e_{1u})^4(1e_{2g})^4(2a_{1g})^2$, thus the ground state is $^1A_{1g}$. Notice that in this bonding scheme, the electrons which are expected to be excited by absorption of a visible/near UV photon reside in molecular orbitals

which are mainly metal in character and that the lowest unoccupied molecular orbital is also mostly metal in character. For this reason, it is sufficient (and much simpler) to discuss the low energy electronic transitions of these metallocenes in the context of ligand field theory: this has led to the designation of the low energy electronic transitions in ferrocene and ruthenocene as ligand field (or d-d) transitions.

The molecular orbitals important for a discussion of the electronic transitions exhibited by the unsubstituted Group 8 metallocenes of interest here are the $1e_{2g}$, $2a_{1g}$, and $2e^{*}_{1g}$ molecular orbitals (indicated in the box in Figure 1.6): as stated above, these orbitals are mainly metal in character. In the case of ferrocene, there are three spin-allowed ligand field transitions from the ground state: the promotion of an electron from the non-bonding $2a_{1g}$ orbital to the anti-bonding empty $2e_{1g}^{*}$ ($^1A_{1g} \rightarrow a^1E_{1g}$), and the promotion of an electron from the weakly bonding $1e_{2g}$ orbital to the anti-bonding $2e_{1g}^{*}$ orbital ($^1A_{1g} \rightarrow {}^1E_{2g}$ and $^1A_{1g} \rightarrow b^1E_{1g}$). Ferrocene has two absorption bands in the visible portion of the spectrum located at 440 nm and 325 nm. The lower energy band consists of two unresolved electronic transitions, the $^1A_{1g} \rightarrow a^1E_{1g}$ and $^1A_{1g} \rightarrow {}^1E_{2g}$ transitions, while the absorption band at 325 nm arises from the $^1A_{1g} \rightarrow b^1E_{1g}$ transition.[35-38] Ruthenocene also has two absorption bands in the near UV/visible region of the spectrum, occurring around 320 nm and at 276 nm. For simplicity (and in accord with the literature), we will assume that ruthenocene has the same symmetry as ferrocene and that the qualitative molecular orbital diagram has the same ordering as shown for ferrocene. Ruthenocene's absorption band at ~320 nm

also arises from two unresolved electronic transitions, the $^1A_{1g} \rightarrow {}^1E_{2g}$ and the $^1A_{1g} \rightarrow a^1E_{1g}$ (arising from the promotion of an electron from the $2a_{1g}$ and $1e_{2g}$ orbitals to the $2e_{1g}^*$ orbitals, respectively). The absorption band at 276 nm arises from the promotion of an electron from the $1e_{2g}$ molecular orbital to the $2e_{1g}^*$ molecular orbital ($^1A_{1g} \rightarrow b^1E_{1g}$).[39-41]

Both ferrocene and ruthenocene are photoinert in solvents such as methanol, cyclohexane, and acetonitrile.[36] However, in electron-accepting solvents such as carbon tetrachloride, both ferrocene and ruthenocene form ground-state electron donor-acceptor (D-A) complexes. These electron D-A complexes are characterized by a new band in the electronic absorption spectrum, which is not due to either the solvent or the metallocene, and is therefore designated a charge-transfer-to-solvent transition (CTTS). Irradiation into the CTTS band causes the one electron oxidation of the metallocene to the metallocenium ion and the reduction of the solvent to its radical anion (equation 1.11).[42-47]

$$M(Cp)_2 + CCl_4 \rightleftharpoons \underset{\text{Ground State D-A Complex}}{\{M(Cp)_2, CCl_4\}} \xrightarrow{h\nu} M(Cp)_2^+ + CCl_4^{\bullet -} \quad (1.11)$$

In the case of ferrocene, the ferricinium ion is a well-characterized species with an absorption maximum at 617 nm.[36,43] In contrast, isolation of the ruthenocenium ion has proven more difficult. There is direct evidence for the

Figure 1.6: Qualitative Molecular Orbital Diagram for Ferrocene

Shown here is the qualitative molecular diagram for ferrocene; the portion of the diagram in the box is responsible for the low energy electronic transitions.[35-38]

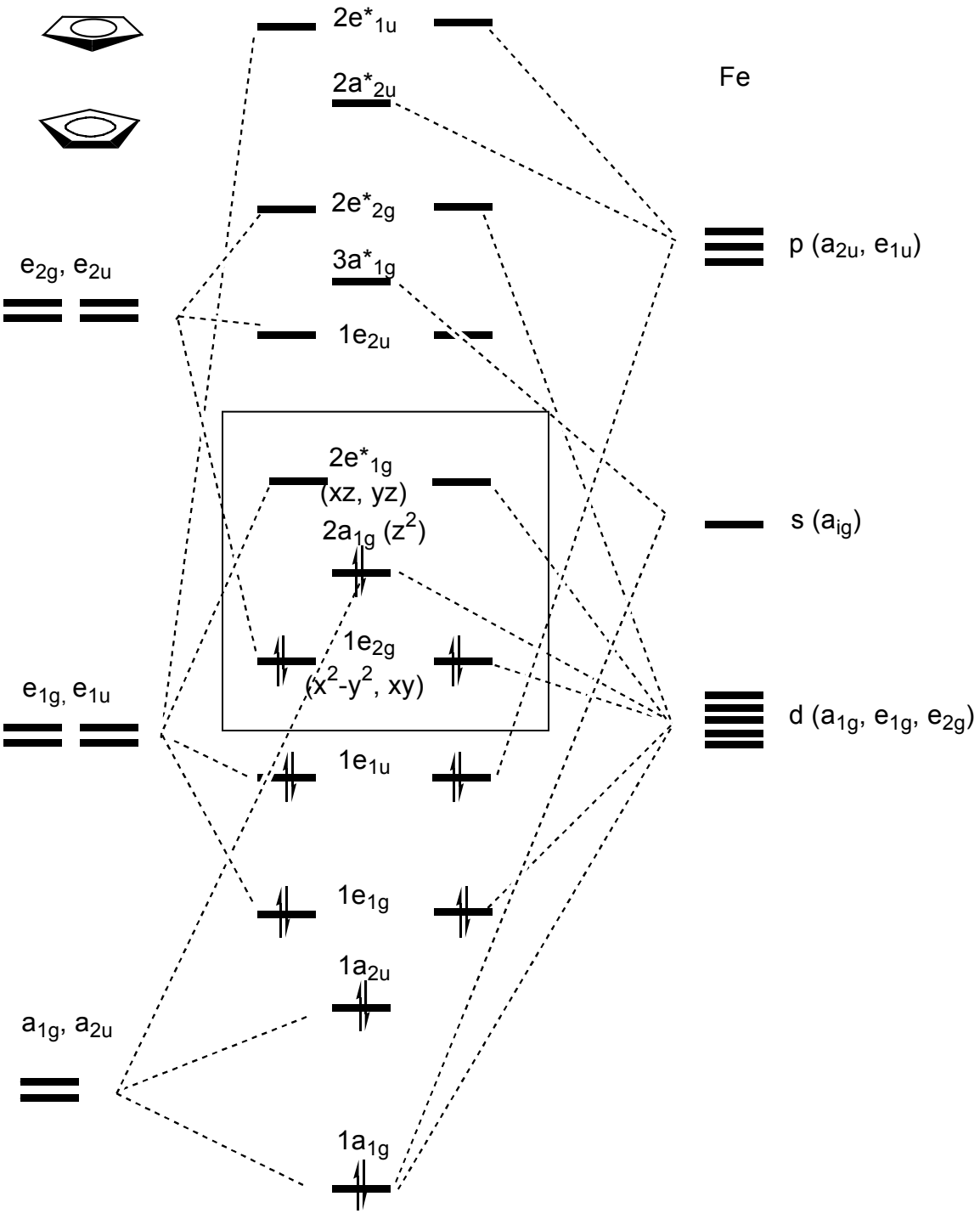
2e*1u
2a*2u
Fe
2e*2g
p (a2u, e1u)
e2g, e2u
3a*1g
1e2u
2e*1g
(xz, yz)
2a1g (z2)
s (aig)
1e2g
(x2-y2, xy)
e1g, e1u
d (a1g, e1g, e2g)
1e1u
1e1g
1a2u
a1g, a2u
1a1g

formation of ruthenocenium in flash photolysis studies;[45,47] but the one electron oxidation product has not been isolated to date.

The radical anion of carbon tetrachloride is very unstable and quickly decomposes to the chloride anion and the trichloromethyl radical. This photochemistry has been used in several different capacities: for example, the trichloromethyl radical generated in equation 1.11 has been utilized to initiate the radical polymerization of various vinylic monomers.[48-51] The type of photochemistry depicted in equation 1.11 has also been used to show that ferrocenes as ligands on other metals are capable of interacting with and causing the oxidation of the second metal.[52] Kunkely and Vogler reported that when a complex containing a ferrocenyl-type ligand linked via a phosphine ligand to either Pd(0) or Re(I) is dissolved in a halocarbon solvent, photooxidation of Fe^{2+} to Fe^{3+} occurs. However, the second metal then reduces the Fe^{3+} back to Fe^{2+}. Systems of this type may help chemists to better understand fundamental biological chromophoric systems, such as photosynthesis. As well, systems such as this may be useful in catalysis and certainly offer insight into supramolecular photochemistry.

In contrast to ferrocene's photoinertness in most solvents, acyl-substituted ferrocenes are photosensitive in many solvents including methanol or acetonitrile. The first report on the photosensitivity of acyl-substituted ferrocenes was by Tarr and co-workers.[53] In the course of this study, it was demonstrated that addition of at least one substituent containing a carbonyl group that was

conjugated to the cyclopentadienyl ring of ferrocene caused a marked increase in the intensity of the low energy electronic absorption band, as well as a shift in band position to lower energy, illustrated in Figure 1.7. This report also states that benzoylferrocene and 1,1'-dibenzoylferrocene both decompose upon exposure to either 470 nm or 354 nm light, with the disubstituted compound being four times more photosensitive than the monosubstituted compound. They proposed that introduction of a carbonyl group conjugated to the cyclopentadienyl ring introduces some amount of instability into the molecule, and therefore interaction between the metal and the oxygen atom of the carbonyl is involved in the breakdown mechanism. The mechanism proposed by this group had the photochemical oxidation of the metallocene, with the reduction of the solvent (methanol), as the primary photochemical step. A subsequent reaction between the metallocenium ion and the solvent radical led to the observed products which consisted of an iron containing precipitate as well as several volatile compounds. The precipitate was not identified; however some of the reported volatile compounds were identified as benzene, methylbenzoate, and acetals. These initial reports on the photosensitivity of acylferrocenes were later confirmed by several other groups; as well, several mechanisms were reported for the photodecomposition of benzoyl-substituted ferrocenes, depending on the solvent used.[54-56] Among these primary photochemical reactions are the aquation of the carbonyl which precedes ring deligation to give ferrocene, cyclopentadiene, and a benzoate product.[54] Additionally, there have

Figure 1.7: Electronic Absorption Spectra of Various Group 8 Metallocenes

This figure shows the electronic absorption spectra of ferrocene (Fc), benzoylferrocene (BFc), and 1,1'-dibenzoylferrocene (DFc) in room temperature methanol.

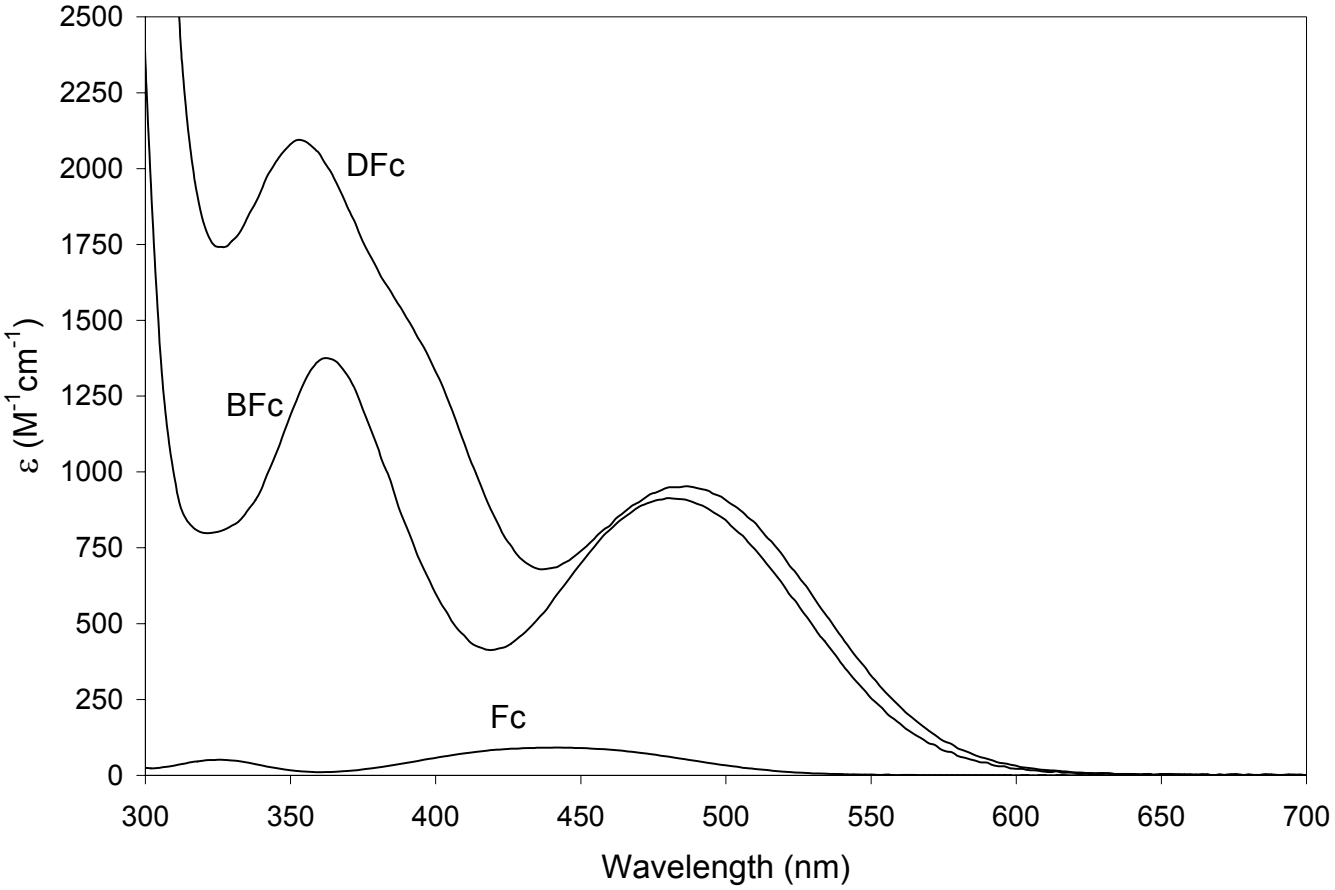
2500
2250
2000
1750
1500
1250
1000
750
500
250
0
ε (M-1cm-1)
DFc
BFc
Fc
300
350
400
450
500
550
600
650
700
Wavelength (nm)

been reports of the photoreaction occurring via protonation of the carbonyl oxygen, followed by metal-ring bond cleavage,[55] and photooxidation of the metallocene to its metallocenium ion.[56]

However, the Kutal group demonstrated that all of these mechanisms do not quite fit the data reported by his group.[57] Yamaguchi and Kutal reported the efficient photodissociation of intact benzoylcyclopentadienide anions from benzoylsubstituted ferrocenes, and therefore the primary photochemical reactions previously reported by others were inaccurate. They showed that oxygen, which can scavenge radicals in solution, had no effect on the disappearance quantum yield for benzoylferrocenes. If the photodissociation mechanism involved a radical, the quantum yield would be lower in the oxygen-saturated solvent; thus discounting the mechanism proposed by Tarr[53] since their mechanism involved the formation of a reactive solvent radical. The Kutal group also pointed out that the photodissociation of a benzoylcyclopentadienide anion occurred without the addition of acid to the solvent, so the mechanism proposed by Bozak was discounted[55] since their mechanism had protonation of the carbonyl oxygen as the first step. Another mechanism, proposed by Kemp,[54] which involves the aquation of the carbonyl group followed by metal-ring bond cleavage, would not yield an intact benzoylcyclopentaidenide anion, and thus could not be accurate. In contrast, Kutal proposed that the primary photochemical reaction was heterolytic cleavage of the metal-ring bond, and the

Figure 1.8: Photochemical Reactions of 1,1'-Dibenzoylferrocene

This figure shows the mechanism proposed by Yamaguchi and Kutal which indicates that the primary photochemical reaction is the loss of an intact benzoylcyclopentadienide anion, and that photoproducts observed by other groups were due to secondary thermal or photochemical processes.[57]

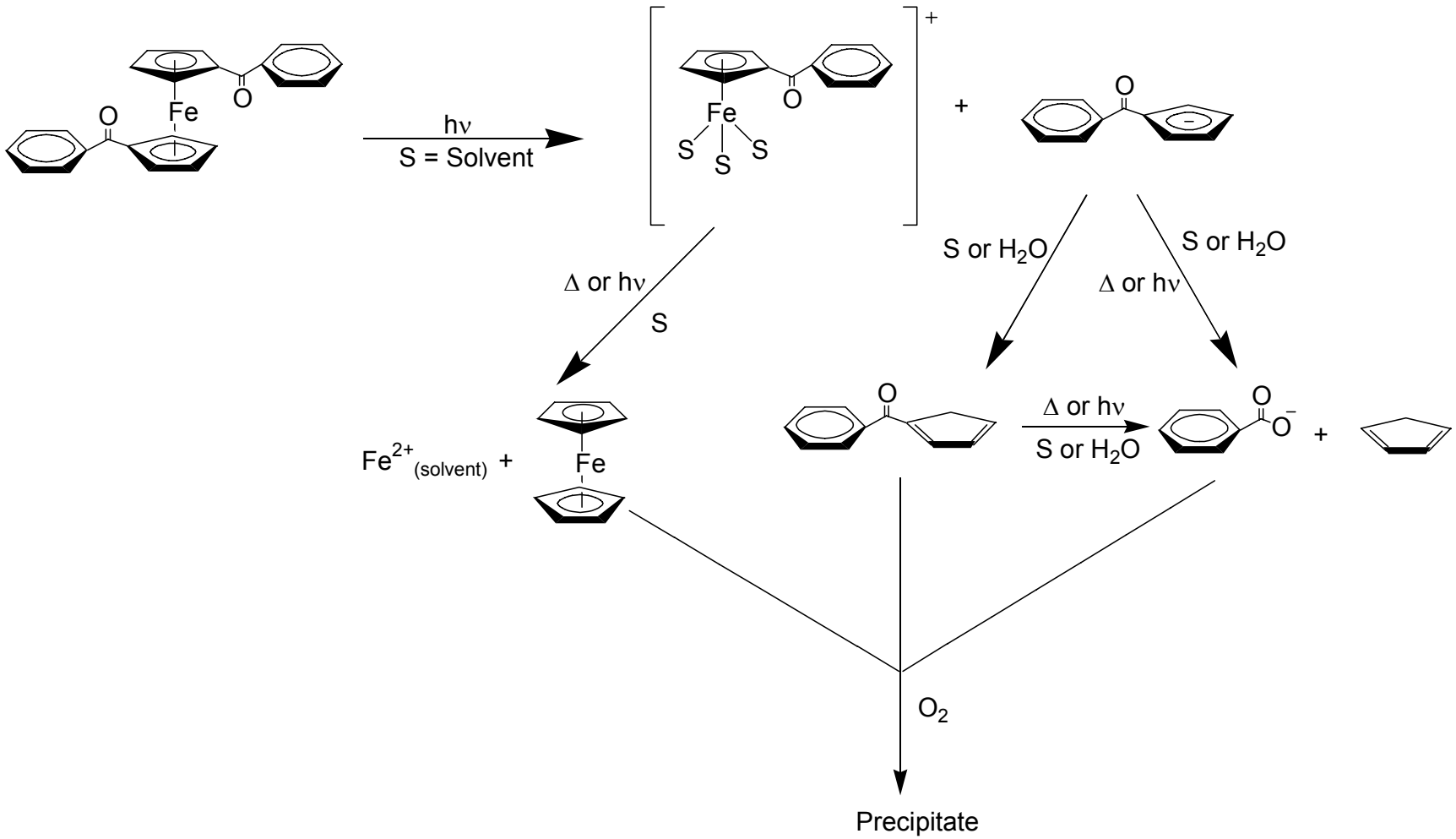
hν
S = Solvent
Fe
O
S
+
Δ or hν
S
S or H2O
Fe2+(solvent) +
O2
Precipitate

products observed by other groups were the result of secondary thermal or photochemical processes as shown in Figure 1.8.[57]

As mentioned before, addition of one or more benzoyl groups to the cyclopentadienyl rings of ferrocene, shifts the low-energy electronic transition to a longer wavelength and increases the intensity of the band. This is believed to arise from conjugation between the carbonyl group and the cyclopentadienyl ring, resulting in the mixing of charge transfer character into the ligand field transitions of the parent ferrocene compound. While the substituted compounds do not exhibit D_{5d} symmetry, one can use the molecular orbital diagram for the parent compounds to draw an analogy to the substituted compounds.[57] If we make that assumption, then irradiation of the compound with 546 nm light causes either the $^1A_{1g} \rightarrow a^1E_{1g}$ or the $^1A_{1g} \rightarrow {}^1E_{2g}$ electronic transition; either of these transitions causes the promoted electron to populate the $2e_{1g}^*$ molecular orbitals, which are anti-bonding, while at the same time vacating either the $2a_{1g}$ or $1e_{2g}$ molecular orbitals, which are non-bonding and weakly bonding, respectively. Either of these transitions would weaken the iron-ring bond, leaving the compound susceptible to nucleophilic attack by an incoming solvent molecule.

Another way to look at this is pictorially through the limiting resonance structure shown in Figure 1.9. In this resonance structure of the photoexcited 1,1'-dibenzoylferrocene molecule, absorption of a photon causes a shift in electron density from the iron atom onto the cyclopentadienyl ring where it is then delocalized onto the carbonyl group. This delocalization causes a reduction in the

hapticity ($\eta^5 \rightarrow \eta^4$) of the cyclopentadienyl ring; thus weakening the iron-ring bond, which facilitates the dissociation of the ring. Additionally, the resulting formal positive charge on the iron atom increases its susceptibility to nucleophilic attack by incoming solvent molecules. Both of these occurrences taken together help to explain why benzoyl-substituted ferrocenes are much more photosensitive than the unsubstituted compound. While this resonance structure seems accurate, direct observation of this metal-to-ligand charge transfer has not been observed. One goal of this project is therefore to test the validity of metal-to-ligand charge transfer assignment using resonance Raman spectroscopy. The photochemistry of the benzoyl-substituted ruthenocenes has not been studied to date, and will also be a subject of part of this project.

1.5 Resonance Raman Spectroscopy

In order to address some of the goals of this project several instrumental techniques will be utilized. A brief summary of some of these techniques are included here. As mentioned above, one goal of this project is to confirm that the low energy absorption band of benzoyl-substituted ferrocenes does in fact contain appreciable metal-to-ligand charge transfer character. One way to assess this assignment is by using resonance Raman spectroscopy, a brief description of which is presented here. For a more thorough treatment, please see the books by P. R. Carey, D. A. Long, and T. G. Spiro listed at the end of this manuscript.[58-60]

Figure 1.9: Resonance Structure of Photoexcited 1,1'-Dibenzoylferrocene

Presented here is a representation of the limiting resonance structure, which illustrates the metal-to-ligand charge transfer in photoexcited 1,1'-dibenzoylferrocene.

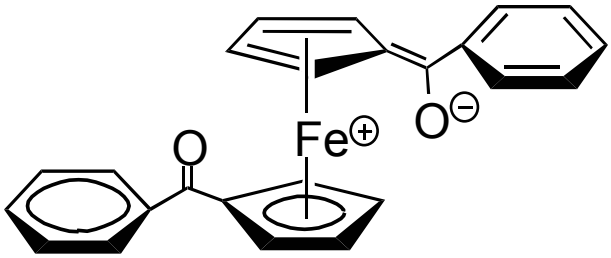
O
Fe⊕
O⊖

When light encounters a molecule, any one of several things can happen: the light can be absorbed and then re-emitted at a different frequency (fluorescence or phosphorescence), the light may encounter the molecule, have an elastic collision and scatter off the molecule with no energy transfer to the molecule (Rayleigh scattering), or the light may encounter the molecule, have an inelastic collision and scatter off of the molecule after transferring some of its energy to the molecule (Raman scattering). These three interactions of light with a molecule are represented in Figure 1.10. The type of interaction discussed here is the inelastic collision known as Raman scattering. Since energy is conserved in an inelastic collision, the energy lost by the incident photon is equal to the energy absorbed by the molecule; this energy absorption causes vibrations in the molecule. Therefore, by measuring the changes in energy of the scattered photons, we are able to measure the energies of the vibrations of a molecule.

Resonance Raman occurs when the incident light used to excite the molecule corresponds to an allowed electronic transition of the molecule. When this happens, certain bands in the Raman spectrum are enhanced, indicating that some bonds have been perturbed more than others. In order to understand the phenomenon of resonance Raman, we need to consider the quantum theory of scattered light. The intensity of a Raman band is dictated by equation 1.12 (for a vibrational transition from state *m* to state *n*):

$$I_{n\leftarrow m} = K(\nu_o + \nu_{mn})^4 \sum_{\sigma\rho} \left| (P_{\sigma\rho})_{mn}{}^2 \right| \qquad (1.12)$$

where K is a constant, ν_o is the frequency of incident light, ν_{mn} is the frequency which corresponds to the energy difference between two vibrational states, m

Figure 1.10: Possible Interactions between Light and a Molecule

This is a pictoral representation of interactions between light and a molecule, including Rayleigh scattering, Raman scattering, resonance Raman scattering, and luminescence.

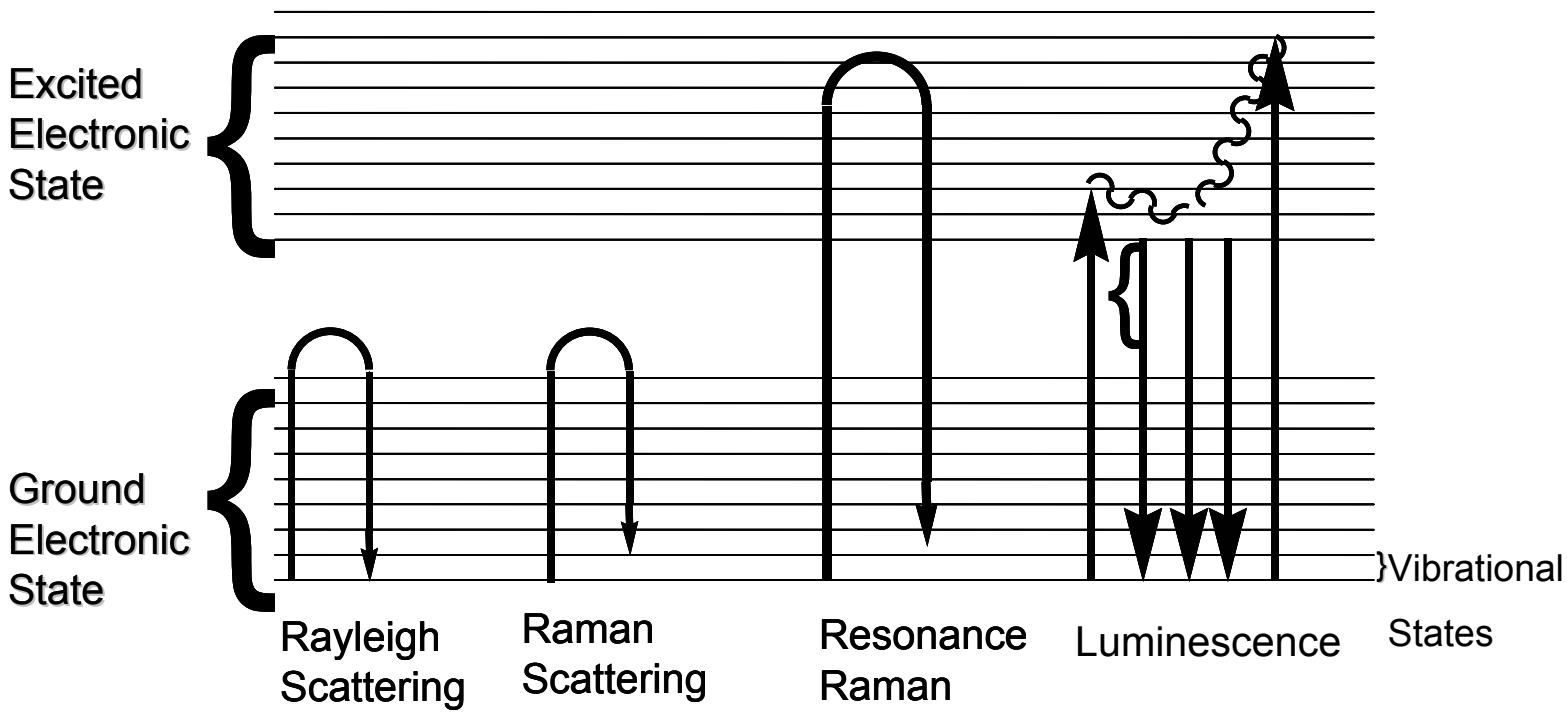
Excited
Electronic
State
Ground
Electronic
State
}Vibrational
States
Rayleigh
Scattering
Raman
Scattering
Resonance
Raman
Luminescence

and n, ρ and σ denote x, y, and z components, and $(P_{\rho\sigma})_{mn}$ (the expanded version) is defined in equation 1.13:

$$(P_{\rho\sigma})_{mn} = \frac{1}{h} \sum_{r} \underbrace{\frac{(M_{\rho})_{rn}(M_{\sigma})_{mr}}{\nu_{rm} - \nu_{o}}}_{\text{A term}} + \underbrace{\frac{E(M_{\rho})_{mr}(M_{\sigma})_{rn}}{\nu_{rn} + \nu_{o}}}_{\text{B term}} \qquad (1.13)$$

where m, n, and r are the initial, final, and intermediate states, respectively, terms of the form $(M_{\rho})_{rn}$ are Cartesian components of the transition moments, E is the electric field, h is Planck's constant, ν_o is the frequency of incident light, ν_{rn}, ν_{rm}, and ν_{mn} are the frequencies which correspond to the energy difference between the two described states. Resonance enhancement arises from the A term above. When the energy of the incident light approaches the energy of an allowed electronic transition, the denominator ($\nu_{rm} - \nu_o$) becomes very small, which causes the overall term to become very large and therefore dominate the spectrum.

The B term denoted above arises from the vibrational mixing of two excited states and allows for scattering by non-totally symmetric modes. In contrast the A term denoted above, which is the active mechanism in the resonance Raman studies presented here, arises from a single electronic transition and involves totally symmetric modes. In this mechanism, there is an increase in band intensities for bonds which are greatly perturbed due to excitation of the molecule. In other words, the vibrational motions observed in the resonance Raman spectra mimic the distortions that occur in the excited state of the molecule, thereby allowing us to visualize said photoexcited state. Since the

carbonyl group is a strong Raman absorber, and is predicted to be greatly perturbed based on the resonance structure shown in Figure 1.9, resonance Raman spectroscopy can be used to monitor changes in the structure of benzoyl-substituted metallocenes upon photoexcitation. Consequently, we can assess the validity of the proposal that the low energy electronic transition contains appreciable metal-to-ligand charge transfer character.

1.6 Electrospray Ionization Time-of-Flight Mass Spectrometry

Electrospray ionization (ESI) is a soft ionization technique which allows ions from solution to enter the gas phase. ESI works by having a high electric field applied to a metal (or other suitable material, such as quartz) capillary. The applied electric field can penetrate into the solution, causing a partial separation of the positively and negatively charged electrolytes in the solution. When operated in the positive ion mode, cations are enriched at the surface of the liquid while anions are driven back toward the inside of the capillary by the applied voltage. As the cations enrich at the surface of the solution, they begin to repel each other, this repulsion coupled with the force exerted on the cations by the applied electric field causes a distortion of the liquid until a cone is formed. This cone continues to elongate and distort until a liquid filament is formed which begins to break up into charged droplets.

As the droplets get smaller, they have an increasing amount of charge in an increasingly smaller volume, which leads to further repulsive forces. Eventually the repulsive force will be strong enough to overcome the cohesive

forces of the solvent, and the droplet will become smaller yet again. This process, called Coulombic fission, continues until one of two things happens: either the droplets become so small that they contain only the analyte ion, or the electric field on the surface of the droplet becomes so high that that analyte ions are desorbed from the droplet. Either way, the result is the same: the ions that were in solution are now intact, in the gas phase, and able to be analyzed (Figure 1.11).[61-63]

Time-of-flight (TOF) detectors separate ions in the gas phase based on the principle that ions of different masses that are moving in the same direction with an approximately constant kinetic energy will have different velocities. Ions acquire kinetic energy as they are accelerated through an applied electric field in the ionization source. Because all of the ions in the same aliquot go through the same field, they will nominally have the same kinetic energy. Once accelerated, the ions enter an evacuated chamber, called a drift tube, which has no applied voltage; here in the drift tube is where ions of different masses are separated.

The kinetic energy of an ion is given by equation 1.14:

$$E_k = zFs = \frac{mv^2}{2} \qquad (1.14)$$

where z is the charge, F is the electric field strength, s is the starting position of the ion, m is the mass, and v is the velocity of the ion. Solving equation 1.14 for velocity gives equation 1.15.

$$v = \left(\frac{2zFs}{m}\right)^{0.5} \qquad (1.15)$$

Figure 1.11: Diagram of an Electrospray Ionization Tip

Depicted here is an ESI tip and the formation of gas-phase ions from the electrospray tip to the skimmer (where the ions enter the mass spectrometer). Also shown are the high voltage power supply, electron flow (in the positive ion mode), and ammeter (I).

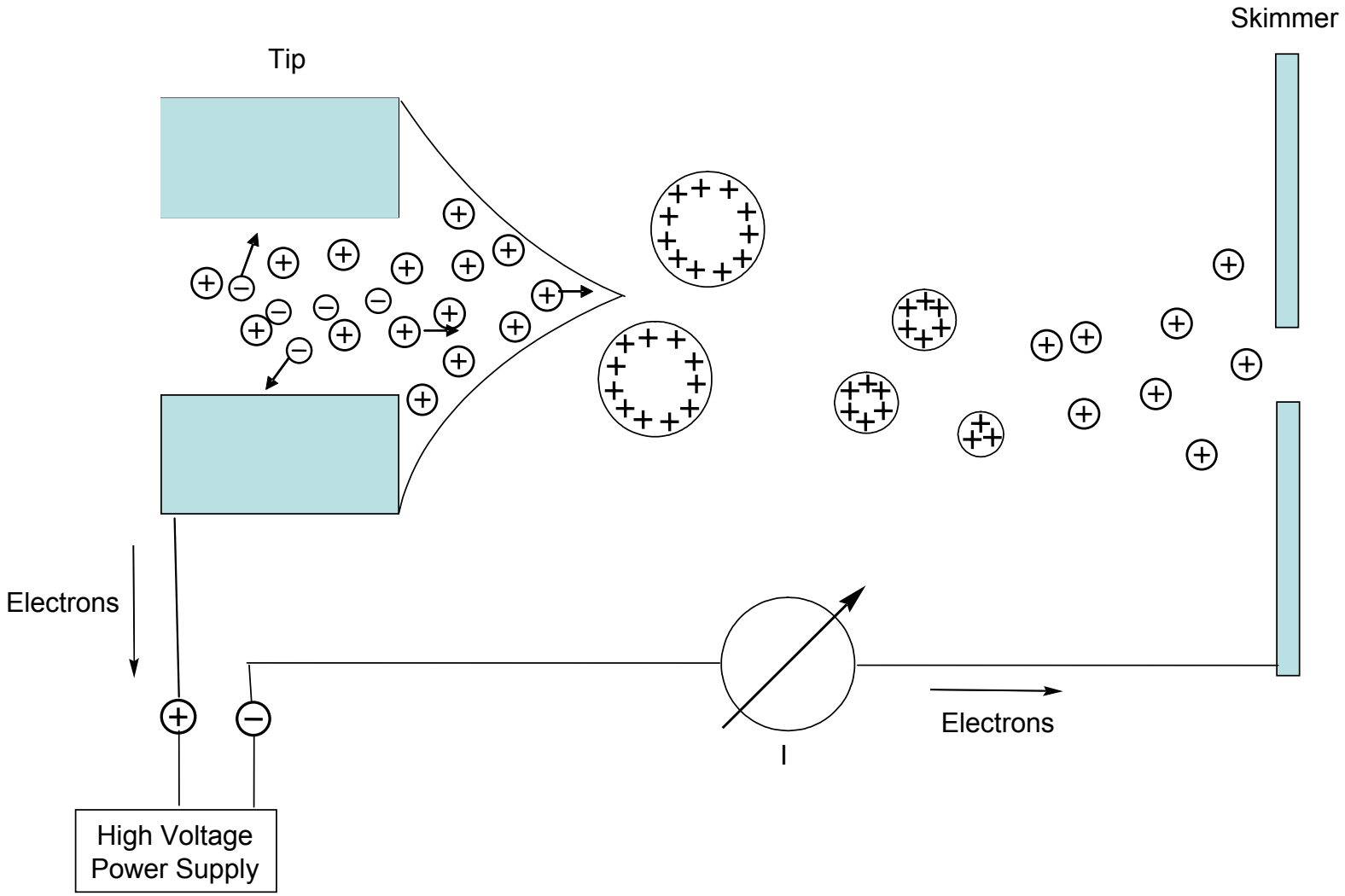
Skimmer
Tip
Electrons
High Voltage
Power Supply
I
Electrons

The time, t, required for the ion to reach the detector is given by the distance traveled divided by the velocity of the ion (equation 1.16a). Plugging equation 1.15 into equation 1.16a gives equation 1.16b where all quantities are as defined above.[64]

$$t = \underset{a}{\frac{d}{v}} = \underset{b}{d\left(\frac{m}{2zFs}\right)^{0.5}} \qquad (1.16)$$

These equations demonstrate that the time required to arrive at the detector is proportional to the mass-to-charge (m/z) ratio. In other words, if we have two singly charged ions with different masses, the lighter ion will reach the detector first, and the heavier ion would take longer to reach the detector.

ESI-TOF has been used to study many organometallic systems,[65-67] and recently Kutal and co-workers have developed an on-line irradiation technique capable of monitoring the photogeneration of intermediates having lifetimes on the order of milliseconds.[68-70] A diagram of the instrumental set-up designed by Kutal and co-workers is seen in Figure 1.12. In this on-line analytical technique, the electrospray tip is a quartz capillary pulled to a fine tip (10-40 μm inner diameter (i.d.)). Aligned to the capillary is a fiber optic cable with laser light shining through it, essentially making the capillary a microphotolysis cell. By knowing the inner diameter of the capillary tip, the flow rate of the solution, and the distance, D, from where the laser light shines on the capillary to where the solution is sprayed out into the gas phase, one can calculate the reaction time. For example, using a typical flow rate of 40 μL/h, an inner diameter of 14 μm, and placing the fiber optic cable at a distance of 0.84 mm from the end of the tip,

the solution takes 12 ms to arrive at the end of the capillary. Once sprayed out of the capillary, any species which are present in the solution (those with lifetimes of 12 ms or more) are essentially trapped in the gas phase and measurement of these species is attained. I have used this on-line photolysis procedure coupled to an ESI-TOF mass spectrometer to identify the short-lived intermediates generated upon 488 nm photolysis of 1,1'-dibenzoylferrocene in solution.

1.7 Attenuated Total Reflectance-Fourier Transform Infrared Spectroscopy

In order to determine the rate of photopolymerization for ethyl 2-cyanoacrylate, (CA), using the photoinitiators mentioned in this manuscript, I will measure the disappearance of the carbon-carbon double bond as a function of time, using IR spectroscopy. In order to facilitate the absorbance measurement, I will use a horizontal attenuated total reflectance (ATR) assembly so that the polymer does not drip into the spectrometer.

A brief description of the theory behind ATR-FTIR is given here. For a detailed discussion of this technique, the reader is referred to the book Internal Reflection Spectroscopy by N. J. Harrick.[71] Internal reflection spectroscopy is a powerful technique which takes advantage of light reflections which occur at the interface of two materials with different refractive indices. This technique was developed by Harrick, and has found many uses including the measurement of optical constants and spectroscopy of thin films as well as chemisorbed materials.

Figure 1.12: Schematic Diagram of an On-Line Photolysis Method

Diagram showing the nanospray tip with the coating removed to expose the optically transparent quartz capillary, where a fiber optic cable transmits light onto the sample. By knowing D, the distance from the cable to the end of the tip, the flow rate, and the inner diameter of the tip, the lifetime of species seen in the mass spectrum can be determined.

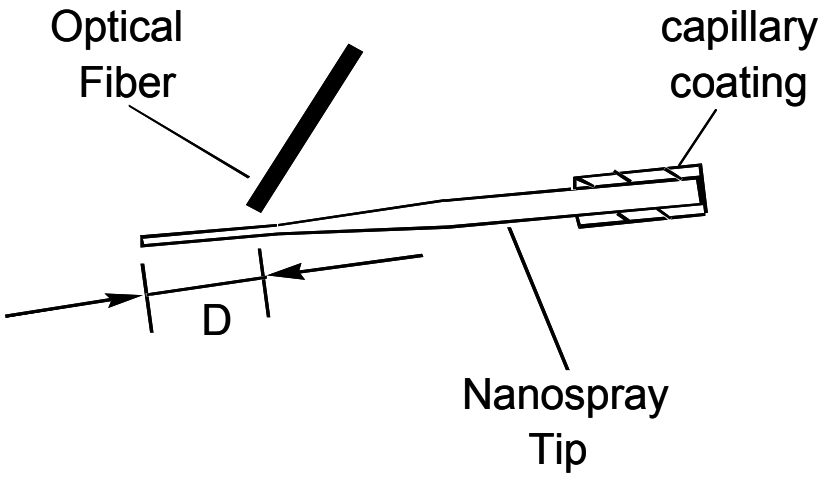
Optical
Fiber
capillary
coating
D
Nanospray
Tip

The idea behind internal reflection spectroscopy is that when light passes through a medium of high (dense) refractive index and that is optically transparent in the desired region, light can be reflected, refracted, or both when it comes into contact with a second medium of lower (rarer) refractive index. Internal reflection spectroscopy deals specifically with the case of total internal reflection, which is when the light is totally reflected back into the denser medium. This phenomenon occurs only when the light strikes the interface at or above a certain angle, called the critical angle (θ_c). The value of the critical angle depends on the difference between the refractive indices and is given by equation 1.17 below:

$$\theta_c = \sin^{-1} \eta_{21} \qquad (1.17)$$

where η_{21} is the ratio of refractive indices of the rarer medium (η_2) to the denser medium (η_1).

Of great importance in internal reflection spectroscopy is the choice of denser medium, or what is called the internal reflection element (IRE). As mentioned previously, the IRE must be optically transparent over the desired region. However, when choosing an IRE there are several other required characteristics. Some of the most important things are the material of construction of the IRE, the shape of the IRE, and the amount of signal obtainable using a given IRE. Let us briefly investigate the nature of these concerns as they apply to the experiments described in Chapter 2 of this manuscript.

With regard to the material composing the IRE, several characteristics must be taken into consideration other than the optical transparency and refractive index of the material. First and foremost, the material must be chemically inert for obvious reasons; one does not want the IRE to react with or be corroded by the sample as this would make experiments difficult. Also, the material should be hard enough so that it may be handled and cleaned without incurring damage. One common material for ATR-FTIR is a Ge crystal which is optically transparent over the range of 4000 cm^{-1} to 900 cm^{-1} (the IR region of interest in this work) and has a refractive index of 4.0.

After a suitable material is chosen, the shape of the IRE must then be considered. Some general requirements are that the opposing sides of the IRE must be parallel and optically polished (flat). If these requirements are not satisfied, then the angle of incidence will not be constant and the light may not be completely reflected.

Since the IRE's used are typically obtained commercially the only other concern is its shape, which has a great effect on the IRE's properties. The shape can dictate whether the IRE is a single or multiple reflection IRE and whether it is a single or multiple pass IRE. As we will see later, depending on the application of interest, one type of IRE may be better than another.

Before we look at the number of reflections and passes of a particular IRE, we should consider how a spectrum is actually measured using ATR-FTIR as this will demonstrate why some features are better than others for any desired application. In ATR-FTIR the incident light is passed through an IRE which is

placed inside the sample chamber of a FT-IR spectrometer. Light from the spectrometer passes into and through the IRE until it encounters the interface between the IRE and the sample which has a lower index of refraction. If the incident angle, θ, is greater than the critical angle, θ_c, the light is then reflected back into the IRE, but not before some of the energy creates what is called an evanescent wave. The evanescent wave has the same energy as the incident light and can be absorbed by the sample. However, the intensity of the wave falls off exponentially at longer distances from the interface, and therefore only penetrates the sample a short distance, called the penetration depth, d_P, which is given by equation 1.18:

$$d_P = \frac{\lambda_1}{2\pi (\sin^2\theta - \eta_{21}^2)^{1/2}} \qquad (1.18)$$

where λ_1 is the wavelength of light divided by the refractive index of the IRE (λ/η_1), θ is the incident angle (which must be greater than the critical angle), and η_{21} is the ratio of refractive indices of the rarer medium (sample) to the denser medium (IRE) (η_2/η_1). In ATR-FTIR the depth of penetration of the evanescent wave, d_P, is usually on the order of a few microns, and the signal intensity is therefore very small.

As a result of the low signal intensity, it is desirable in ATR-FTIR to use a multiple reflection IRE rather than a single reflection IRE. In the case of a single reflection IRE, the light enters the IRE and then encounters the interface between the IRE and the sample only once before being reflected back into the IRE and passing through to the detector. In contrast, when a multiple reflection IRE is

employed the incident light will encounter the interface between the IRE and the sample several times before being transmitted to the detector. This has an important implication, namely that as the number of reflections increases so does the quality of the spectra since the data collected comes from the changes in the reflectivity of the sample (*R*), which is exponentially related to the number of reflections (N). This is illustrated by equation 1.19:

$$R = (1-a)^N \qquad (1.19)$$

where *R* is the reflectivity, or the amount of signal, *a* is the absorption parameter (the signal loss per reflection), and N is the number of reflections.

A double pass IRE is one in which the light is transmitted throughout the length of the IRE and is then doubled back to exit the IRE at the same end (though not through the same opening) as the entering incident light. In contrast, a single pass IRE is one in which the light is transmitted through the length of the IRE and then exits through the opposite end. Since the IR spectrometer I plan to use is organized so that the source is one side of the sample chamber, and the detector is on the other, the IRE of choice for these experiments is a single-pass multiple reflection IRE.

We chose to use a trapezoidal shaped germanium crystal for our experiments. A drawing of the ATR setup is shown in Figure 1.13. In the drawing, the IR light passes from the source in to the IRE at an angle of 45^o. Upon encountering the sample, the light is reflected back into the IRE. The drawing shown indicates that the Ge ATR crystal used was a single pass, multiple reflection IRE. The expanded region of the drawing shows the angle of incidence

Figure 1.13: Schematic Diagram of an Attenuated Total Reflectance Set-up

Diagram showing a single-pass, multiple-reflection, trapezoidal-shaped ATR crystal oriented in the beam path of an IR instrument. This diagram also shows the interface between the IRE (of refractive index, η_1) and the sample (of refractive index, η_2) as well as the angle of incidence (θ) and the penetration depth of the evanescent wave, d_P.

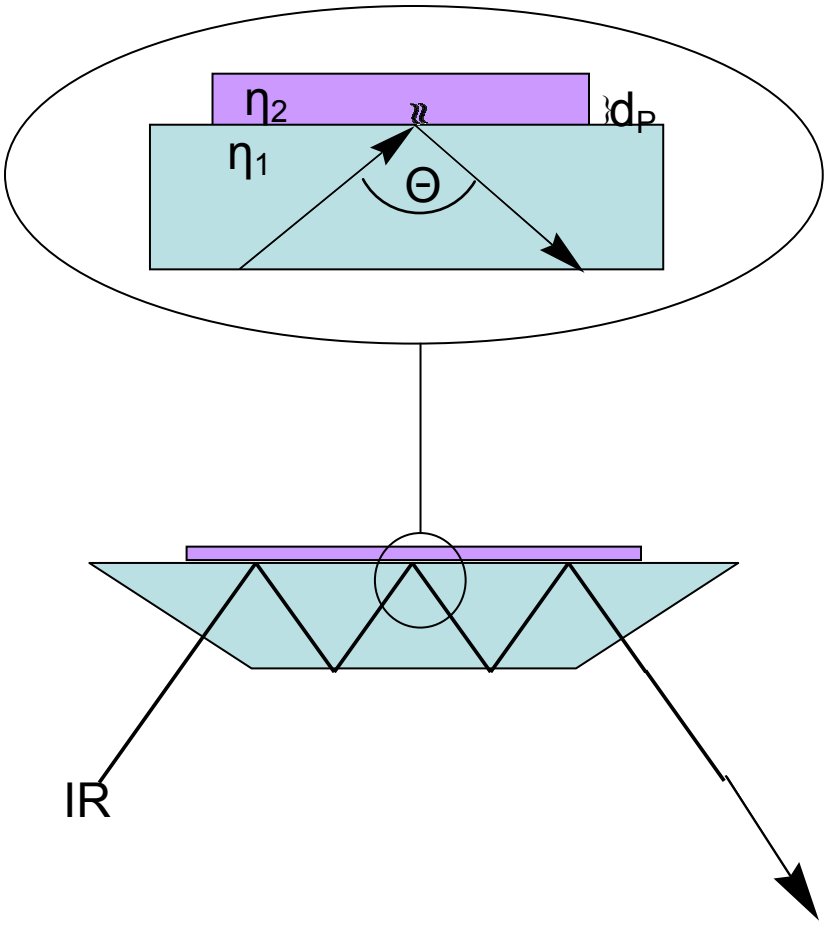
η2
dP
η1
Θ
IR

(θ), creation of the evanescent wave, and the depth of penetration of said evanescent wave.

1.8 Restatement of the Goals of this Project

Presented here are the goals of this work:

1. Determination whether benzoylruthenocene, 1,1'-dibenzoylruthenocene, and ferrocene can function as photoinitiators for the anionic polymerization of ethyl 2-cyanoacrylate.
2. Determination of the rate of photopolymerization of ethyl 2-cyanoacrylate using 1,1'-dibenzoylferrocene and ruthenocene as photoinitiators. If ferrocene, benzoylruthenocene, and/or 1,1'-dibenzoylruthenocene act as photoinitiators, then the rate of photopolymerization for these photoinitiators is determined as well.
3. Determination of the mechanism by which ruthenocene and (possibly) ferrocene act as photoinitiators for the anionic polymerization of ethyl 2-cyanoacrylate.
4. Verification, using resonance Raman spectroscopy, of previous assessments that the low energy electronic transitions for benzoylferrocene and 1,1'-dibenzoylferrocene contain appreciable metal-to-ligand charge transfer character. Also, determine if the ruthenium analogs also exhibit this metal-to-ligand charge transfer character.

5. Investigation of the mechanism by which benzoylruthenocene and 1,1'-dibenzoylruthenocene function as photoinitiators for the anionic polymerization of ethyl 2-cyanoacrylate, if applicable.
6. Expansion of this work to include the photoinitiated anionic polymerization of other monomers, specifically methyl methacrylate which is also susceptible to anionic attack. The polymerization of MMA will be discussed in Chapter 5 as an entity separate from the first five goals.

CHAPTER 2

MATERIALS AND METHODS

2.1 General Materials and Methods

General Reagents:

Unless otherwise stated, all chemicals were of reagent grade or better and used without further purification.

Photolysis Equipment:

Continuous photolysis experiments were performed with an Illumination Industries 200 W high-pressure mercury-arc lamp. Polychromatic light (λ > 290 nm) was obtained by passing the full output of the lamp through a pyrex filter. When stated, monochromatic light was isolated using a narrow band-pass (10 nm at half height) interference filter, and light intensity at this wavelength was determined by either ferrioxalate[72] or Reinecke's salt[31] actinometry.

UV-Vis Spectra:

All UV-VIS spectra were collected at room temperature (23 ^{o}C ± 3 ^{o}C) on either a Varian DMS 300 or a Cary 300 spectrophotometer. All cells used for both spectrochemical and photochemical experiments were either standard quartz or optically transparent methacrylate cells.

2.2 Synthesis and/or Purification of Photoinitiators:

Purification of Commercial Metallocenes:

All commercial metallocenes were purified according to literature procedures.[39,57] Ferrocene (98%, Sigma), ruthenocene (99%, Strem), and benzoylferrocene (Aldrich) were each sublimed in vacuo and condensed onto a

cold finger cooled to −70 ^{o}C with dry ice/acetone. 1,1'-Dibenzoylferrocene (DFc) (reagent grade, Sigma) was purified by recrystallization from warm n-hexanes.

Preparation of Benzoylruthenocene and 1,1'-Dibenzoylruthenocene:

Benzoylruthenocene (BRc) and 1,1'-dibenzoylruthenocene (DRc) were prepared according to methods adapted from the literature.[73,74] Methylene chloride was dried over calcium hydride overnight until no more bubbles were produced indicating that there was no more water present. The solvent was then distilled under argon and the distillate was collected and used for the synthesis. To a flame dried and argon filled two neck round bottom flask fitted with stoppers and containing a magnetic stir bar, which had been placed in a glove box with an argon atmosphere, were added 1.281 g (9.60 mmole) of aluminum chloride and 1.00 mL (8.61 mmole) of benzoyl chloride. This flask was then set up to reflux with stirring under an argon atmosphere using standard glassware. To a second round bottom flask which had been flame dried and argon filled was added 1.0020 g (4.32 mmole) ruthenocene. The flask with ruthenocene was flushed with argon for 15 minutes, and approximately 45 mL of purified methylene chloride was added via a cannula to dissolve the metallocene. The ruthenocene solution was then added to the mixture of benzoyl chloride and aluminum chloride causing the yellowish-orange solution to immediately turn a dark red color. From this point forward, all solutions were wrapped in foil to protect them from light.

The reaction mixture was refluxed under a constant argon stream for nine and a half hours. After refluxing, the solution was allowed to cool to room

temperature and then left to stir under argon for an additional fourteen hours. After stirring, the solution was hydrolyzed over approximately 30 g of ice, and a dark yellow organic layer was separated from the aqueous layer. The aqueous layer was then washed three times with 50 mL portions of methylene chloride. All of the organic layers were then combined and washed twice with 100 mL portions of water and dried over magnesium sulfate. The magnesium sulfate was filtered off and the methylene chloride was then removed by rotary evaporation to give 2.2 g of an oily brownish-yellow crude product.

The crude product was dissolved in approximately 1 mL of methylene chloride and placed on a column packed with silica gel (9 cm long, 2.5 cm inner diameter). Elution with reagent grade methylene chloride yielded band 1 (later determined to be benzoylruthenocene, BRc). After band 1 was collected, the eluent was changed to a 5% (by volume) acetonitrile in methylene chloride solution; this yielded band 2 (later determined to be 1,1'-dibenzoylruthenocene, DRc). The solvent was then removed from each band by rotary evaporation. BRc was recrystallized from 250 mL of warm n-hexanes by placing the solution in a freezer at −20 ^{o}C; while DRc was recrystallized from a mixture of 6.6% (by volume) benzene and 6.6% (by volume) petroleum ether in warm n-hexanes by placing the solution in a freezer at −20 ^{o}C. After filtering the crystals from the solvent and drying them overnight in a vacuum dessicator, 0.1942 g of BRc and 0.7409 g DRc were isolated. The melting point for BRc was 124-124.5 ^{o}C, and elemental analysis results indicated a pure compound as follows: %C 60.88 theoretical, 60.91 actual; %H 4.22 theoretical, 4.13 actual. The melting point for

DRc was 125.5-126.2 ^{o}C, and elemental analysis results indicated a pure compound as follows: %C 65.58 theoretical, 65.54 actual; %H 4.14 theoretical, 4.15 actual.

2.3 Rate of Anionic Polymerization of Ethyl 2-Cyanoacrylate:

Cell Method:

All studies were conducted on freshly prepared solutions of the metallocene photoinitiators in ethyl 2-cyanoacrylate (CA). Approximately 2 mL of a sample were placed in a 1 cm rectangular, optically transparent methacrylate plastic cuvette containing a magnetic stirring bar. In most runs, no special precautions were taken to exclude air or ambient moisture. Samples were irradiated at 23 ± 1 ^{O}C, and t_{poly}, the time required for solution viscosity to increase to the point that the stirring bar ceased to spin, was recorded. For a series of samples run under identical conditions of incident light intensity and stirrer speed, t_{poly} values provide a simple, yet reliable, measure of the relative rates of photoinitiated polymerization.

ATR-FTIR:

In another, more quantitative set of experiments, the rate of polymerization was monitored using attenuated total reflectance Fourier-transform infrared spectroscopy (ATR-FTIR). All IR spectra (with the exception of ferrocene, 1,1'-dibenzoylferrocene, and the ruthenocene sample at low (33mW/cm^2) light intensity, which will be described later) were collected on a BIO-RAD FTS-7000 spectrophotometer equipped with a narrow band HgCdTe detector. A small strip

of solution containing a metallocene dissolved in CA was placed on top of a germanium ATR crystal mounted on a horizontal ATR accessory (CIC Photonics) inside the sample chamber of the spectrophotometer. Assuming a refractive index of 1.5 for CA and 4.0 for Ge, and a 45° angle of incidence, we calculate that the electric field of the monitoring IR beam penetrated the sample to a depth of 2-3 μm.[71] Polymerization of CA began after the sample was irradiated with the polychromatic output from a mercury arc lamp, which was reflected down onto the sample. Incident light intensity was measured with a Coherent Model-10 power meter. Infrared spectra were collected every 1 s using the following parameters: three co-added scans, triangular apodization with one level of zero filling, and 4 cm^{-1} resolution. Spectra were analyzed with a Grams 32/AI spectral software package (Galactic Industries). Peak heights, frequencies, and areas were calculated with a center-of-gravity algorithm[75] using a program written by R. A. Dluhy. The area of the C=O stretching band of CA at 1734 cm^{-1} was used as an internal standard to correct the area of the C=C stretching band at 1616 cm^{-1} for changes in sample thickness.

The only experimental differences for the ferrocene, 1,1'-dibenzoylferrocene, and low (33 mW/cm^2) light intensity ruthenocene samples are as follows: The instrument employed was a FTS-60 spectrophotometer, and the parameters were such that one co-added scan was collected every 1.5 s.

2.4 Theoretical Methods

I wish to explicitly state here that I did not perform the calculations included in this paper. The calculations were performed by Nicole Brinkmann (at the time a PhD student in Dr. Schaefer's group). However, I believe that the theoretical results complete the story of the mechanism by which ferrocene and ruthenocene photoinitiate the anionic polymerization of CA: for that reason, they are included here. A brief summation of the technique is provided here. Full details are provided in a recent publication.[76] As well, there are several references on the subject; the book I found most helpful was "A Chemist's Guide to Density Functional Theory".[77]

The theoretical data reported in this manuscript were calculated using the DZP++ basis set. A basis set is a group of mathematical functions which describe the space of a molecule, which is then used, in conjunction with a functional, to construct an approximate wave function. The DZP++ basis set represents each atomic orbital by two primitive Gaussian functions which then have polarization and diffuse functions added. When bonds are formed in molecules, the shapes of atomic orbitals are distorted (polarized) from their ideal shape to provide bonding. This distortion (or polarizability) can be mimicked by adding polarization functions to the basis set of atomic orbitals. Diffuse functions are added to the basis set when computing anions since they better describe the lengthening of the orbitals in the anion. The functional used in these studies is the B3LYP hybrid functional. The B3LYP functional includes terms that account

for electron-electron repulsion, the electron gradient which results from having different atoms in the molecule, and both local and non-local electron density.

2.5 Resonance Raman Spectroscopy

Instrumentation:

Raman spectra were recorded by Dr. Richard Conover using an Instruments SA Ramanor U1000 spectrometer fitted with a cooled RCA-31034 photomultiplier tube. Spectra were recorded digitally using photon counting electronics and improvements in signal-to-noise were achieved by signal averaging multiple scans. Absolute band positions were calibrated using the excitation frequency and CCl_4 and are accurate to ±1 cm^{-1}. Lines from a Coherent Sabre 100 10-W argon ion laser or Coherent Innova 200-K2 krypton ion laser were used for excitation, and plasma lines were removed using a Pellin Broca prism pre-monochromator. Scattering was collected from the surface of the sample using 90° scattering geometry and a custom-designed sample cell,[78] which was attached to the cold finger of an Air Products Displex Model CSA-202E closed cycle refrigerator maintained at 17 K. Solid state spectra were recorded using samples prepared as KBr disks, containing a known weight percentage of K_2SO_4 as an internal standard, and the disks were attached to the surface of the sample holder using Crycon grease. Frozen solution spectra with $CHCl_3$ as the solvent were recorded using samples frozen as 15-μL droplets on the sample holder, and the solvent bands were used as an internal standard. The time course of the effect of laser exposure on Raman band intensities was

monitored by optimizing alignment using a solvent or sulfate band, blocking the laser beam, adjusting the position of the sample so that the focused laser beam hits a different spot on the surface of the sample, initiating a time-based scan at fixed frequency, and then unblocking the laser beam at time zero.

2.6 Mass Spectral Analysis of Metallocenes

Instrumentation:

Electrospray ionization mass spectrometry (ESI-MS) experiments were performed in the positive ion mode on a Mariner Biospectrometry Workstation (PerSeptive Biosystems, Inc.), which combines a time-of-flight mass spectrometer with an electrospray ionization source. The optically transparent nanospray tip was made from fused silica capillary tubing (100 μm inner diameter (i.d.)). The tubing was drawn to a fine point (30-40 μm i.d. as determined by optical microscopy) at the spray-delivery end and connected at the other end to a syringe pump that delivered the sample solution at a constant flow rate. Typical operating parameters for the ESI experiments follow: spray tip potential, 1.9 kV; nozzle potential, 60 V; first skimmer potential, 11.5 V; nozzle temperature, 150 °C. The temperature in the interface region between the spray chamber and the time-of-flight mass analyzer was maintained at 150 °C to aid desolvation of electrosprayed ions.

Online Photolysis of 1,1'-Dibenzoylferrocene:

Details of the instrumental setup are provided in the literature.[70] Solutions containing 1,1'-dibenzoylferrocene and a carrier cation (Na^+ or K^+ added as the iodide salt) were irradiated directly in the nanospray tip by an optical fiber that transmitted 488-nm light from an argon ion laser. The distance between the midpoint of the irradiated zone and the tip end could be varied by adjusting the position of the fiber with a precision translation stage.

General Procedure for ESI-MS Analysis of Ruthenium Compounds:

Freshly prepared solutions of the metallocene were made in either carbon tetrachloride (HPLC grade, Aldrich) or acetonitrile (spectral grade, Fisher). The solutions were made so that the absorbance would be 2 at the wavelength maximum (λ_{max}) for each compound, indicating that at the λ_{max} 99% of the light intensity was being absorbed by the sample. A 2 mL aliquot of each solution was photolyzed with the full output (λ>290 nm) of a high pressure mercury lamp for 10 to 30 minutes while stirring in a 1 cm quartz spectrophotometric cell. Then, 1 mL of the photolyzed solution was diluted to 10 mL with acetonitrile (purified by refluxing over and distilling from calcium hydride), sodium iodide (in acetonitrile) was added to give a 10 fold excess of sodium as compared to ruthenium, and the solution was filtered through a 0.2 μm syringe filter. The solution was then analyzed.

CHAPTER 3

DETERMINATION OF THE RATE AND MECHANISM OF PHOTOINITIATED ANIONIC POLYMERIZATION OF ETHYL 2-CYANOACRYLATE USING GROUP 8 METALLOCENES AND THEIR BENZOYL-SUBSTITUTED ANALOGS

3.1 Qualitative Kinetic Data

One way to get qualitative data on the rate of polymerization is to irradiate a sample of photoinitiator dissolved in neat CA while stirring in a methacrylate cuvette. This qualitative method is referred to as the cell method in Chapter 2. While the data collected are not quantitative in nature, if runs are performed under the same conditions with the same stirring rate, then it is possible to get a qualitative idea of the rate of polymerization reported as t_{poly}, the time required for a solution to become so viscous that a magnetic stirring bar in the sample stops spinning.

The morphology of the polymer produced depends on which photoinitiator is used. When ruthenocene is used as the photoinitiator the polymerization reaction occurs very rapidly and the polymer product is a hard plastic-like solid with bubbles in it. The bubbles are presumably formed by the large amount of heat generated during the polymerization which may be boiling the monomer. (Enough heat is evolved in these experiments to melt the cell.) This rapid polymerization process makes it very easy to determine when the reaction has stopped since the polymer product looks different from the monomer solution. In contrast, the polymer product that forms when ferrocene is used as the photoinitiator is a thick, viscous syrup-like liquid which later hardens into a plastic-like solid when left to sit in the dark. Owing to this thick syrupy state, there is more uncertainty associated with the polymerization time (t_{poly}) reported.

Polymerization proceeds differently when benzoylruthenocene (BRc) or 1,1'-dibenzoylruthenocene (DRc) is used as the photoinitiator. For the first 3

minutes for BRc (and the first 8 minutes for DRc) of irradiation time, it is unclear whether or not the viscosity of the solution is changing. It appears as though a film of polymer might be forming on the front face of the cuvette which causes the stirbar to stop spinning even though the rest of the solution does not appear to be polymerizing, then polymerization suddenly proceeds rapidly with the evolution of heat. The polymer that forms has the same appearance as that formed when ruthenocene is used as a photoinitiator (a hard plastic-like solid with bubbles in it).

Qualitative kinetic data for the photopolymerization of ethyl 2-cyanoacrylate using various photointiators are shown in Table 3.1. Data for BRc and DRc are not present in Table 3.1 owing to difficulties in determining a polymerization time as stated above. The data in Table 3.1 indicate that ruthenocene and 1,1'-dibenzoylferrocene are especially good photoinitiators for the polymerization of CA (runs 4-10); within seconds of exposure to the full output of a high pressure mercury lamp (λ>290 nm), these samples have polymerized. In fact, even low-intensity monochromatic light (filtered through a narrow band pass interference filter) caused polymerization to commence in a relatively short period of time (runs 5 and 10). This is in stark contrast to ferrocene which is not a particularly good photoinitiator. Looking at Table 3.1, it may seem that DFc is a better photoinitiator than ruthenocene, however the DFc data were not collected on the same day (and therefore not under the same conditions) as the ruthenocene data, so direct comparison between DFc and ruthenocene cannot be made.

Table 3.1. Qualitative Kinetic Data for the Photoinitiated Anionic Polymerization of Ethyl 2-Cyanoacrylate

Run	Photoinitiator (PI)	[PI], mM	λ_{excit}, nm[a]	t_{poly}, s[b]
1	$FeCp_2$	7.96	>290	285
2	$FeCp_2$	7.78	365[c]	2094
3	$FeCp_2$	8.1	>290	292[d]
4	$RuCp_2$	12.1	>290	9
5	$RuCp_2$	11.4	365[c]	405
6	$RuCp_2$	2.42	>290	17
7	$RuCp_2$	2.42	>290	19[e]
8	$RuCp_2$	2.42	>290	>600[f]
9	DFc	1.06	>290	3.8[g]
10	DFc	2.39	546[h]	29[g]

[a]Excitation wavelength(s).

[b]Irradiation time required for sample viscosity to increase to the point where the magnetic stirbar in the photolysis cell ceased to spin.

[c]Light intensity = 2.50×10^{-8} einstein/s.

[d]Sample bubbled with argon for 10 min to remove O_2.

[e]Hydroquinone (400 ppm) was added to sample.

[f]Methanesulfonic acid (494 ppm) was added to sample.

[g]Data from reference 79.

[h]Light intensity = 1.0×10^{-7} einstein/s.

Also, several other runs were performed to test the effects of oxygen, hydroquinone, and methanesulfonic acid (MSA) (runs 3, 7, and 8). Both oxygen and hydroquinone are known radical scavengers, while MSA would scavenge any anion produced. As seen in runs 3 and 7, neither hydroquinone nor oxygen have any effect on the time required for polymerization to occur. Furthermore, run 8 shows that the addition of acid greatly inhibits polymerization. These bits of information confirm that polymerization occurs via an anionic mechanism and not a radical mechanism.

3.2 Quantitative Kinetic Data

While the qualitative rates discussed above are a good starting point, it was desirable to have a more quantitative method for determining the rate of polymerization, particularly in the cases of Fc, BRc, and DRc where the polymerization time was difficult to determine using the qualitative method. Quantitative data on the rate of photopolymerization of a solution of ethyl 2-cyanoacrylate (CA) containing millimolar concentrations of a photoinitiator were obtained using attenuated total reflectance Fourier transform infrared spectroscopy (ATR-FTIR). By using a horizontal ATR assembly, we were able to reflect the polychromatic output of a high pressure mercury arc lamp down onto the top of the sample, while continuously monitoring the progress of the reaction by looking at the disappearance of the carbon-carbon double bond of the monomer (at 1616 cm^{-1}) in real time. The percent polymerization of the monomer can be calculated using equation 3.1:

$$\% \text{ Polymerization} = \frac{A_o - A_t}{A_o} * 100 \qquad (3.1)$$

where A_o is the normalized area of the carbon-carbon double bond at time 0, and A_t is the normalized area of the carbon-carbon double bond at time t. These areas are normalized to account for any inhomogeneity in film thickness since ATR only looks at the 2-3 μm of sample nearest the crystal. The area of the carbonyl band (1734 cm^{-1}) of the monomer is relatively constant over the time period of the experiment, so this was chosen as our internal standard. The maximum rate (R_P) of polymerization can be calculated using equation 3.2,

$$R_P = \frac{M(A_{t1} - A_{t2})}{A_o(t_2 - t_1)} \qquad (3.2)$$

where M is the molarity of vinyl groups in the monomer (8.4 M for CA) and A_o, A_{t1}, and A_{t2} are the normalized areas of the carbon-carbon double bond at times 0, t_1, and t_2, respectively.

Graphs of the photopolymerization of CA as a function of time using ferrocene (Fc), 1,1'-dibenzoylferrocene (DFc), ruthenocene (Rc), benzoylruthenocene (BRc), and 1,1'-dibenzoylruthenocene (DRc) as photoinitiators are given in Figures 3.1, 3.2, 3.3, 3.4, and 3.5 respectively. In all these cases, there is an induction period at the beginning of the reaction; this induction period is attributed to the presence of a small amount of methanesulfonic acid (MSA) present in the commercial monomer as a stabilizing

agent. The acid stabilizer reacts with any anions which are initially formed by the photoreaction, and only when the acid stabilizer is consumed does polymerization of the monomer commence. Once polymerization begins, there is rapid consumption of the monomer until the reaction stops at approximately 70 – 85 % conversion. We also see that the addition of small amounts of MSA either lengthen the induction period, or completely inhibit the polymerization over the time period monitored. In all of these cases, we see that polymerization does not occur without light, and, as illustrated in the case of ruthenocene (Figure 3.3), the rate increases with the light intensity as expected in any photochemical process.

For iron containing metallocenes, the addition of benzoyl groups to both cyclopentadienyl rings greatly decreases the induction period and drastically increases the rate of photopolymerization of CA. The rates of polymerization are 0.06 and 1.7 Ms^{-1} for ferrocene and 1,1'-dibenzoylferrocene, respectively, when using comparable light intensity. In contrast, for the ruthenium compounds addition of one or more benzoyl groups to the cyclopentadienyl ring lengthens the induction period and decreases the rate of photopolymerization. The rates are 0.94, 0.68, and 0.14 Ms^{-1} respectively for the unsubstituted, monosubstituted, and disubstituted ruthenocenes when using comparable light intensities.

3.3 Proposed Mechanism of Photoinitiation for Ferrocene and Ruthenocene

All of the compounds looked at in the previous section photoinitiate the anionic polymerization of CA. Furthermore, it has been shown that 1,1'-

Figure 3.1: Percent Polymerization of CA Using Ferrocene (Fc) as the Photoinitiator

Plots of percent polymerization vs. time for a solution containing 9.6 mM Fc in neat CA without light (dark sample) (a), upon exposure to 110 mW/cm^2 of polychromatic light (b), and upon exposure to 110 mW/cm^2 polychromatic light after addition of 150 ppm MSA (c).

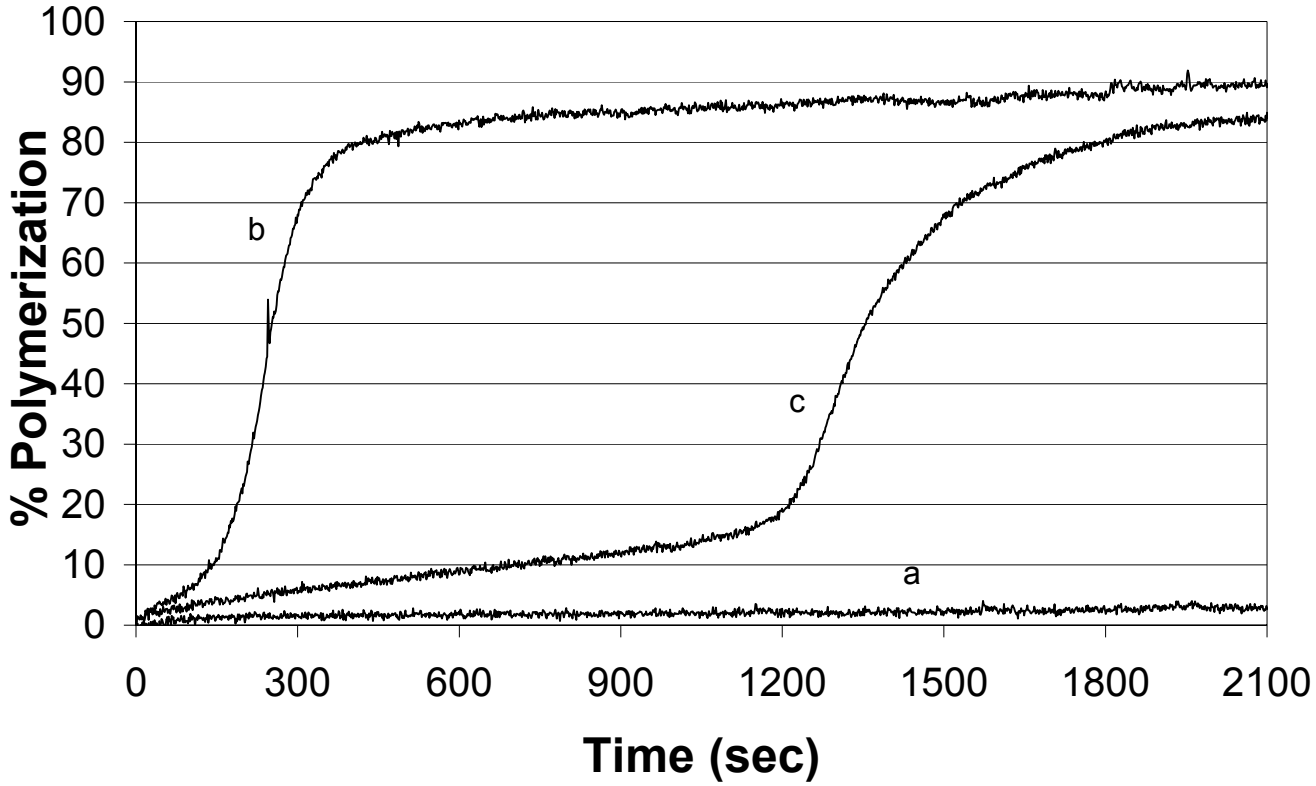
100
90
80
70
60
50
40
30
20
10
0
% Polymerization
b
c
a
0
300
600
900
1200
1500
1800
2100
Time (sec)

Figure 3.2: Percent Polymerization of CA Using 1,1'-Dibenzoylferrocene (DFc) as the Photoinitiator

Plots of percent polymerization vs. time for a solution containing 2.7 mM DFc in neat CA without light (dark sample) (a) and upon exposure to 30 mW/cm^2 of polychromatic light (b).

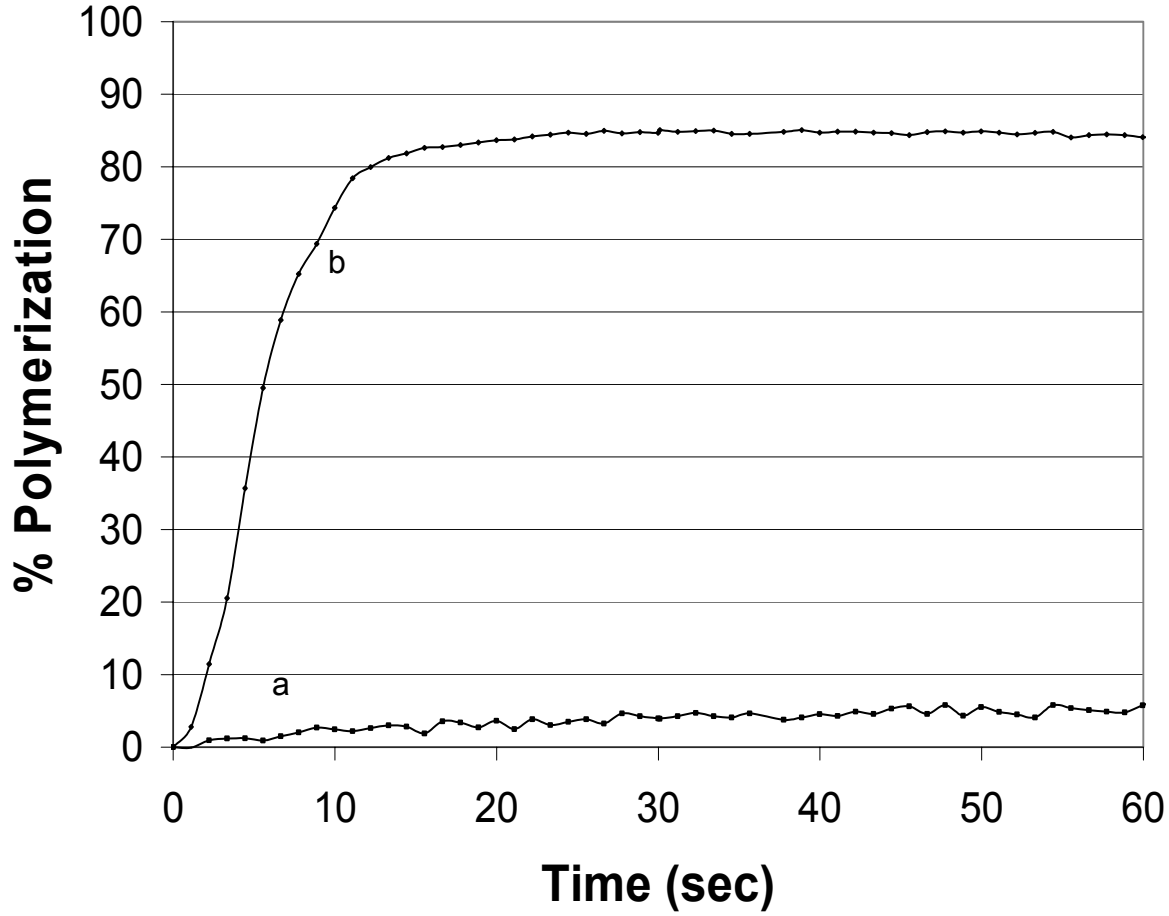
% Polymerization
100
90
80
70
60
50
40
30
20
10
0
0
10
20
30
40
50
60
Time (sec)
a
b

Figure 3.3: Percent Polymerization of CA Using Ruthenocene (Rc) as the Photoinitiator

Plots of percent polymerization vs. time for a solution containing 10.0 mM Rc in neat CA without light (dark sample) (a), upon exposure to 33 mW/cm^2 of polychromatic light (b), upon exposure to 117 mW/cm^2 polychromatic light (c), and upon exposure to 117 mW/cm^2 polychromatic light after addition of 133 ppm MSA (d).

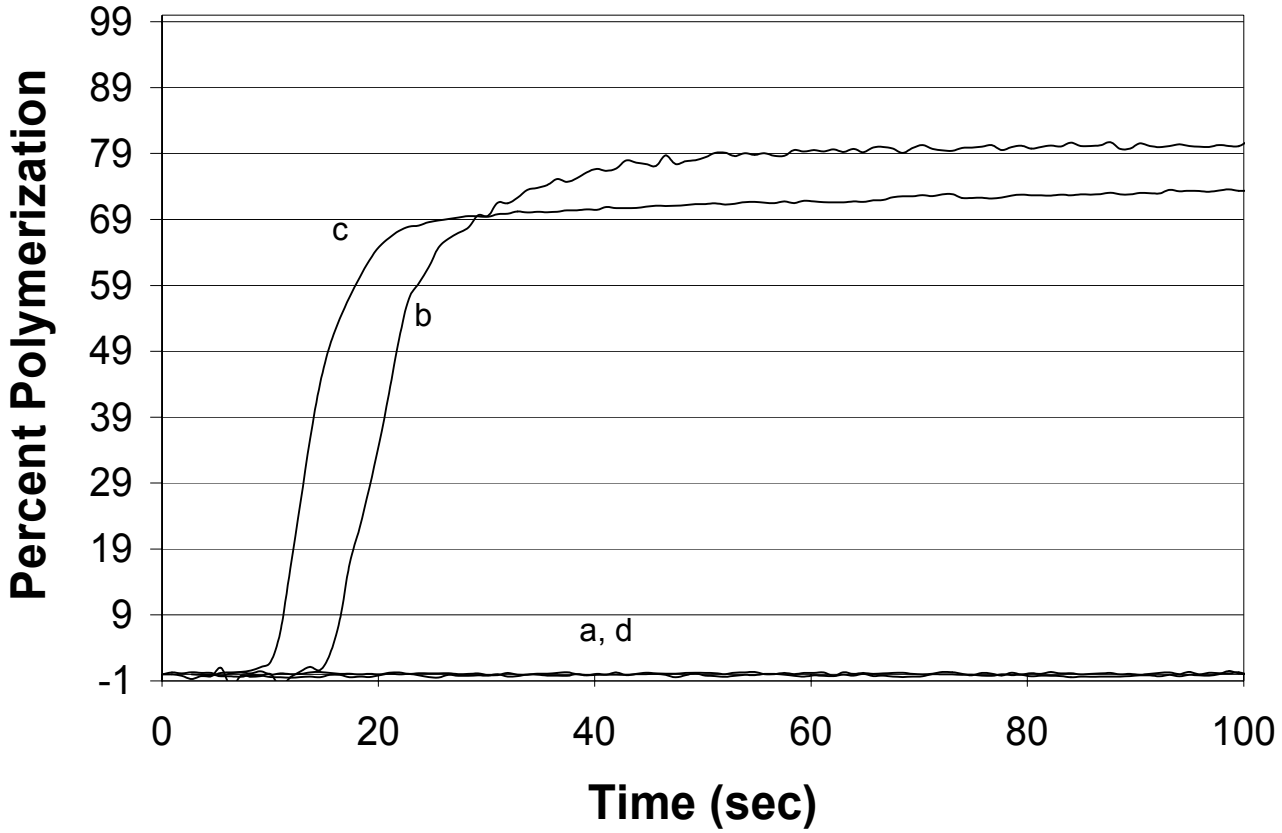
Percent Polymerization
99
89
79
69
59
49
39
29
19
9
-1
0
20
40
60
80
100
Time (sec)
c
b
a, d

Figure 3.4: Percent Polymerization of CA Using Benzoylruthenocene (BRc) as the Photoinitiator

Plots of percent polymerization vs. time for a solution containing 10.5 mM BRc in neat CA without light (dark sample) (a), upon exposure to 126 mW/cm^2 polychromatic light (b), and upon exposure to 126 mW/cm^2 polychromatic light, after addition of 141 ppm MSA (c).

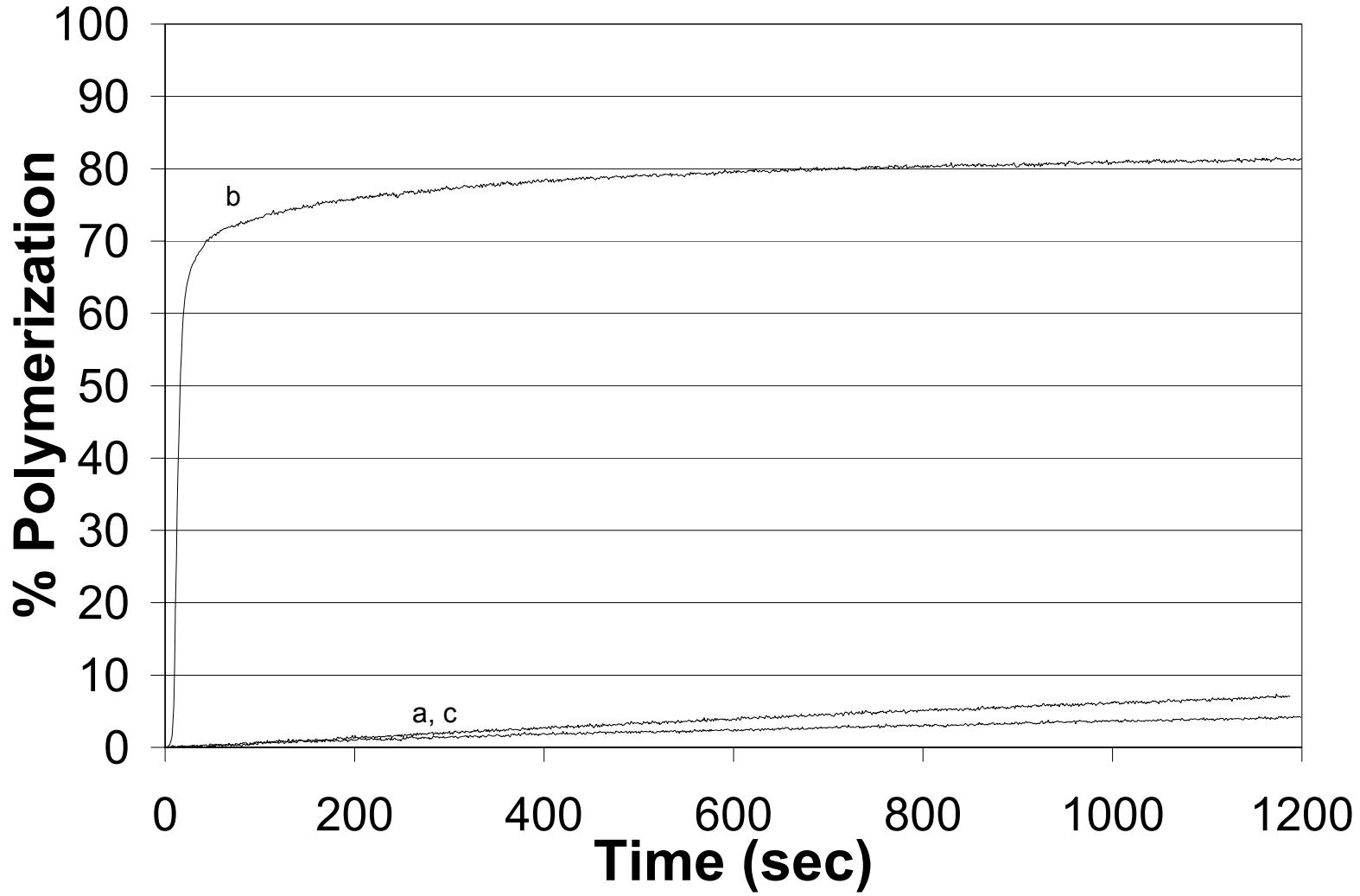
% Polymerization
100
90
80
70
60
50
40
30
20
10
0
b
a, c
0
200
400
600
800
1000
1200
Time (sec)

Figure 3.5: Percent Polymerization of CA Using 1,1'-Dibenzoylruthenocene (DRc) as the Photoinitiator

Plots of percent polymerization vs. time for a solution containing 11.6 mM DRc in neat CA without light (dark sample) (a), upon exposure to 105 mW/cm^2 polychromatic light (b), and upon exposure to 105 mW/cm^2 polychromatic light, after addition of 113 ppm MSA (c).

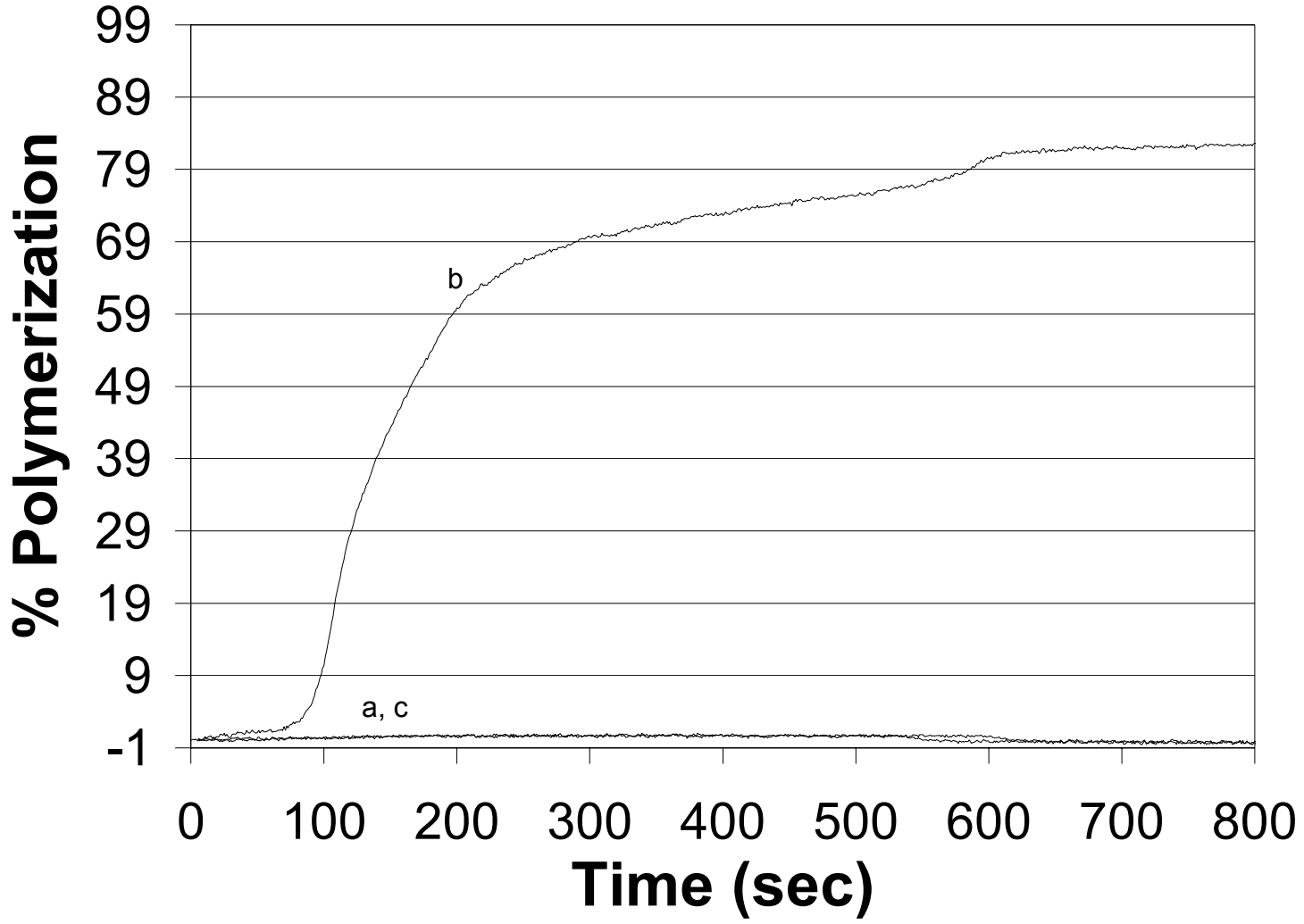
% Polymerization
99
89
79
69
59
49
39
29
19
9
-1
b
a, c
0
100
200
300
400
500
600
700
800
Time (sec)

dibenzoylferrocene undergoes heterolytic iron-ring bond cleavage to release a benzoylcyclopentadienide anion which then initiates the polymerization of CA. In contrast, ferrocene and ruthenocene resist ring loss upon photolysis.[36] Since both of these compounds act as photoinitiators, studies were undertaken to elucidate the mechanism of photoinitiation. As mentioned previously (c.f. section 1.4), ferrocene and ruthenocene are not photosensitive in solvents such as methanol. However in electron-accepting solvents such as carbon tetrachloride, these metallocenes undergo the photochemical reaction shown in equation 3.3.[42,44-47]

$$M(Cp)_2 + CCl_4 \rightleftharpoons \{M(Cp)_2, CCl_4\} \xrightarrow{h\nu} M(Cp)_2^{+} + CCl_4^{\bullet -} \quad (3.3)$$

In equation 3.3, the metallocene first forms an electron donor-acceptor complex with the solvent. This ground state complex is characterized by a new band in the electronic absorption spectrum which is not attributable to either the solvent or the metallocene; this new band has been assigned as a charge-transfer-to-solvent (CTTS) transition. Irradiation into the new absorption band causes the one electron oxidation of the metallocene to the corresponding metallocenium ion, accompanied by the reduction of the solvent to its radical ion.

Since ethyl 2-cyanoacrylate (CA) is a good electron acceptor, it seems reasonable to propose that the parent metallocenes, ferrocene (Fc) and ruthenocene (Rc), might form a similar type of electron donor-acceptor complex with CA as that which is formed with halocarbon solvents. In analogy to the photochemical reaction shown in equation 3.3, we propose that this ground-state

complex between the metallocene and CA is the photochemically active species and the reaction occurs as shown in equation 3.4. In this mechanism, the CA radical anion formed in the photochemical reaction then attacks a neutral monomer molecule to begin the polymerization process, and is therefore the actual initiating species in accordance with equation 3.5.

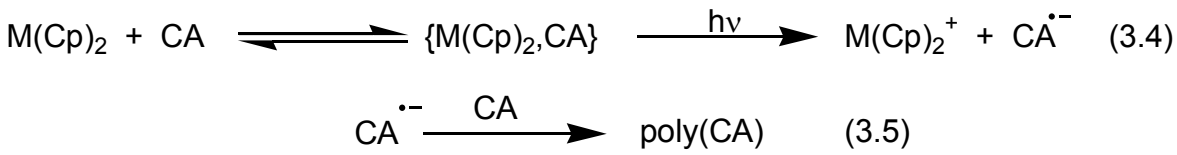

Studies were undertaken to look for evidence to support this mechanism. Specifically, we looked for evidence that a ground state electron donor-acceptor (charge-transfer-to-solvent) complex is formed between the metallocene and CA, and we looked for evidence of the photoproducts, either the metallocenium ion or the reduced form of CA.

3.4 Evidence for a Charge-Transfer-to-Solvent Complex

Presented in Figure 3.6 are the spectra of ferrocene in tetrahydrofuran, THF (spectrum a), 40% (v/v) CA in THF (spectrum b), and the difference spectrum (inset). In THF, the parent metallocene has two low intensity absorption bands in the visible/near uv region. These weak bands occur at 325 and 442 nm and have been assigned as arising from ligand field transitions which are predominantly metal in character (c.f. section 1.4). However, when mixed with an appreciable portion of CA, the valley at 365 nm fills in. The difference spectrum

(inset) clearly shows that a new band is formed, which indicates the presence of a donor-acceptor type of ground state complex. We have assigned this transition as ferrocene to CA ($(Cp)_2Fe \rightarrow CA$). In the case of ruthenocene (Rc), we see the same type of interaction as illustrated in Figure 3.7. In this case, the new absorption band overlaps with the ligand field transition of Rc at ~320 nm. The new band uncovered by looking at the difference spectrum (inset) is therefore not as well defined as it was in the case of ferrocene. This new band is assigned as ruthenocene to CA ($(Cp)_2Ru \rightarrow CA$). Since we now have evidence that both Fc and Rc form a ground state electron donor-acceptor complex with CA, we can begin to look for the photoproducts of the reaction shown in equation 3.4.

3.5 Electron Affinity of Ethyl 2-Cyanoacrylate

As mentioned in the introduction (section 1.2), cyanoacrylates are extremely susceptible to attack by either anions or Lewis bases. While it seems perfectly reasonable to suggest that this electrophilic monomer is capable of accepting an electron to give its radical anion, the reduction potential for ethyl 2-cyanoacrylate (CA) has not been determined experimentally. Since the poly(CA) formed would harm instrumentation, experimental determination of the reduction potential is ill-advised. However, density functional theory (DFT) is capable of predicting the electron affinity of a molecule reasonably well (to within 0.2 eV depending on the level of theory used for the calculations). In particular, using the DZP++ basis set and the B3LYP functional results in predicted electron

Figure 3.6: Electronic absorption spectra of Ferrocene (Fc) in pure THF and 40% (v/v) CA in THF

Shown here are the electronic absorption spectra of 25 mM Fc in THF (spectrum a) and 40% (v/v) CA in THF (b). Inset is the difference spectrum showing the presence of a new absorption band which has been assigned as a charge-transfer-to-solvent band.

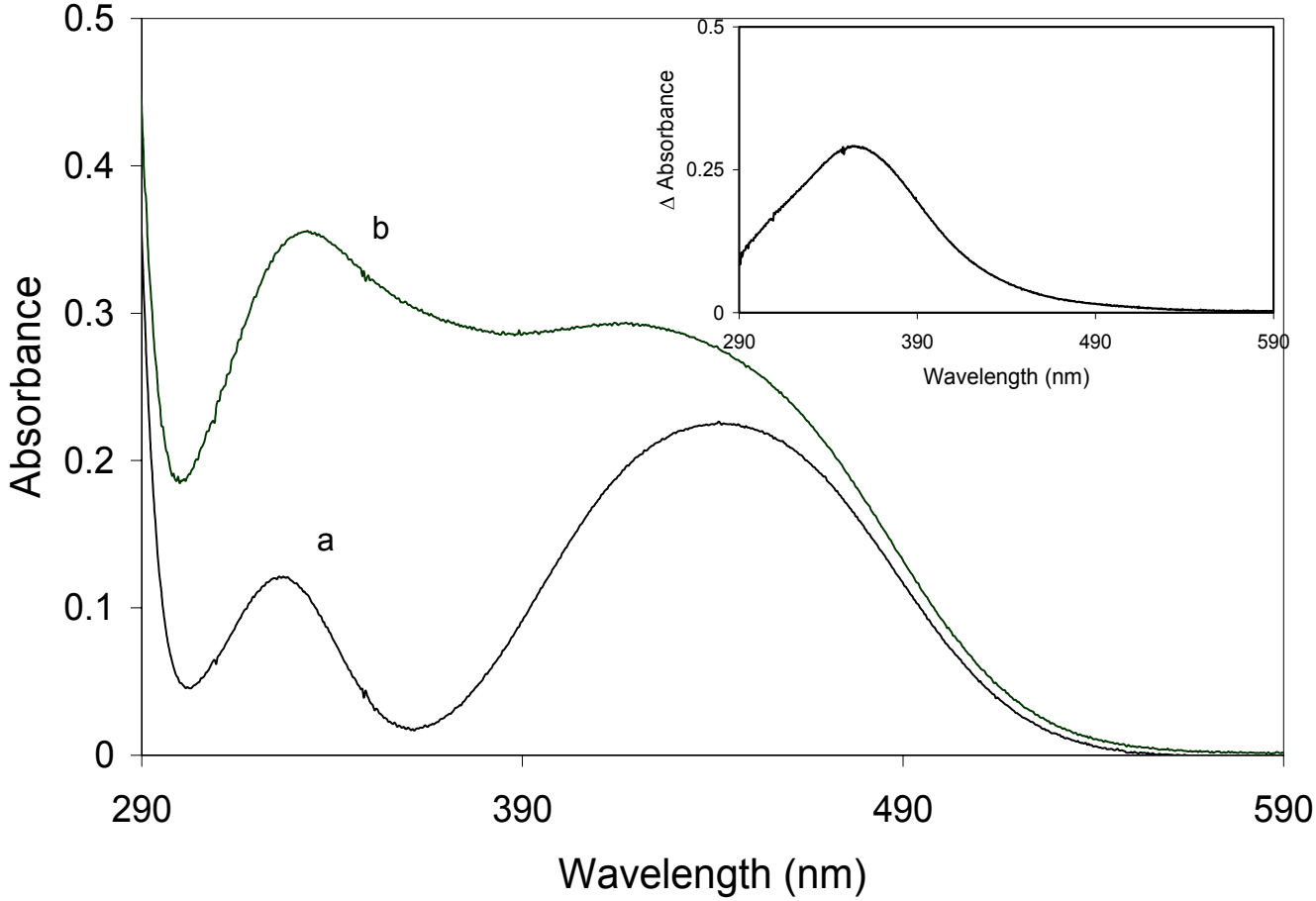
0.5
0.4
0.3
0.2
0.1
0
Absorbance
290
390
490
590
Wavelength (nm)
b
a
0.5
0.25
0
Δ Absorbance
290
390
490
590
Wavelength (nm)

Figure 3.7: Electronic absorption spectra of Ruthenocene (Rc) in pure THF and 40% (v/v) CA in THF

Shown here are the electronic absorption spectra of 15 mM Rc in THF (spectrum a) and 40% (v/v) CA in THF (b). Inset is the difference spectrum showing the presence of a new absorption band which has been assigned as a charge-transfer-to-solvent band.

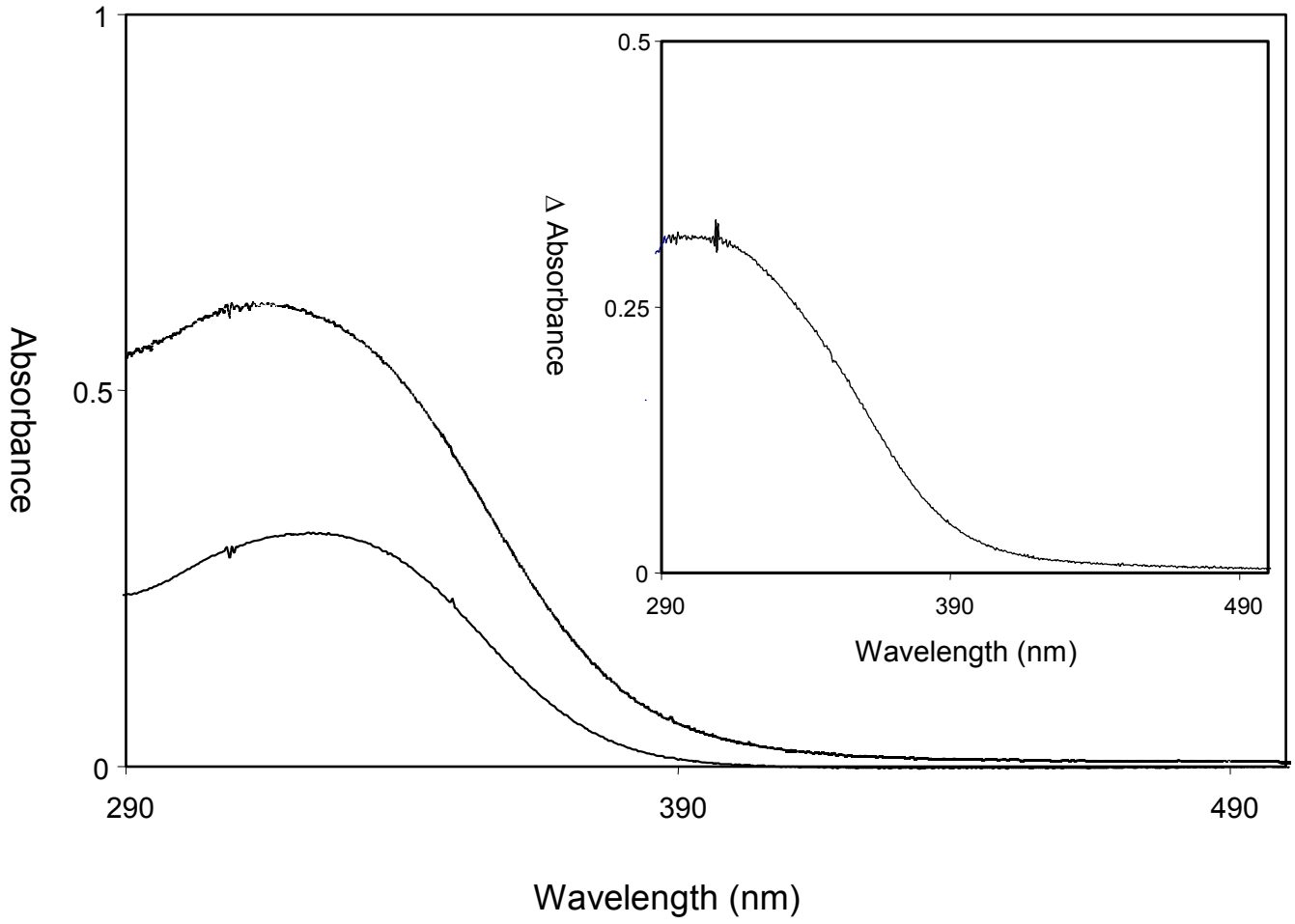
1
0.5
0
Absorbance
290
390
490
Wavelength (nm)
0.5
0.25
0
Δ Absorbance
290
390
490
Wavelength (nm)

affinities which are in good agreement with experimentally determined values.[80] Since the electron affinities obtained using this theoretical method are consistent with experimental values, we surmised that this method may predict (with some accuracy) the electron affinity of a molecule for which there is no experimental value. In addition, this method allows the calculation of an electron spin density (the probability of finding an electron on any particular nucleus in the molecule).[81] Since most of the electrons will be paired, their spins will cancel out, thereby allowing us to predict where the one unpaired electron in the radical anion is most likely to reside on the molecule.

The adiabatic electron affinity of a molecule can be defined as the difference in energy between a neutral molecule and its anion (equation 3.6); this energy is calculated at the equilibrium geometry of the molecule. In Figure 3.8 we see the numbering scheme used for the discussion of the theoretical data. Since the addition of an electron to the CA molecule causes no change in the ethyl group on the ester end of the molecule, the hydrogen atoms in this portion of the molecule (and their bond distances) have been omitted from the figure for clarity. Upon addition of an electron to the neutral molecule there is no significant change in the terminal CH_2 (r_1 and r_5) group. However, the distance between C_1 and C_2 (r_2) increases from 1.349 to 1.430 Å and the distance between C_3 and N increases from 1.167 to 1.178 Å. In addition the bond between C_2 and C_4 (r_6) decreases from 1.508 to 1.437 Å, while the bond between C_4 and O_1 (r_7) increases from 1.215 to 1.244 Å. As well, the angle made between $O_1C_4C_2$ increases by 5° from 123.1 to 128.3°.

$$EA_{ad} = E_{(optimized\ neutral)} - E_{(optimized\ anion)} \quad (3.6)$$

Figure 3.8: Atomic Numbering Scheme for Ethyl 2-Cyanoacrylate

The atoms referred to in the text are numbered here (r_n denotes a bond between two atoms). Hydrogen atoms in the ethyl ester portion of the molecule have been omitted for clarity.

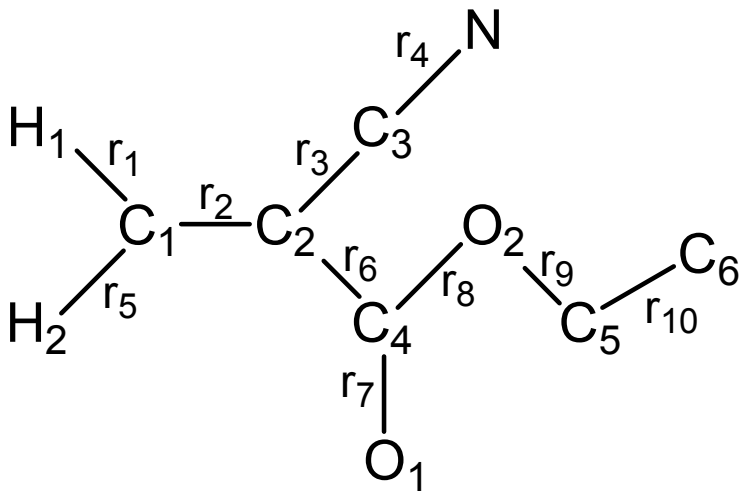
r4
N
H1
r1
C3
r3
r2
C1
C2
O2
r9
C6
r6
r8
r5
H2
C4
C5
r10
r7
O1

Table 3.2: Calculated spin densities at the optimized geometry for the ethyl 2-cyanoacrylate radical anion.[76]

Atom	Spin Density
$^{13}C_1$	0.045187
$^{13}C_2$	−0.015587
$^{13}C_3$	−0.006423
$^{13}C_4$	0.001372
$^{13}C_5$	−0.000602
$^{13}C_6$	0.005446
$^{1}H_1$	−0.009603
$^{1}H_2$	−0.009652
$^{1}H_3$	−0.000016
$^{1}H_4$	0.000119
$^{1}H_5$	−0.000029
$^{1}H_6$	−0.000029
$^{1}H_7$	−0.000003
$^{14}N_1$	0.00400
$^{17}O_1$	0.015177
$^{17}O_2$	−0.008960

All of these results are consistent with a molecule possessing a $C{=}C{-}C{\equiv}N$ type of π-conjugated system, where addition of an electron to a π^* orbital causes a weakening of the C-C double bond and the C-N triple bond.[82] The presence of the ester group serves to further stabilize the radical anion by allowing the electrons to be delocalized over these additional atoms. Calculated spin densities are found in Table 3.2. The large positive value (in relation to the values for the other atoms in the molecule) of ~0.045 for C_1 indicates that this is the most likely place for an unpaired electron to reside in the CA radical anion. Figure 3.9 shows the proposed structure for the CA radical anion where the unpaired electron is located on the C_1 atom, and the negative charge is located on the C_2 atom with additional resonance structures resulting from the delocalization of the negative charge onto the electronegative N or O atoms of the cyano and ester groups.

Finally, the calculated adiabatic electron affinity of the ethyl 2-cyanoacrylate molecule is + 1.08 eV. While this is not a reduction potential per se, the adiabatic electron affinity does indicate whether or not a radical anion is stable. The large positive value for the electron affinity of the ethyl 2-cyanoacrylate indicates that the electrophilic molecule is likely to accept an electron to form a stable radical anion. Furthermore, we propose that the radical anion is nucleophilic enough to attack a second monomer and initiate the anionic polymerization of CA.

Figure 3.9: Possible Resonance Structures of the Ethyl 2-Cyanoacrylate Radical Anion

The resonance structures shown indicate the delocalization of the anionic site over the electronegative nitrogen and oxygen atoms; as well the resonance structures indicate that the unpaired electron resides primarily on the C_1 atom.

H
H
C
N
O
O
H
H
C
N
O
O
H
H
C
N
O
O

3.6 Spectral Evidence for Metallocenium Ions

At this point, experimental evidence for the formation of an electron donor-acceptor complex between either ruthenocene (Rc) or ferrocene (Fc) and ethyl 2-cyanoacrylate (CA) has been presented. As well, theoretical data predict that the radical anion of CA is stable. In order to verify experimentally whether or not our charge-transfer-to-solvent (CTTS) mechanism (equation 3.4) is valid, we undertook studies to look for the photooxidation products of the metallocenes in CA.

When ruthenocene is photooxidized in a halocarbon solvent, the resulting ruthenium-containing compound absorbs in the UV region. This, coupled with the fact that the polymer product is a hard plastic-like solid with bubbles, makes it difficult to determine if the oxidized form of ruthenocene is present. In contrast, the oxidized form of ferrocene, ferricinium, has a characteristic absorption band at 617 nm[43] which would not be interfered with by the metallocene, the solvent, or the complex formed between the two. Furthermore, the polymer product is a syrupy liquid, and we can therefore measure the electronic absorption spectrum of the photolyzed solution with a minimum of difficulties.

Figure 3.10 shows the electronic absorption spectrum of a ferrocene solution in CA before and after irradiation with the full output (λ > 290 nm) of a high pressure mercury lamp for 350 s. After irradiation, a new band appears at 617 nm which has been assigned as ferricinium ($Fe(Cp)_2^+$). The formation of the ferricinium ion is consistent with our proposal that anionic photoinitiation occurs via the photoinduced charge transfer between the metallocene and CA. Both

Figure 3.10: Electronic Absorption Spectra of Ferrocene (Fc) in CA Before and After Irradiation

Shown here is a solution of 10.5 mM Fc in CA before (spectrum a) and after (spectrum b) irradiation for 350 s with the full output of a high pressure mercury lamp. The peak that forms at 617 nm upon irradiation is assigned as $Fe(Cp)_2^+$.

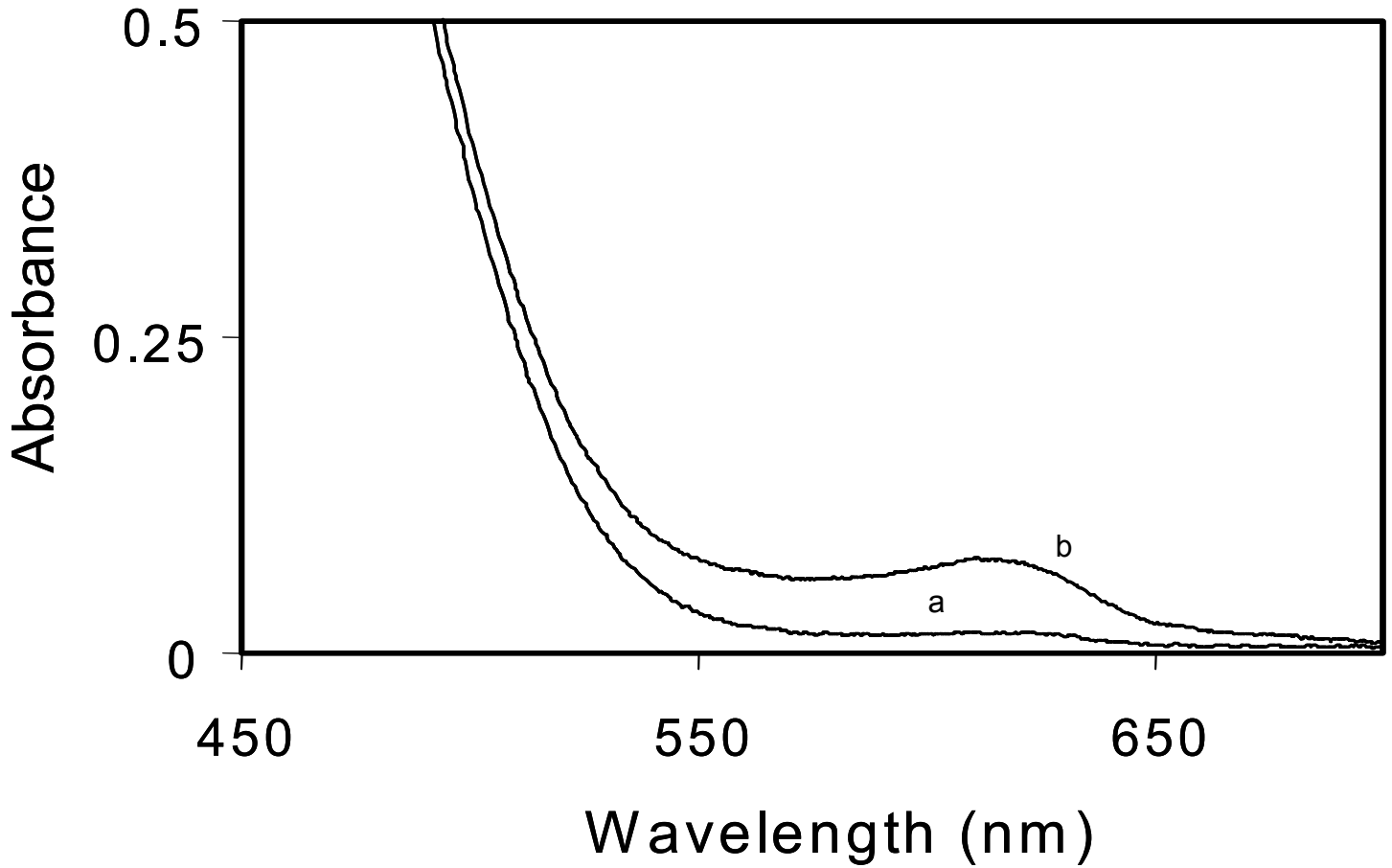
0.5
0.25
0
Absorbance
450
550
650
Wavelength (nm)
a
b

ferrocene and ruthenocene undergo analogous photochemical oxidation in halocarbon solvents.[42,44-47] It therefore seems reasonable to conclude that the photoinitiated anionic polymerization of CA by ruthenocene proceeds via the same mechanism as just shown for ferrocene, despite the lack of direct observation of the ruthenocenium ion.

3.7 Metal-to-Ligand Charge Transfer Character for Photoexcited Benzoyl-Substituted Ruthenocenes

As previously stated (in section 1.4), adding one or more benzoyl substituents to the cyclopentadienyl rings of ferrocene causes marked spectral changes. Compared to the ligand field transitions of ferrocene, the absorption bands in the spectra of the benzoyl-substituted compounds are shifted to lower energy and are much more intense. It has been proposed that these spectral changes arise from the mixing of metal-to-ligand charge transfer (MLCT) character into the ligand field bands of the parent compounds.[57] Since the benzoyl substituted ruthenocenes had not been characterized in this way, we undertook studies to determine if adding benzoyl groups has a similar effect on the electronic transitions of ruthenocene.

All spectral data of interest are summarized in Table 3.3. Figure 3.11 shows the electronic absorption spectra of ruthenocene (Rc), benzoylruthenocene (BRc), and 1,1'-dibenzoylruthenocene (DRc) in room temperature methanol. The parent compound, Rc, exhibits an absorption band at 324 nm. This has been assigned as arising from a LaPorte forbidden ligand field

Figure 3.11: Electronic Absoprtion Spectra Benzoyl-Substituted Ruthenocenes.

Shown here are the room temperature electronic spectra of ruthenocene (a), benzoylruthenocene (b), and 1,1'-dibenzoylruthenocene (c) in methanol.

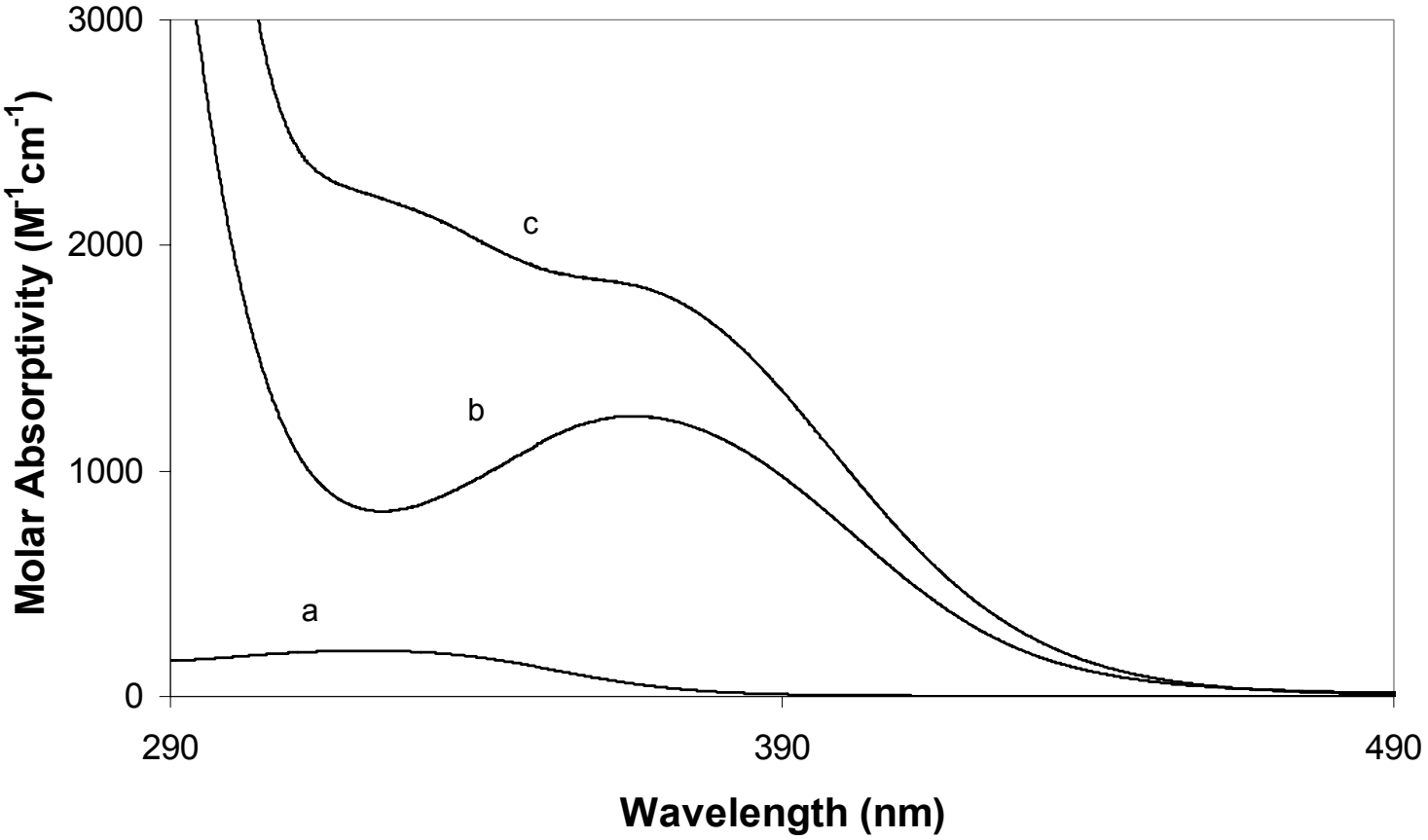
3000
2000
1000
0
Molar Absorptivity ($M^{-1}cm^{-1}$)
c
b
a
290
390
490
Wavelength (nm)

transition. In the monosubstituted compound, BRc, this band has red-shifted to 365 nm and has a marked increase in intensity (200 $M^{-1}cm^{-1}$ for Rc vs. 1250 $M^{-1}cm^{-1}$ for BRc). The disubstituted compound, DRc, has a feature in its absorption spectrum at 367 nm (determined by looking at the second derivative of the spectrum); however, this feature appears as a shoulder on a more intense band at 329 nm. The extinction coefficients for these features are also higher than those for the unsubstituted parent compound (1830 $M^{-1}cm^{-1}$ and 2200 $M^{-1}cm^{-1}$ for the lower and higher energy features, respectively). The shoulder present in the spectrum of DRc indicates that there are at least two bands, corresponding to at least two different transitions, occurring in the same region of the spectrum.

Figure 3.12 shows the electronic absorption spectra of BRc in methanol, acetonitrile, and cyclohexane. As can be seen, the low energy absorption band is sensitive to the polarity of the solvent, shifting to lower energy in more polar solvents. In cyclohexane, the absorption band appears at 342 nm with an extinction coefficient of 1020 $M^{-1}cm^{-1}$. However, in acetonitrile and methanol this band is shifted to lower energy (356 nm (ε = 977 $M^{-1}cm^{-1}$) and 365 nm (ε = 1240 $M^{-1}cm^{-1}$), respectively). Figure 3.13 shows the electronic absorption spectra of DRc in cyclohexane, acetonitrile, and methanol. It is interesting to note that in cyclohexane, the higher energy transition occurs at 321 nm (ε = 1800 $M^{-1}cm^{-1}$) and the lower energy shoulder, which appears to be centered at about 363 nm (determined by looking at the second derivative of the spectrum), is barely

Figure 3.12: Electronic Absorption Spectra of Benzoylruthenocene in Various Solvents

Shown here are the room temperature electronic absorption spectra of benzoylruthenocene in cyclohexane (a), acetonitrile (b), and methanol (c).

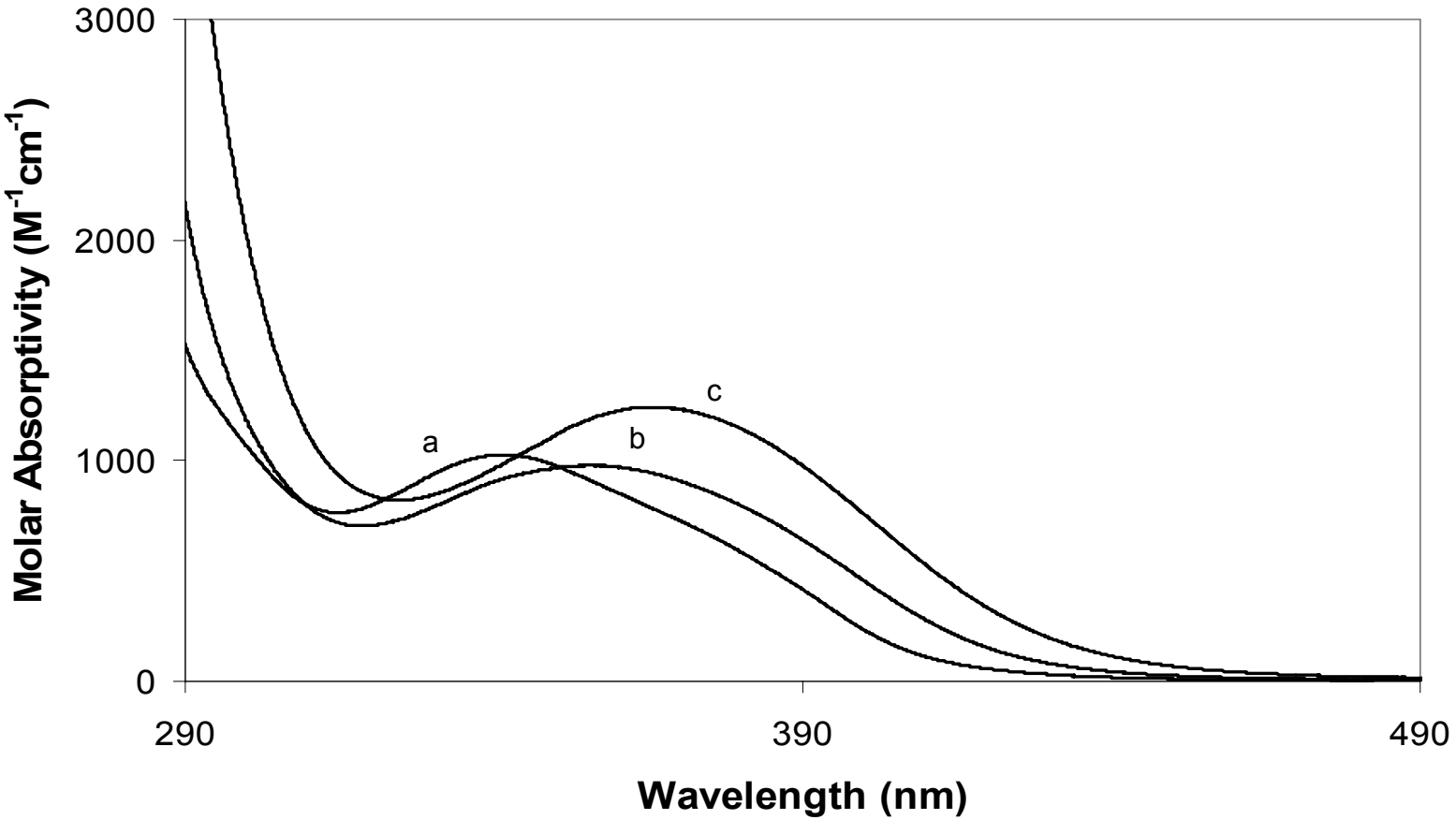
3000
2000
1000
0
Molar Absorptivity (M-1cm-1)
290
390
490
Wavelength (nm)
a
b
c

Figure 3.13: Electronic Absorption Spectra of 1,1'-Dibenzoylruthenocene in Various Solvents

Shown here are the room temperature electronic absorption spectra of 1,1'-dibenzoylruthenocene in cyclohexane (a), acetonitrile (b), and methanol (c).

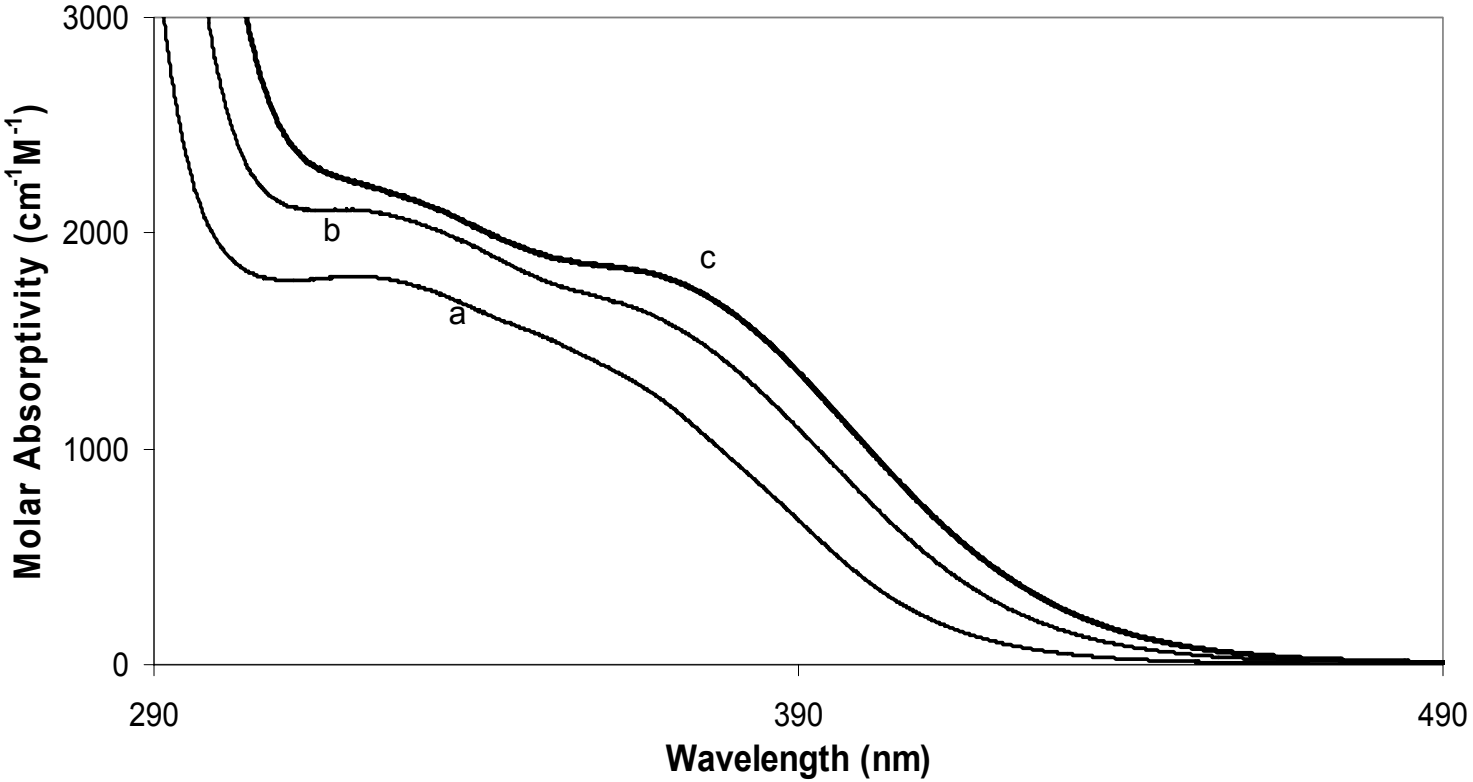
3000
2000
1000
0
Molar Absorptivity (cm-1M-1)
290
390
490
Wavelength (nm)
a
b
c

Table 3.3: Summary of electronic absorption spectra for Rc, BRc, and DRc.

Compound	Solvent[a]	Absorption (nm)[b]	Extinction Coefficient ($M^{-1}cm^{-1}$)
Rc	MeOH	324	200
BRc	MeOH	365	1250
	ACN	356	977
	C_6H_{12}	342	1020
DRc	MeOH	367	1830
	ACN	366	1630
	C_6H_{12}	363	1340
	MeOH	329	2200
	ACN	323	2100
	C_6H_{12}	321	1800

[a] MeOH is methanol, ACN is acetonitrile, and C_6H_{12} is cyclohexane.

[b] For Rc and BRc, the wavelength reported is the λ_{max} for the absorption band. In the case of DRc, the wavelengths reported are the inflection points as determined by looking at the second derivative spectra.

distinguishable in the spectrum (ε = 1340 $M^{-1}cm^{-1}$). In acetonitrile the higher energy band occurs at 323 nm (ε = 2110 $M^{-1}cm^{-1}$) and the lower energy band occurs at 366 nm (ε = 1630 $M^{-1}cm^{-1}$) (determined by looking at the second derivative of the spectrum). In addition, the lower energy band is much more defined than it was in cyclohexane. This same observation is even more pronounced in the methanol spectrum. The lower energy band occurs at 367 nm (ε = 1830 $M^{-1}cm^{-1}$) and is a well defined shoulder to the larger band that occurs at 329 nm (ε = 2200 $M^{-1}cm^{-1}$). In addition to the red shift and increase of intensity, as the polarity of the solvent increases, the features in DRc absorption spectrum become much more defined, indicating that the more polar solvent is causing the bands to separate.

The spectral changes that occur upon addition of one or more benzoyl groups to ruthenocene (Table 3.3) are consistent with the mixing of charge transfer character into the ligand field transition of the parent compound. Specifically, if the excited state of the compound has a greater separation of charge than the ground state, it will occur at lower energy in a more polar solvent due to coloumbic stabilization, thus accounting for the shifting of these bands to lower energy in more polar solvents. More specifically, since the benzoyl groups on the cyclopentadienyl ring are electron withdrawing, it is logical to propose that the charge transfer is metal-to-ligand (MLCT) in nature. One representation of the proposed excited state is shown in Figure 3.14. A similar photoexcited state has previously proposed for benzoyl-substituted ferrocenes (Figure 1.9), and this

Figure 3.14: Proposed Photoexcited State for 1,1'-Dibenzoylruthenocene

This is a limiting resonance structure of the photoexcited state of 1,1'-dibenzoylruthenocene which illustrates metal-to-ligand charge transfer character in the low energy absorption band. This is the same resonance structure that has been proposed for the photoexcited state of 1,1'-dibenzoylferrocene.

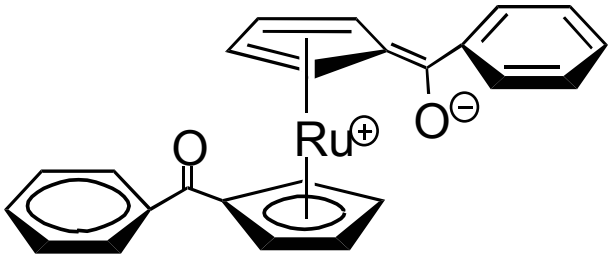
O
Ru⊕
O⊖

photoexcited state has been used to explain why benzoylferrocene and 1,1'-dibenzoylferrocene exhibit heterolytic cleavage of one of the cyclopentadienyl rings upon photolysis. We were interested to learn whether or not the same type of photochemistry might occur in the case of BRc and DRc.

3.8 Confirmation of Metal-to-Ligand Charge Transfer Character

Resonance Raman spectroscopy is a technique for determining which molecular vibrations are coupled to an electronic transition. Specifically, when the laser irradiation used to excite the compound lies within the vicinity of an allowed electronic transition, the intensities of some vibrational modes are enhanced relative to others. The molecular vibrations which are most perturbed are those that mimic the distortions in the excited state populated by the electronic transition that occurs upon absorption of a photon. In effect, resonance Raman allows us to see which molecular vibrations mimic the excited state structure of a molecule. The resonance structures shown in Figures 1.9 and 3.14 indicate that upon excitation there is a redistribution of charge leading to a significant change in the carbonyl bond (from double bond to single bond in character). Therefore, if the resonance structure shown in these figures is an accurate representation of the electronic excited state, then we should see a large intensity enhancement in the carbonyl region of the resonance Raman spectrum.

Raman spectra of BRc, DRc, BFc and DFc are shown in Figures 3.15, 3.16, 3.17, and 3.18, respectively. In order to visualize the resonant enhancement, the Raman intensities have been normalized to an internal

standard (the 985 cm^{-1} band in K_2SO_4) which is not resonantly enhanced. Using the literature assignments for ferrocene, ruthenocene, and benzoic acid, we have assigned the major bands in the Raman spectra (Table 3.4); all of the bands arise from either stretching or bending modes of either the substituted or unsubstituted rings.

The Raman spectrum of BRc (Figure 3.15) acquired using 568 nm excitation (off resonance) is dominated by the carbonyl stretching mode at 1633 cm^{-1}. Also present is the symmetric ring breathing mode of the unsubstituted ring at 1100 cm^{-1}, and several internal modes for the benzoyl-substituted ring. When 406 nm light is used for the excitation (on resonance) of BRc, we see that the carbonyl stretching mode at 1633 cm^{-1} is greatly enhanced with respect to the sulfate band at 985 cm^{-1}. This enhancement indicates that the electronic transition that occurs causes a pronounced perturbation of the carbonyl bond. In contrast, we see that certain bands, namely the unsubstituted ring breathing mode at 1100 cm^{-1}, and the in-plane bending (deformation) mode of the substituted ring at 1058 cm^{-1} actually decrease in intensity. The cause for this decrease in intensity is most likely due to decomposition of the sample.

The Raman spectra of DRc, shown in Figure 3.16, are similar to the spectra of BRc in that the spectra are also dominated by the carbonyl stretching mode at 1633 cm^{-1}. However, there are several differences between the two compounds; the most notable of which is that the ring breathing mode of the unsubstituted cyclopentadienyl ring is absent. Also, due to luminescence, many of the bands arising from the internal modes of the benzoyl-substituted

Table 3.4: Vibrational assignments in the resonance Raman spectra of BFc, DFc, BRc, and DRc.

BFc[a]	DFc	BRc	DRc	Assignment[b]
1000	998	1000	1000	$\delta(CCC)_{Ph}$
1028	1028			$\nu(CC)_{Ph}$
1059	1050	1058	1058	$\delta(CCH)_{Cp'}$
1105		1100		$\nu(CC)_{Cp}$
1167	1170	1169	1169	$\delta(CCH)_{Cp'}$ or $\delta(CCH)_{Ph}$
1176	1180			$\delta(CCH)_{Cp'}$ or $\delta(CCH)_{Ph}$
		1406		$\nu(CC)_{Cp}$
1440	1446	1442	1442	$\nu(CC)_{Cp'}$
1579	1580	1578		$\nu(CC)_{Ph}$
1598	1598	1597	1597	$\nu(CC)_{Ph}$
1624	1630	1633	1633	$\nu(CO)$

a: All band positions are quoted in cm^{-1}.

b: Where Ph is phenyl, Cp is the unsubstituted cyclopentadienyl ring, and Cp' is the substituted cyclopentadienyl ring.

Figure 3.15: Raman Spectra of Benzoylruthenocene

The Raman spectrum taken with 568 nm excitation is off resonance, and the Raman spectrum taken with 406 nm excitation is on resonance.

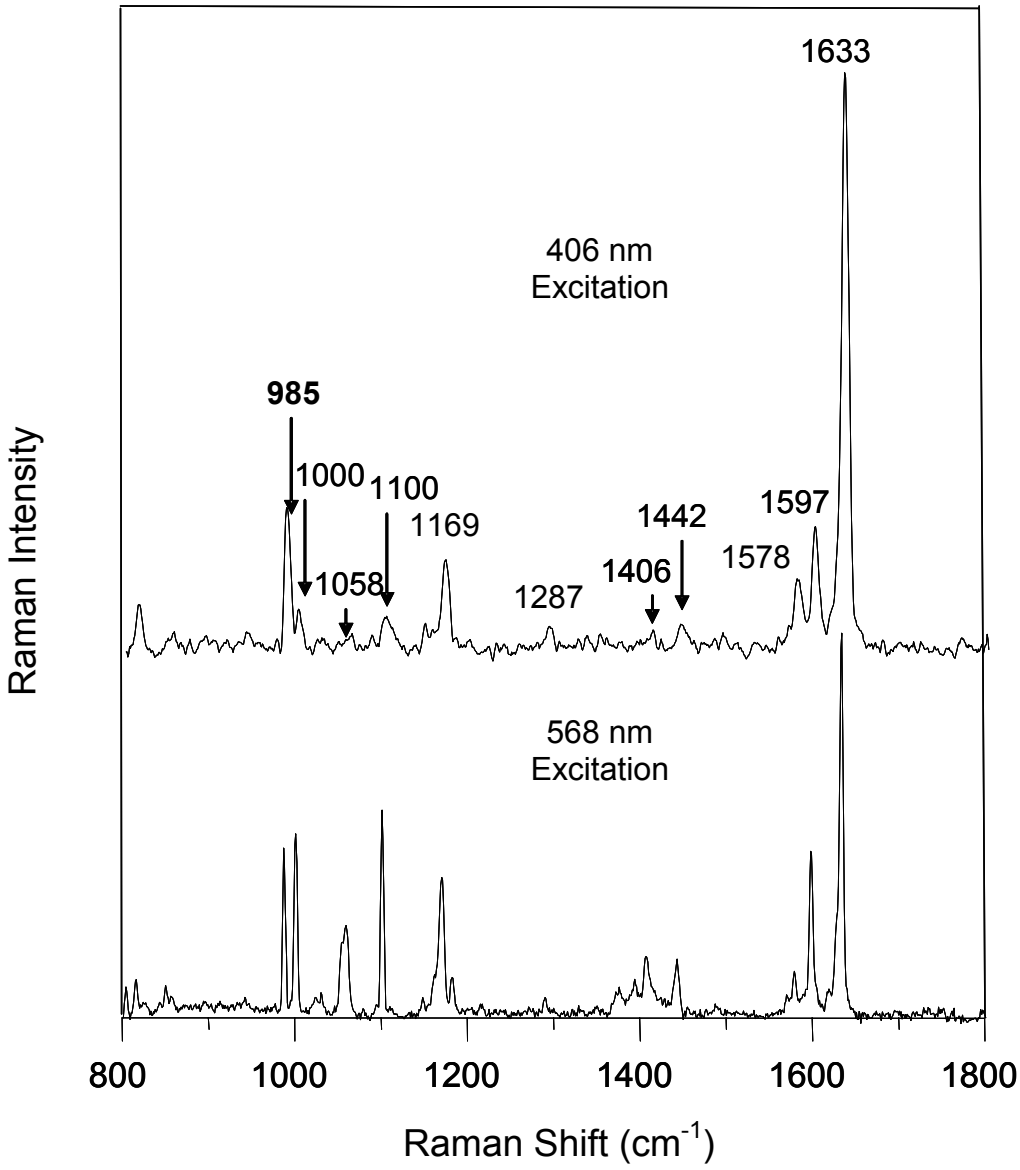
1633
406 nm
Excitation
985
1000
1100
1169
1058
1287
1406
1442
1597
1578
568 nm
Excitation
Raman Intensity
800
1000
1200
1400
1600
1800
Raman Shift (cm-1)

Figure 3.16: Raman Spectra of 1,1'-Dibenzoylruthenocene

The Raman spectrum taken with 568 nm excitation is off resonance, and the Raman spectrum taken with 406 nm excitation is on resonance. Noise in the spectrum taken with 406 nm excitation is due to luminescence of the compound.

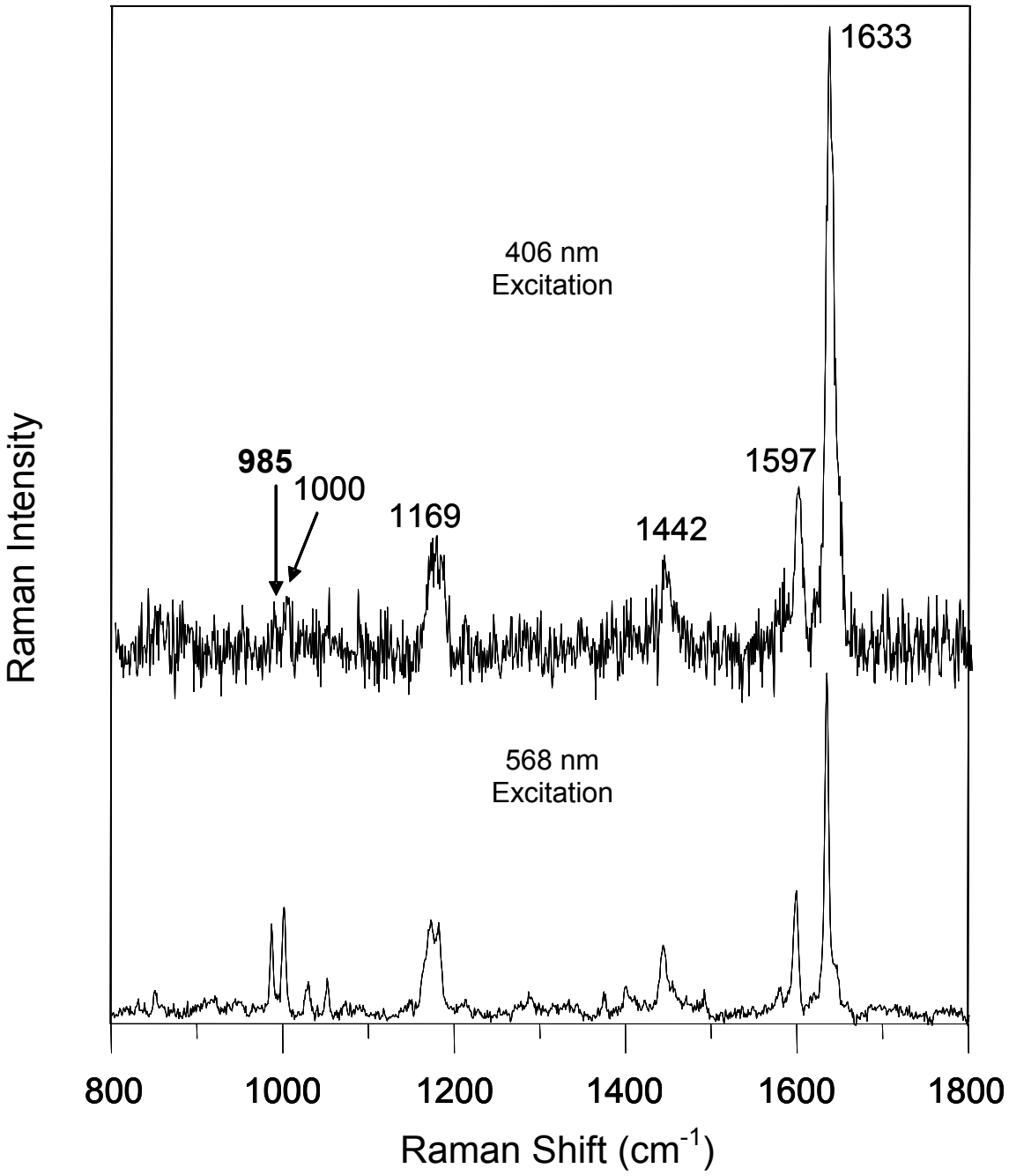
1633
406 nm
Excitation
985
1000
1169
1442
1597
Raman Intensity
568 nm
Excitation
800
1000
1200
1400
1600
1800
Raman Shift (cm-1)

cyclopentadienyl rings are not seen above the noise threshold. In spite of this luminescence, the spectrum excited with 406 nm light (on resonance) shows a marked increase in the carbonyl stretching mode at 1633 cm^{-1}. This indicates that absorption of a photon causes a significant perturbation of this particular bond.

The Raman spectrum of BFc (Figure 3.17) acquired using 647 nm excitation (off resonance) is also dominated by the carbonyl stretching mode at 1624 cm^{-1} and the symmetric ring breathing mode at 1105 cm^{-1}. Also present are several internal modes for the benzoyl-substituted ring. When 568 nm light (on resonance, in the tail end of the absorption band) is used for excitation, we see that the carbonyl stretching mode at 1624 cm^{-1} is greatly enhanced with respect to the sulfate band at 985 cm^{-1}; as well the other bands attributable to the internal modes of the substituted rings are enhanced, though not nearly as much. This enhancement indicates that the electronic transition that occurs causes a pronounced perturbation of the carbonyl bond. In contrast, the ring breathing mode of the unsubstituted ring shows no resonance enhancement indicating that the bonding in this ring does not change significantly upon population of the excited state represented by the low energy electronic transition. When 488 nm light (on resonance, near the absorption maximum) was used as the excitation source, we see a decrease in signal intensity. We attribute this to photodegradation of the sample induced by the laser.

The Raman spectra of DFc, shown in Figure 3.18, are similar to the spectra of BFc. The spectrum taken with 647 nm light (off resonance) is still

dominated by the carbonyl stretching mode at 1633 cm^{-1}. However, as expected the symmetric breathing mode of the unsubstituted ring at 1105 cm^{-1} is absent. Upon excitation of DFc with 568 nm light (on resonance, near the tail of the absorption band), there is still enhancement of the carbonyl band; though the degree of enhancement is much less than for BFc, and much less than was expected. When 488 nm light is used for excitation, there is very little signal. One possible reason for this is that there is more photodecomposition in the case of DFc than for BFc. This makes sense in light of the fact that DFc is much more (5-10 times more) photosensitive than BFc in solution.[53]

In order to verify our assertion that the iron-containing samples were decomposing over the time period required for the spectra to be taken, a second set of spectra were collected. In these experiments, the intensity of the carbonyl band of DFc was monitored as a function of laser light exposure time in both a solid sample and a frozen solution in $CHCl_3$ (the 1227 cm^{-1} band of $CHCl_3$ was used as the internal standard in the solution spectra); these results are shown in Figure 3.19. Spectrum (a) shows that, in the solid state, the intensity of the carbonyl band decreases appreciably over the first 20 s of exposure to the light, indicating that significant photodegradation has occurred. Spectrum (b) shows that the same decrease in intensity occurs when a frozen solution is used to acquire the spectra, but much faster (the carbonyl band has significantly decreased in the first 5 s of exposure).

The data presented here indicate that excitation into the low energy electronic transition results in some resonance enhancement of in-plane

Figure 3.17: Raman spectra of Benzoylferrocene

The Raman spectrum collected with 647 nm excitation is off resonance, the Raman spectrum collected with 568 nm excitation is right at the tail end of the low-energy absorption band (on resonance), and the Raman spectrum collected using 488 nm excitation is near the maximum of the low-energy band (on resonance).

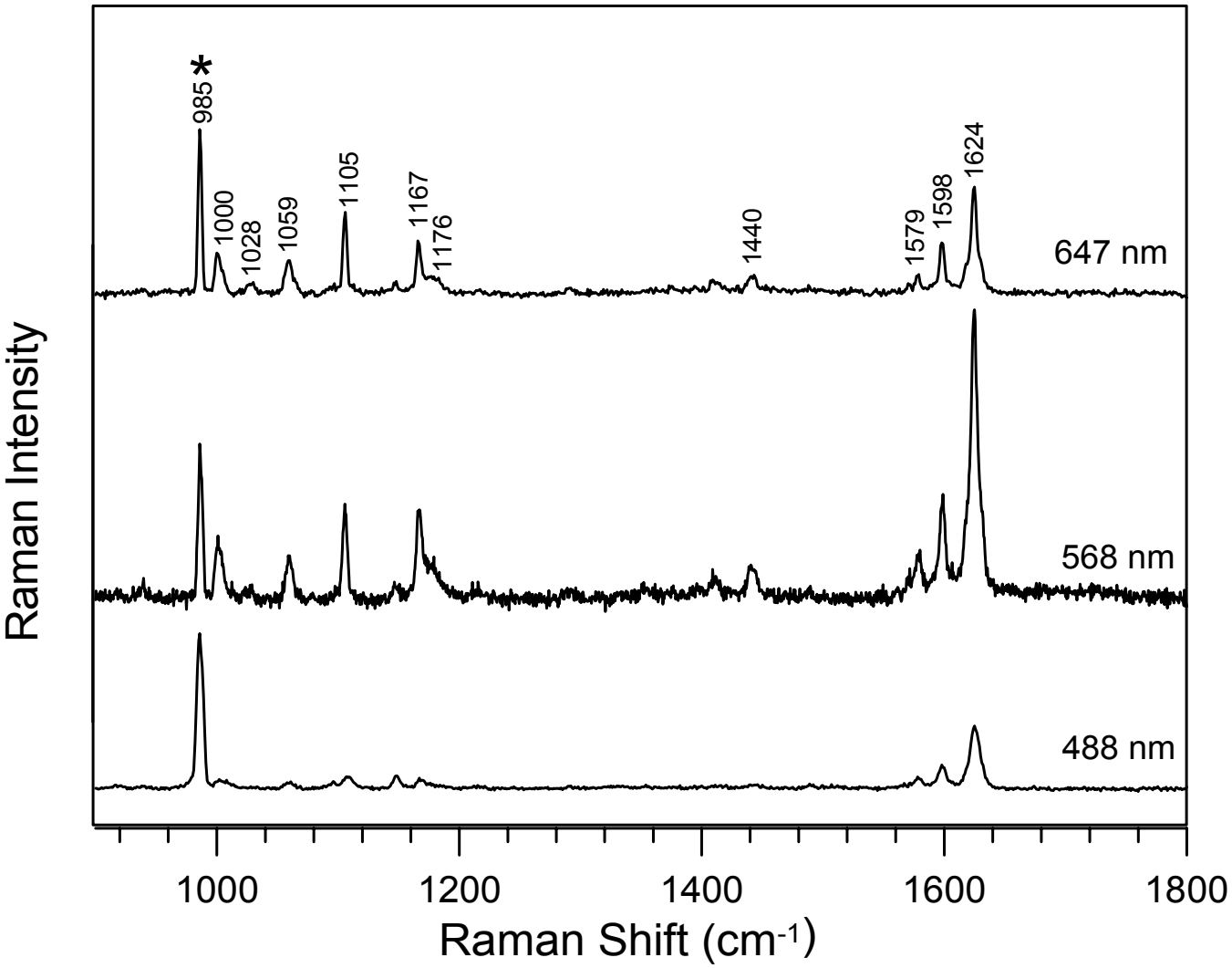
985 *
1000
1028
1059
1105
1167
1176
1440
1579
1598
1624
647 nm
568 nm
488 nm
Raman Intensity
1000
1200
1400
1600
1800
Raman Shift (cm-1)

Figure 3.18: Raman spectra of 1,1'-Dibenzoylferrocene

The Raman spectrum collected with 647 nm excitation is off resonance, the Raman spectrum collected with 568 nm excitation is right at the tail end of the low-energy absorption band (on resonance), and the Raman spectrum collected using 488 nm excitation is near the maximum of the low-energy band (on resonance).

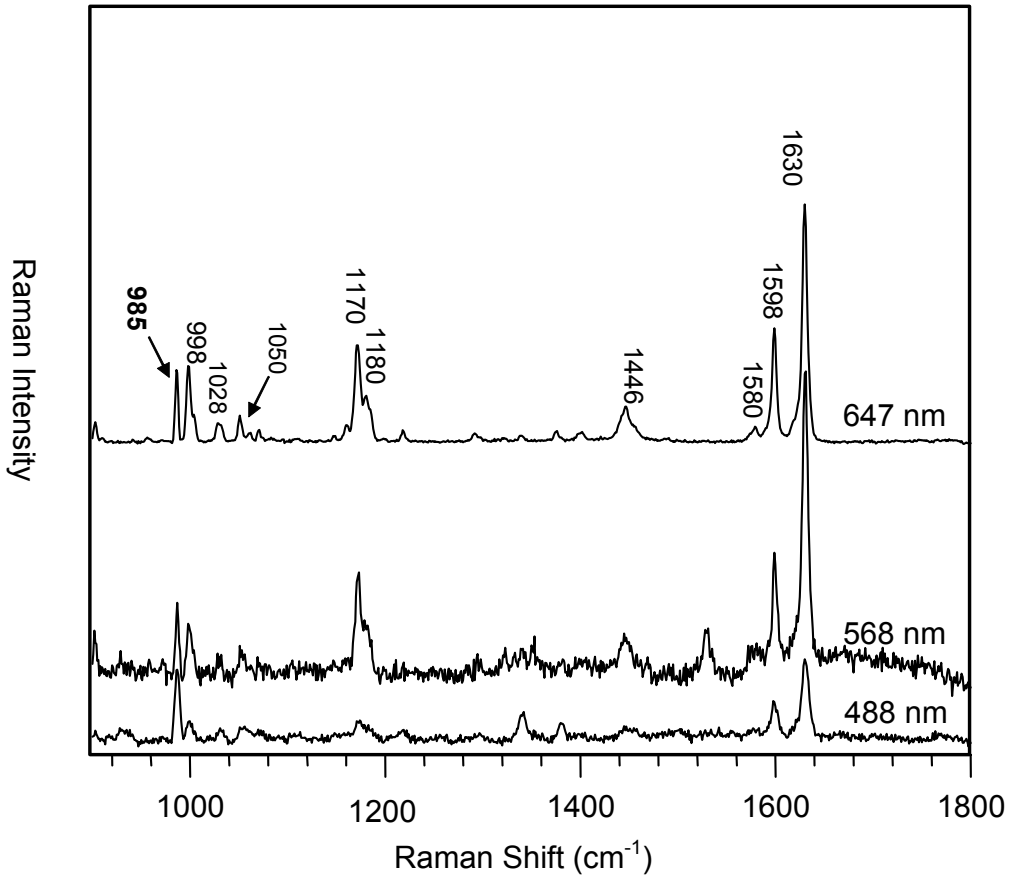
Raman Intensity
985
998
1028
1050
1170
1180
1446
1580
1598
1630
647 nm
568 nm
488 nm
1000
1200
1400
1600
1800
Raman Shift (cm-1)

Figure 3.19: Raman Spectra Showing the Decomposition of 1,1'-Dibenzoylferrocene Upon 568 nm Excitation

Graph of Raman intensity of DFc as a function of time upon excitation with 568 nm light to illustrate the decrease in intensity of the carbonyl band at 1630 cm^{-1} as compared to either the solid Raman standard (985 cm^{-1} band of sulfate) in spectrum (a) or the solution Raman standard (1227 cm^{-1} band of $CHCl_3$) in spectrum (b) over the time period required for the Raman spectra to be acquired.

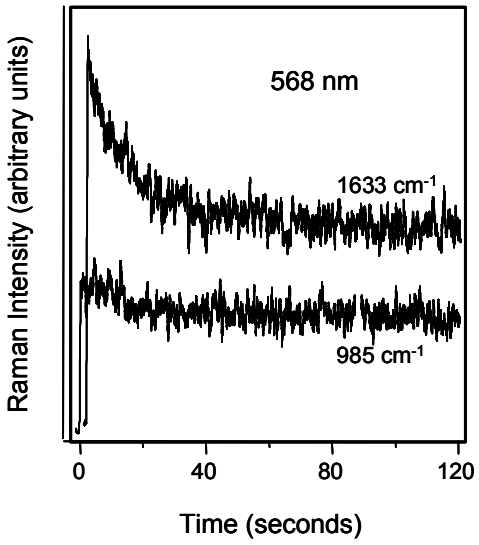
568 nm
1633 cm-1
985 cm-1
Raman Intensity (arbitrary units)
0
40
80
120
Time (seconds)

a

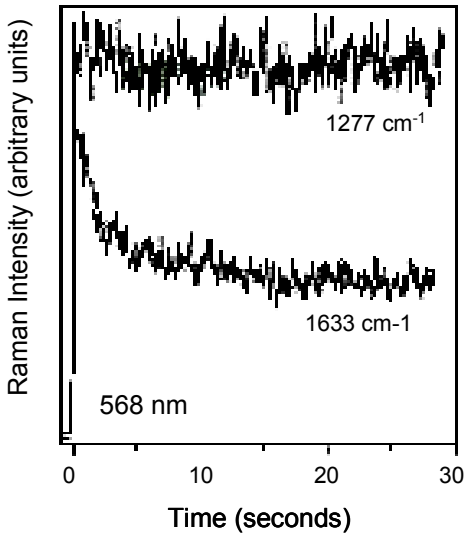
1277 cm-1
1633 cm-1
568 nm
Raman Intensity (arbitrary units)
0
10
20
30
Time (seconds)

b

vibrations of the benzoyl substituted cyclopentadienyl rings as well as a very strong resonance enhancement of the carbonyl bond. This enhancement is consistent with our proposal that the low energy electronic transition contains an appreciable amount of metal-to-ligand charge transfer (MLCT) character. Moreover, these results lend credibility to the proposed photoexcited states depicted by the resonance structures in Figures 1.9 and 3.14, which show electron density shifting from the metal center onto the conjugated benzoyl-substituted cyclopentadienyl ring. It is interesting to note that in the case of the iron compounds, excitation of the compound with 488 nm (and even 568 nm) light causes a large amount of photoinduced degradation of the sample whereas in the ruthenium compounds this photoinduced degradation is much less of a problem. This is consistent with the kinetic observations that the 1,1'-dibenzoylferrocene is a better photoinitiator for the anionic polymerization of CA than the benzoyl-substituted ruthenium compounds. At this point, it seemed reasonable to look for photoproducts, and while there are several different ways to go about this, we chose to use mass spectrometry.

3.9 Identification of Photoproducts Using Mass Spectrometry

Mass spectrometry is a powerful technique which allows the detection of ionic species in the gas phase. The ionization method employed here is electrospray ionization, and it is coupled to a time of flight detector, (ESI-TOF). Electrospray ionization (ESI) is a soft ionization technique which transfers species from solution into the gas phase with little or no fragmentation of the

species. Once the ions are in the gas phase, they can no longer react with other species present in the system. It had previously been shown that irradiation of DFc in methanol gave a non-iron-containing product which was determined by gas chromatography-mass spectrometry (GC-MS) to be protonated benzoylcyclopentadiene.[57] These data supported the assertion that photolysis of DFc caused heteroytic ring cleavage (equation 3.7 where 'S' is a solvent molecule); however, it is possible that the primary photoproducts had decomposed or reacted further to give the observed products since the nature of the experimental method required that the solution be analyzed after sitting around for a while (~30 min). In order to minimize the amount of time the photoproducts spent in solution, a method has been developed by a co-worker that irradiates a solution while it flows through the electrospray tip.[70]

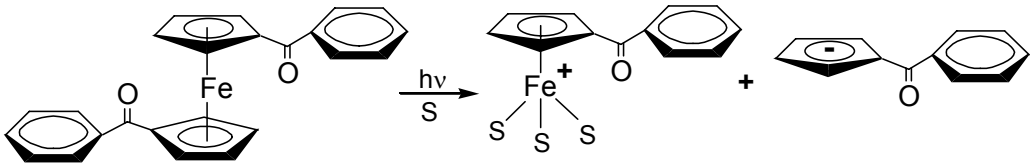

(3.7)

In one set of experiments, the mass spectra of solutions containing DFc and either Na^+ or K^+ (to act as a carrier ion) dissolved in acetonitrile (ACN) were taken before irradiation (the 'dark' sample) and during irradiation (the 'light' sample) with 488 nm light. The dark samples are shown in Figure 3.20. Spectrum (a) is the unirradiated DFc solution containing Na^+ as the carrier ion. Major peaks occur at m/z 417.0 and 811.1; these correspond to the 1:1 and 2:1 DFc:Na^+ adducts, and each species has a 1^+ charge. The adducts are the result of Lewis acid-base interactions between the Na^+ ion and the carbonyl oxygen in DFc. The

presence of both the 1:1 and 2:1 adducts can be explained by the solution equilibria described in equations 3.8 and 3.9.

$$DFc + Na^+ \rightleftharpoons [DFc + Na]^+ \qquad (3.8)$$

$$[DFc + Na]^+ + DFc \rightleftharpoons [2DFc + Na]^+ \qquad (3.9)$$

The occurrence of these equilibria can be tested by adding a larger excess of Na^+ to the solution, which should favor the formation of the 1:1 adduct. This is illustrated in spectrum (b) which shows less of the 2:1 adduct as compared to the 1:1 adduct as the ratio of DFc to Na^+ is increased from 1:1.6 to approximately 1:20. In spectrum (c) we see that changing the carrier ion from Na^+ to K^+ keeps the stoichiometry intact, but shifts the mass by 16 units, the difference in mass between Na^+ and K^+.

Irradiation, using 488 nm light, of a solution containing DFc and Na^+ in approximately a 1:1 ratio causes a plethora of new species to appear in the mass spectrum (Figure 3.21). The photoproducts can be divided into three series: non iron-containing species, half sandwich compounds (compounds containing one substituted cyclopentadienyl ring and the iron atom), and solvated iron atoms. The parent compound forms the 1:1 adducts with H^+ and Na^+, which appear at m/z 395.0 and 417.0, respectively. The non iron-containing series consists of 1^+ peaks at m/z 171.1, 193.1, 234.1, and 363.1 which correspond to $[PhC(O)C_5H_5 + H]^+$, $[PhC(O)C_5H_5 + Na]^+$, $[PhC(O)C_5H_5 + Na + ACN]^+$, and $[2(PhC(O)C_5H_5) + Na]^+$, respectively. The half sandwich series consists of 2^+ peaks at m/z 154.0

and 174.5, which correspond to the protonated half sandwich complex with 2 and 3 ACN molecules occupying the vacated coordination sites, respectively. The solvated iron (II) atoms occur with 4 and 5 ACN molecules coordinated to give 2^+ species at m/z 110.0 and 130.5, respectively.

The presence of the half sandwich complexes and the benzoyl-cyclopentadiene series provides evidence that the primary photochemical reaction is heterolytic ring cleavage as shown in equation 3.7. The solvated iron atoms arise from losing the second ring from the half sandwich compound which is originally produced (as seen in equation 3.10, where 'S' is a solvent molecule). Whether this reaction happened photochemically or thermally is not known at this time.

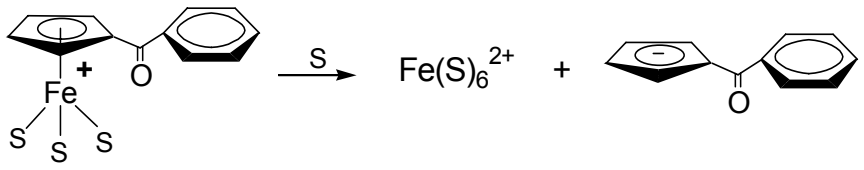

(3.10)

Online photolysis of DFc works well to identify the intermediates of the photoreaction and shows that the primary photoproducts of the reaction are the half-sandwich compound and the (protonated) benzoyl-substituted ring consistent with equation 3.7. Interestingly, these same products were seen using an off-line photolysis procedure, even though the photolyte had sat in solution for 30 minutes in the latter case. Since the ruthenium analogs of these compounds have essentially no absorbance at 488 nm, samples of the benzoyl-substituted ruthenocenes were irradiated off-line (λ>290 nm) and then analyzed by ESI-MS within 30 minutes of photolysis.

Figure 3.20: ESI Mass Spectrum of 1,1'-Dibenzoylferrocene in ACN (Dark Sample)

Shown here are the mass spectra of a DFc solution in ACN with approximately a 1:1.6 ratio of DFc:Na^+ (a), approximately a 1:20 ratio of DFc:Na^+ (b), and approximately a 1:13 ratio of DFc:K^+ (c).

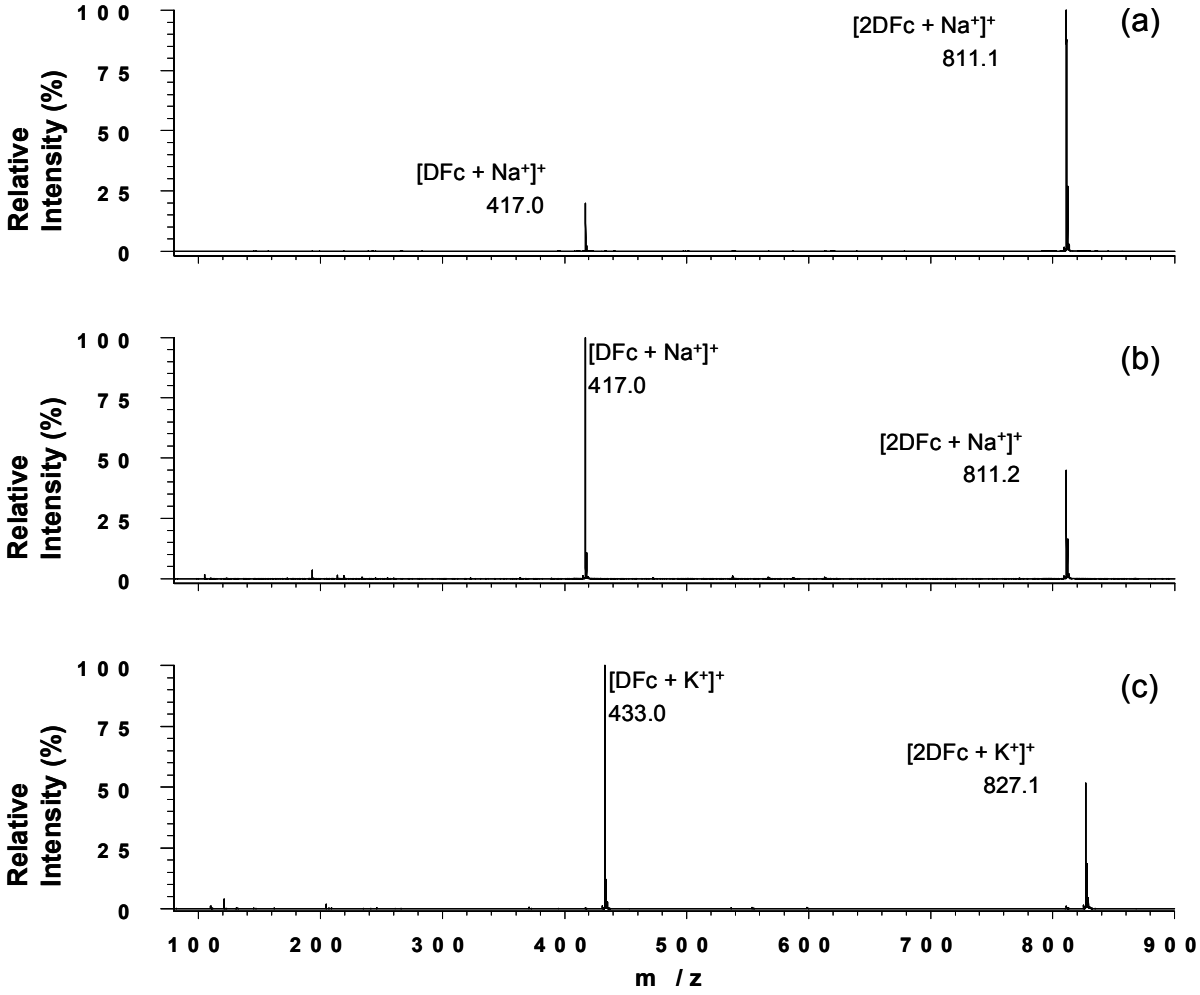
(a)
[2DFc + Na+]+
811.1
[DFc + Na+]+
417.0
(b)
[DFc + Na+]+
417.0
[2DFc + Na+]+
811.2
(c)
[DFc + K+]+
433.0
[2DFc + K+]+
827.1
Relative Intensity (%)
100
75
50
25
0
100 200 300 400 500 600 700 800 900
m /z

Figure 3.21: ESI Mass Spectrum of 1,1'-Dibenzoylferrocene in ACN (Irradiated with 488 nm Light)

Shown here is the mass spectrum of an irradiated sample which originally contained approximately equimolar amounts of DFc and Na.

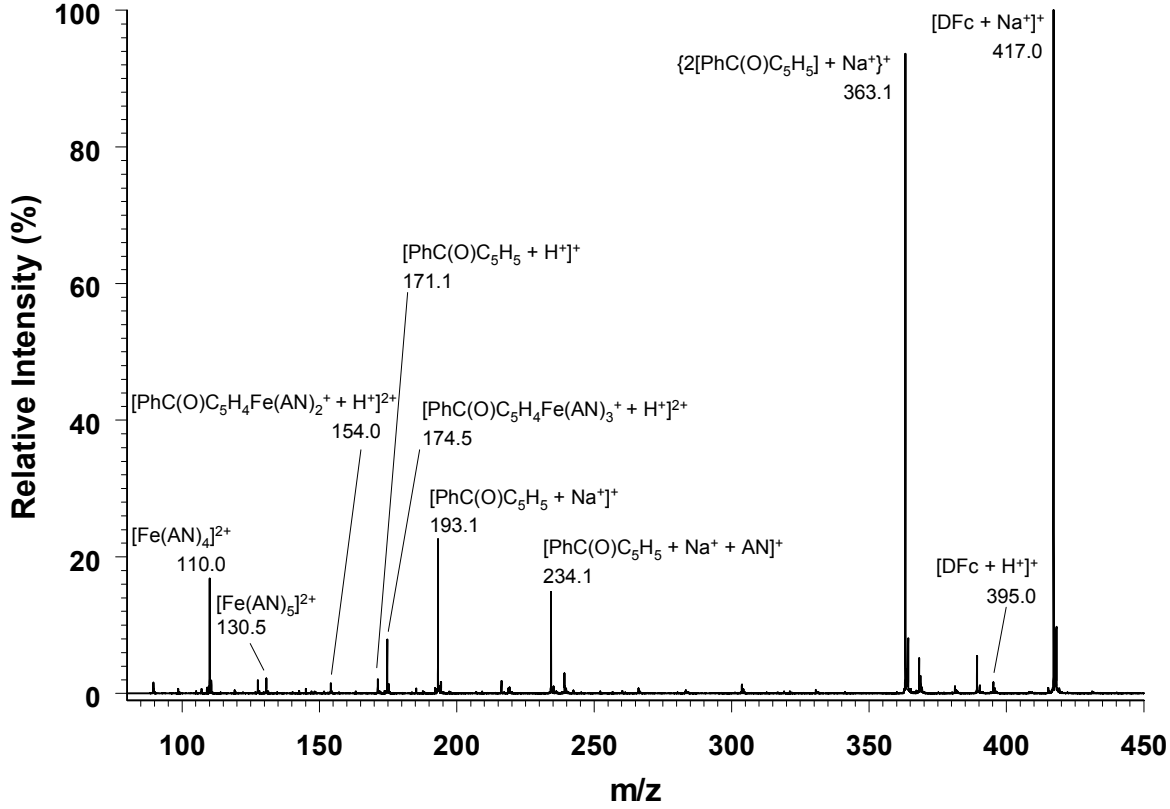
Relative Intensity (%)
m/z
[DFc + Na+]+
417.0
{2[PhC(O)C5H5] + Na+}+
363.1
[PhC(O)C5H5 + H+]+
171.1
[PhC(O)C5H4Fe(AN)2+ + H+]2+
154.0
[PhC(O)C5H4Fe(AN)3+ + H+]2+
174.5
[PhC(O)C5H5 + Na+]+
193.1
[Fe(AN)4]2+
110.0
[PhC(O)C5H5 + Na+ + AN]+
234.1
[DFc + H+]+
395.0
[Fe(AN)5]2+
130.5

In one experiment, samples of either DRc or BRc in ACN were photolyzed for 20 to 30 minutes before analysis by ESI-TOF mass spectrometry. The resulting mass spectra are shown in Figure 3.22 and 3.23 for DRc and BRc, respectively. Non ruthenium-containing 1^+ peaks are seen at m/z 241.2, 529.3, and 599.3. The peak at m/z 241.2 corresponds to $(n\text{-}Bu)_4N^+$ which was added as a standard to calibrate the mass spectrum. The latter two non ruthenium-containing peaks correspond to impurities which are present in all samples. Also, there is a ruthenium-containing 2^+ peak at m/z 265.5, which is an unknown impurity present in all samples. In addition to the impurity peaks mentioned above, the spectra contain peaks corresponding to the 2:1 and 1:1 adducts of the metallocene with sodium (m/z 903.0 and 463.0 for DRc and 694.9 and 359.0 for BRc). No peaks were seen that corresponded to half-sandwich-type compounds despite the fact that ACN is a good coordinating solvent for ruthenium. This indicates that these ruthenium compounds do not exhibit photoinduced ring loss in ACN.

Since we knew that irradiation of BRc and DRc causes the anionic photoinitiation of CA, we decided to repeat these photolysis experiments using CCl_4 as the solvent. These results are shown Figures 3.24 and 3.25 for DRc and BRc, respectively. Upon photolysis in CCl_4, the solutions became cloudy with a brown precipitate, indicating that a photochemical reaction has taken place. After diluting the photolyte with ACN, we see that the non ruthenium-containing 1^+ peaks at m/z 241.2, 529.3, and 599.3 are still present, as well as the ruthenium-containing 2^+ peak at 265.5. The major difference between any set of two spectra

Figure 3.22: Mass Spectrum of 1,1'-Dibenzoylruthenocene in ACN

Shown here is the mass spectrum of a solution of DRc in ACN before (dark sample, spectrum a) and after (spectrum b) irradiation with white light (λ>290 nm) for 30 minutes.

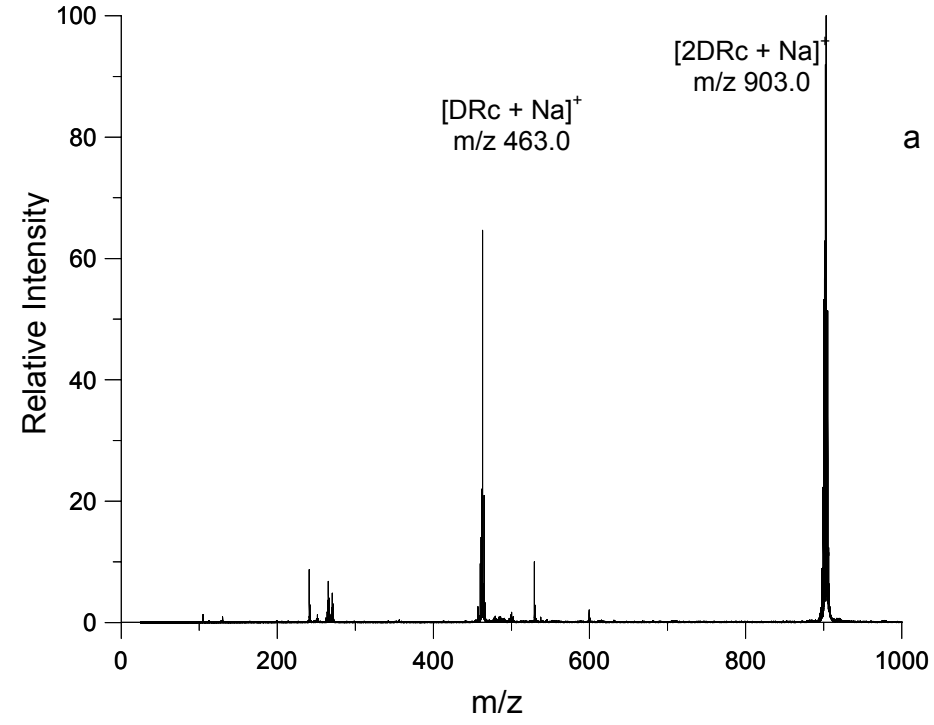
[DRc + Na]+
m/z 463.0
[2DRc + Na]+
m/z 903.0
a
Relative Intensity
m/z
0
20
40
60
80
100
0
200
400
600
800
1000

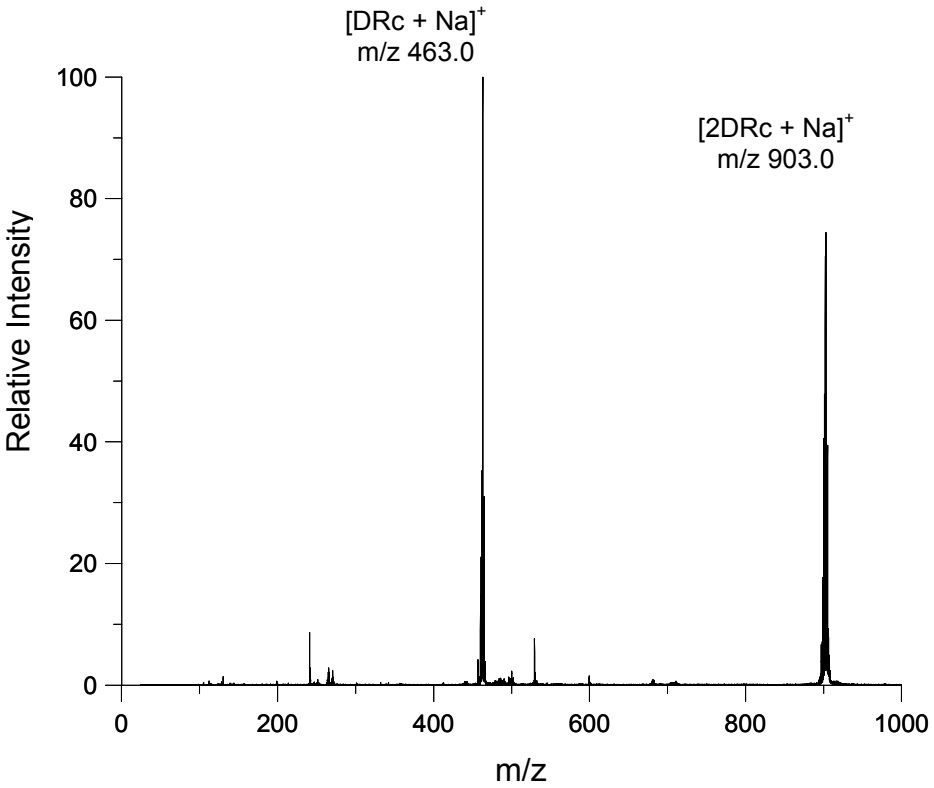
[DRc + Na]+
m/z 463.0
[2DRc + Na]+
m/z 903.0
b
Relative Intensity
m/z
0
20
40
60
80
100
0
200
400
600
800
1000

Figure 3.23: Mass spectra of Benzoylruthenocene in ACN

Shown here is the mass spectrum of a solution of BRc in ACN before (dark sample, spectrum a) and after (spectrum b) irradiation with white light (λ>290 nm) for 20 minutes.

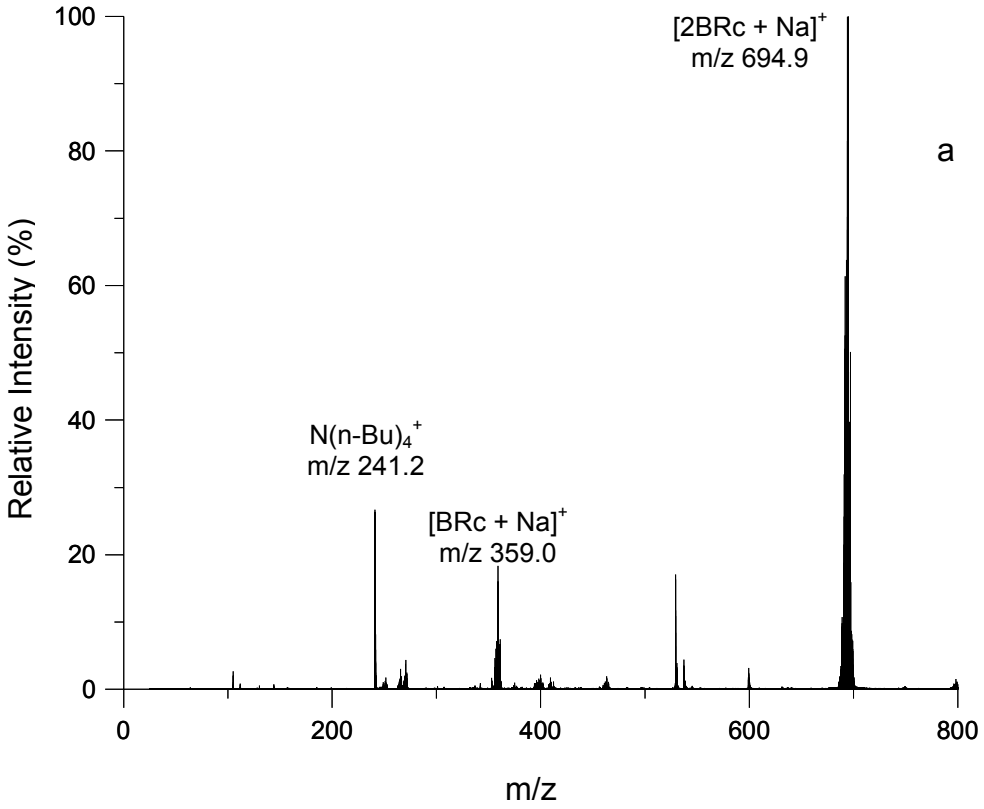
100
80
60
40
20
0
Relative Intensity (%)
[2BRc + Na]+
m/z 694.9
a
N(n-Bu)4+
m/z 241.2
[BRc + Na]+
m/z 359.0
0
200
400
600
800
m/z

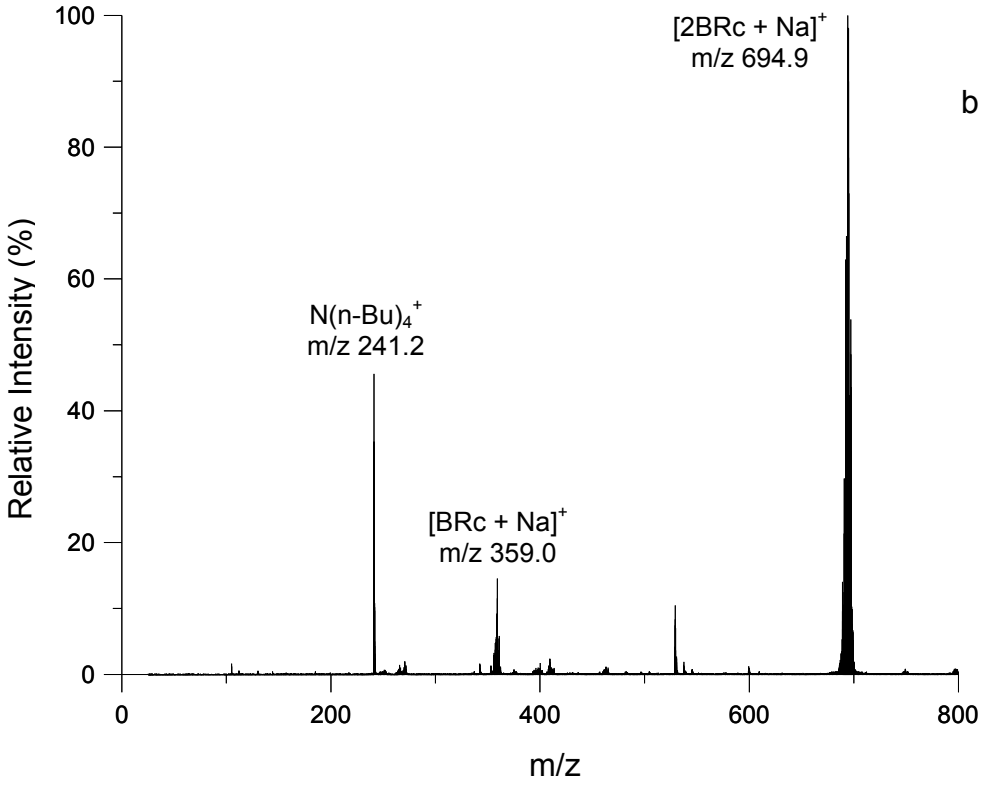
100
80
60
40
20
0
Relative Intensity (%)
[2BRc + Na]+
m/z 694.9
b
N(n-Bu)4+
m/z 241.2
[BRc + Na]+
m/z 359.0
0
200
400
600
800
m/z

Figure 3.24: Mass Spectra of 1,1'-Dibenzoylruthenocene in CCl_4

Mass Spectrum of a solution of DRc in CCl_4 before (spectrum a) and after (spectrum b) 20 minutes of irradiation with white light (λ>290 nm).

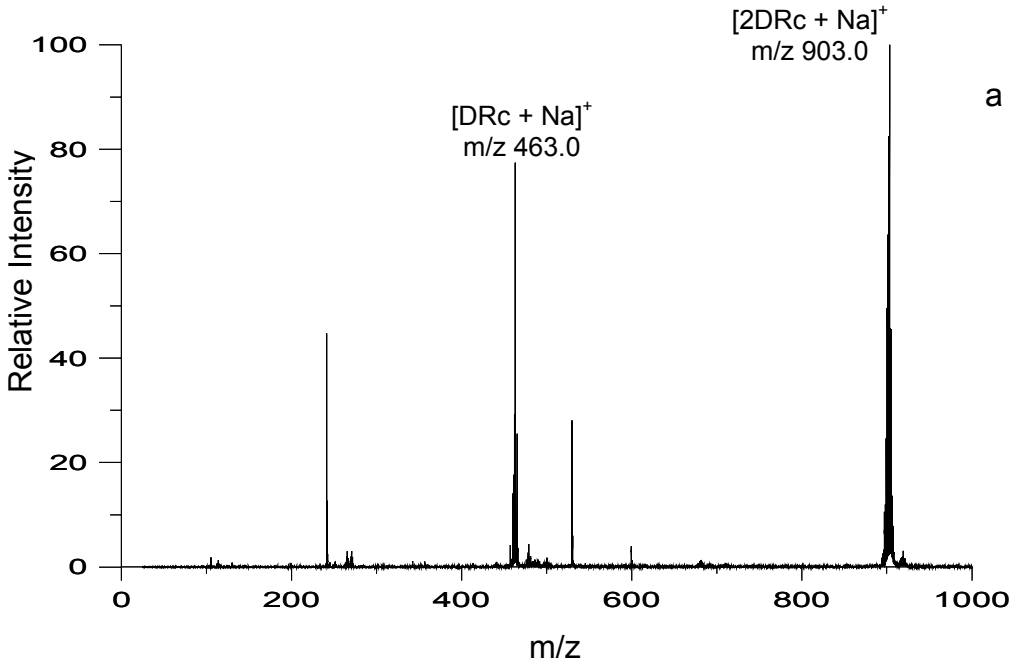
[2DRc + Na]+
m/z 903.0
a
[DRc + Na]+
m/z 463.0
Relative Intensity
m/z

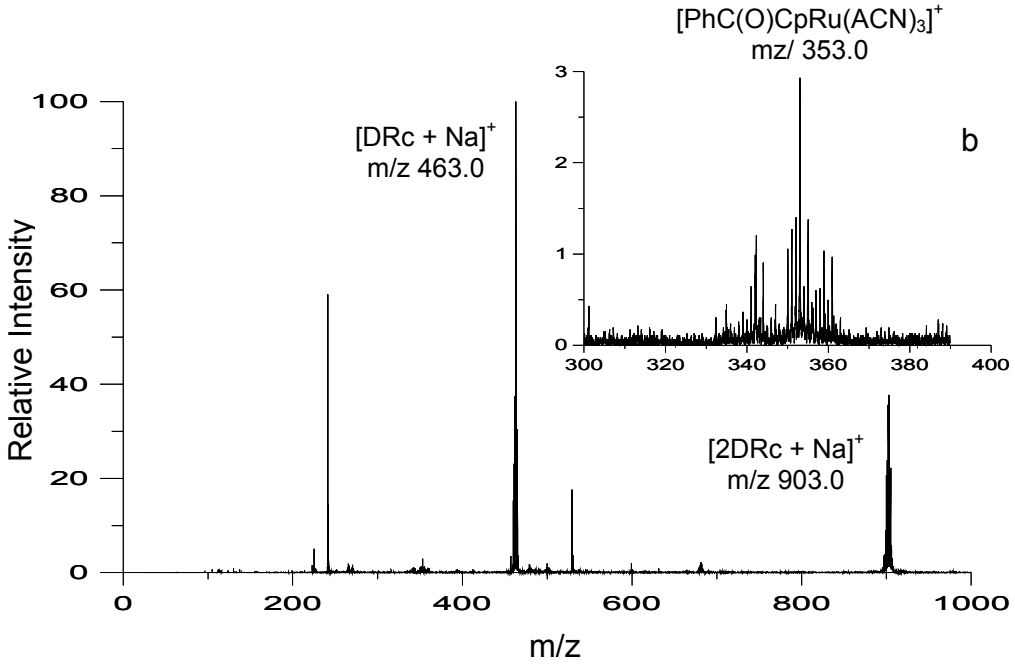
[PhC(O)CpRu(ACN)3]+
mz/ 353.0
b
[DRc + Na]+
m/z 463.0
[2DRc + Na]+
m/z 903.0
Relative Intensity
m/z

Figure 3.25: Mass Spectrum of Benzoylruthenocene in CCl_4

Mass spectrum of a solution of BRc in CCl_4 before (spectrum a) and after (spectrum b) 10 minutes of irradiation with white light (λ>290 nm).

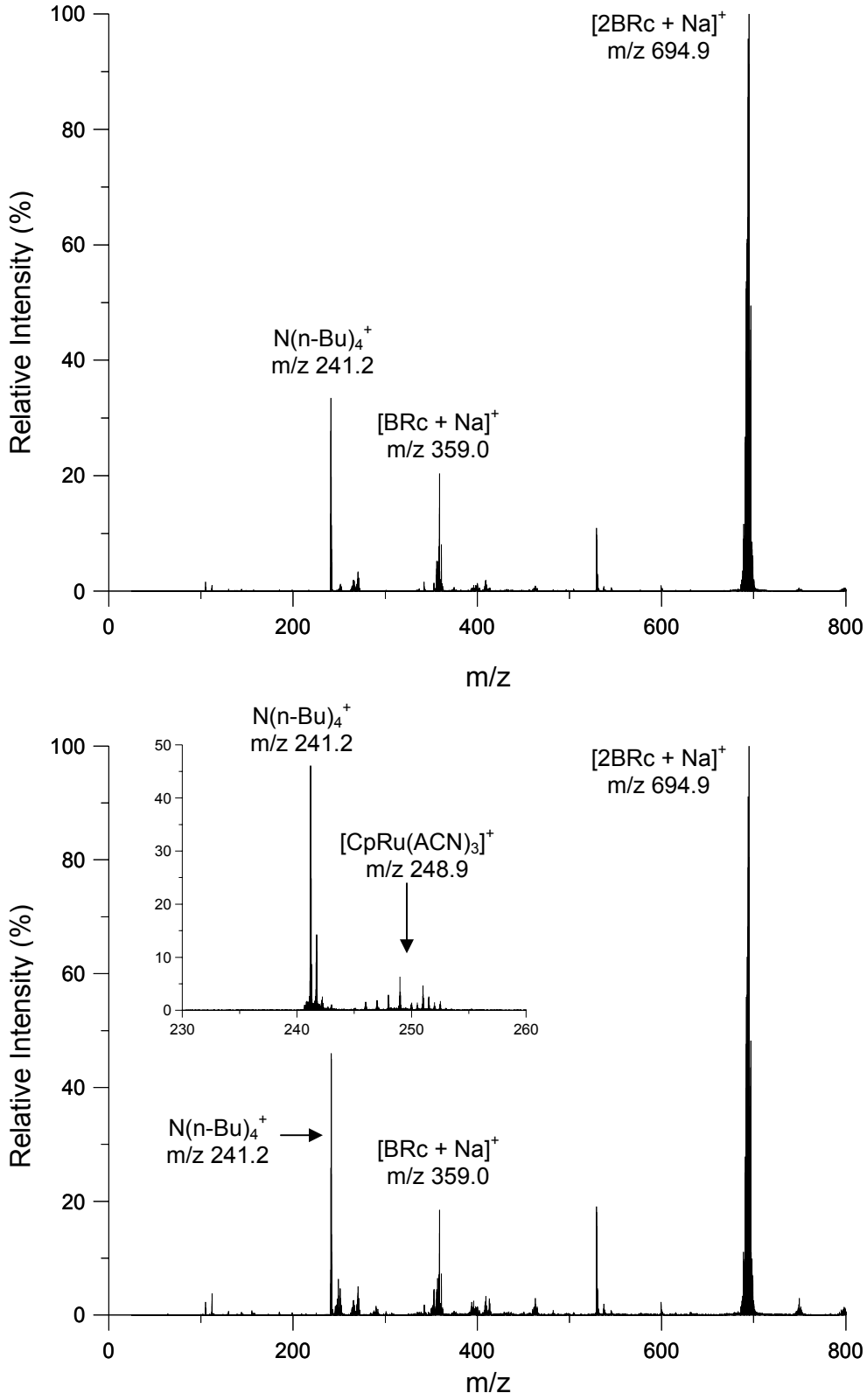
[2BRc + Na]+
m/z 694.9
N(n-Bu)4+
m/z 241.2
[BRc + Na]+
m/z 359.0
Relative Intensity (%)
m/z
[CpRu(ACN)3]+
m/z 248.9

is the presence of either $[PhC(O)CpRu(ACN)_3]^+$ at m/z 353.0 in the case of DRc or $[CpRu(ACN)_3]^+$ at m/z 248.9 in the case of BRc. These half sandwich structures are seen in very low intensity (~5% relative abundance) indicating that heterolytic ring cleavage akin to that shown for the iron analogs in equation 3.7 is not the favored photochemical process for the ruthenium compounds. To illustrate this point, consider the online photolysis procedure for DFc where micromolar concentrations of the metallocene in ACN were exposed to monochromatic light for less than one second, and the half sandwich complex was still seen. While in the case of DRc and BRc, millimolar concentrations of metallocene in ACN were exposed to white light for a minimum of 20 minutes, and no half-sandwich compounds were seen. We suspect that the major ruthenium-containing photoproduct is the precipitate produced during photolysis in CCl_4. Furthermore, since the brown precipitate is only produced when CCl_4 is used as the solvent, we propose that the favored photochemical pathway is the photooxidation of the metallocene.

3.10 An Alternative Mechanism for Anionic Photoinitiation When Using Benzoyl-Substituted Ruthenocenes

When mass spectrometry failed to indicate that heterolytic ring cleavage was the favored photochemical pathway, we undertook studies to determine the mechanism of photoinitiation for the anionic polymerization of ethyl 2-cyanoacrylate (CA) using benzoylruthenocene (BRc) and 1,1'-dibenzoylruthenocene (DRc). Since a photochemical reaction was noticed in

CCl_4 and not ACN, we thought that perhaps the active mechanism is the charge-transfer-to-solvent (CTTS) mechanism described for ferrocene (Fc) and the parent ruthenocene (Rc) compound (equation 3.4). To test this theory, we undertook studies to determine if a ground-state electron donor-acceptor complex is formed between the benzoyl-substituted metallocene and an electron accepting solvent. A search of the literature showed that no one had yet determined if these benzoyl-substituted ruthenocenes formed a ground state donor-acceptor complex with CCl_4, so we sought to determine if this did in fact happen by measuring the electronic absorption spectra of BRc in a mixture containing various amounts of cyclohexane and CCl_4. Cyclohexane was chosen as the second solvent because the low energy band of BRc is very sensitive to the polarity of the solvent, and cyclohexane and CCl_4 have similar dielectric constants, (ε = 2.238 and 2.023 for CCl_4 and cyclohexane, respectively), but cyclohexane is not a good electron acceptor. Since the dielectric constants are similar, any spectral changes that occur are most likely not due to changes in solvent polarity, but rather they are due to the electron accepting nature of CCl_4, and therefore indicate the formation of a ground state electron donor-acceptor complex between the CCl_4 and the metallocene.

Figure 3.26 shows the electronic absorption spectra of BRc in cyclohexane and carbon tetrachloride; inset is the difference spectrum. The maximum absorption in CCl_4 occurs at 346 nm, with an extinction coefficient of 1320 $M^{-1}cm^{-1}$. While it is possible that this increase in absorption is due to solvent effects, there is much more of an effect seen than was expected based

Figure 3.26: Electronic Absorption Spectra of Benzoylruthenocene in Cyclohexane and Carbon Tetrachloride

Shown here are the spectra of BRc in cyclohexane (a) and carbon tetrachloride (b). Inset is the difference spectrum indicating the formation of a charge-transfer-to-solvent band.

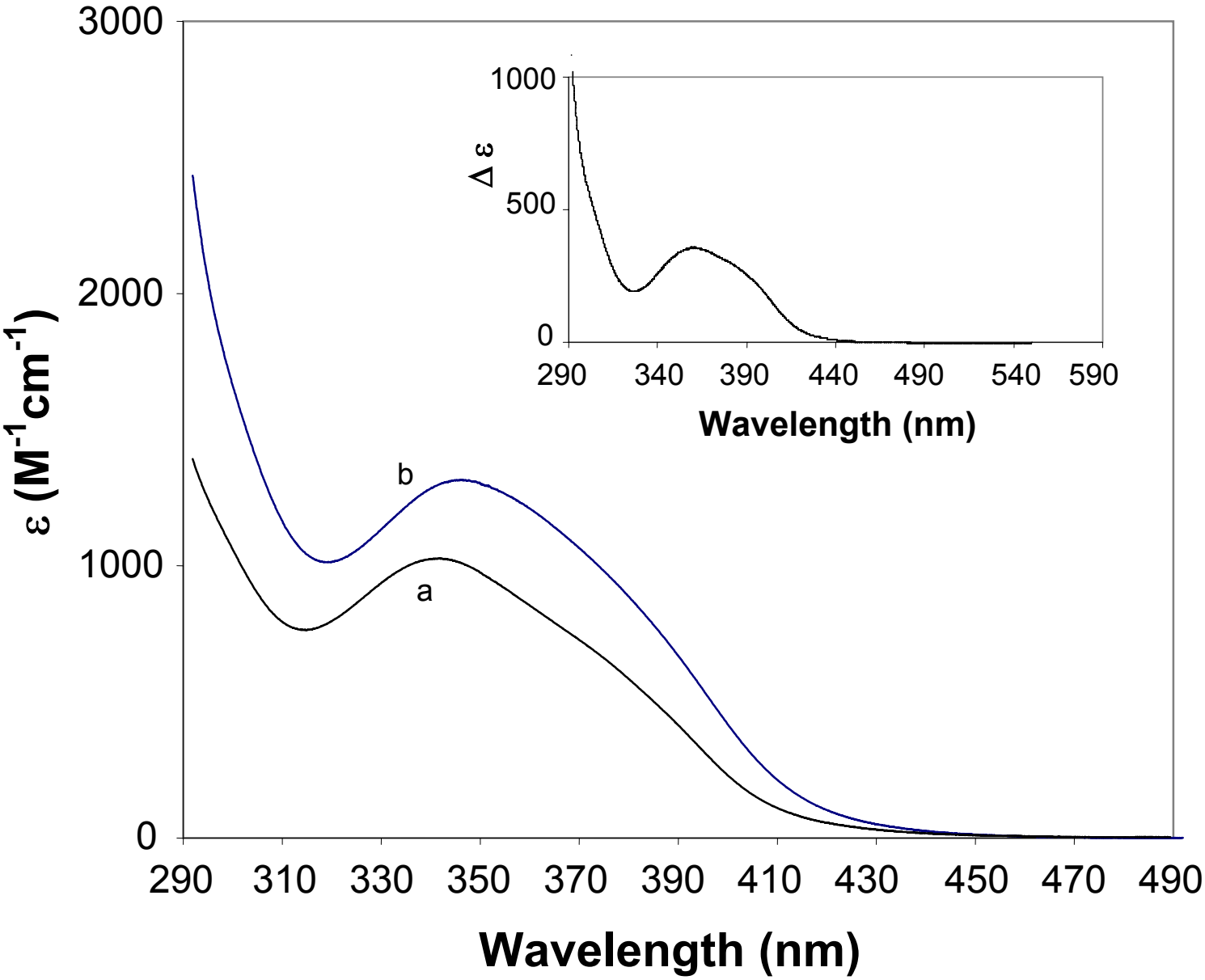
3000
2000
1000
0
ε (M-1cm-1)
290
310
330
350
370
390
410
430
450
470
490
Wavelength (nm)
a
b
1000
500
0
Δ ε
290
340
390
440
490
540
590
Wavelength (nm)

on the data reported in Table 3.3. Therefore, the new band that appears at 357 nm in the difference spectrum is assigned as charge-transfer-to-solvent (CTTS). Since the same sort of interaction is seen in the case of ferrocene or ruthenocene in CCl_4 and CA, it seems logical that the same CTTS mechanism for the photoinitiation of CA that occurs with the unsubstituted metallocenes occurs with the benzoyl-substituted ruthenocenes (equation 3.11).

$$BRc + CA \rightleftharpoons \{BRc, CA\} \xrightarrow{h\nu} BRc^{+} + CA^{\bullet -} \qquad (3.11)$$

CHAPTER 4

CONCLUDING REMARKS ON THE USE OF BENZOYL-SUBSTITUTED GROUP 8 METALLOCENES AS PHOTOINITIATORS FOR THE ANIONIC POLYMERIZATION OF ETHYL 2-CYANOACRYLATE

4.1 Concluding Remarks

In this study I have demonstrated (section 3.1) that in addition to 1,1'-dibenzoylferrocene and ruthenocene, which were known photoinitiators, ferrocene, benzoylruthenocene, and 1,1'-dibenzoylruthenocene also function as photoinitiators for the anionic polymerization of ethyl 2-cyanoacrylate. Further, I have shown ruthenocene and 1,1'-dibenzoylferrocene are more efficient photoinitiators than the other metallocenes studied. The data in section 3.2 indicate that 1,1'-dibenzoylferrocene, and ruthenocene are the best photoinitiators, meaning that they initiate the anionic polymerization of ethyl 2-cyanoacrylate with the fastest rate, while 1,1'-dibenzoylruthenocene and ferrocene are the poorest photoinitiators for the desired reaction. It is interesting to note that in the iron compounds, the efficiency of a metallocene towards the photoinitiated anionic polymerization of CA increases upon the addition of benzoyl groups to the cyclopentadienyl rings. In contrast, we see the opposite order of reactivity in the ruthenium compounds; in other words, as benzoyl groups are added to one or more of the cyclopentadienyl rings of ruthenocene, the resulting compound becomes a less efficient photoinitiator for the anionic polymerization of CA. A detailed study of the spectroscopic properties of these compounds was then undertaken in an attempt to understand this order of reactivity.

The unsubstituted ferrocene compound is a fairly poor photoinitiator, whereas 1,1'-dibenzoylferrocene is a good photoinitiator for the anionic polymerization of CA. This disparity in efficiency is due to a duality of

mechanism. Both of these iron-containing compounds undergo a charge-transfer photoreaction; however, the nature of the charge-transfer character in each system is inherently different. The parent compound, ferrocene, undergoes an *inter*molecular charge transfer reaction where an electron is passed from the iron atom to an electron accepting solvent molecule, such as the CA monomer (equation 3.4). To lend more credibility to this intermolecular charge-transfer-to-solvent (CTTS) mechanism, evidence has been presented indicating the formation of a ground-state electron donor-acceptor complex between the metallocene and monomer. As well, theoretical data predict the radical anion of the cyanoacrylate monomer to be a stable species, and direct spectral evidence for the formation of the oxidized ferrocene product (ferricinium) has been presented.

In the case of the benzoyl-substituted ferrocenes, the nature of this charge transfer character is an *intra*molecular charge transfer from the iron atom onto the cyclopentadienyl ring where it is then delocalized over the carbonyl group conjugated to the cyclopentadienyl ring (Figure 1.9). Data to support this assignment has been presented in the form of resonance Raman spectra which indicate a large perturbation of the carbonyl bond upon absorption of a photon of light corresponding to the low-energy electronic transition of these compounds. This metal-to-ligand charge transfer character has been used to explain the weakening of the iron-ring bond which leads to photoinduced ring loss. Further support that ring loss is the primary photochemical reaction has been presented in the form of mass spectral data, which indicate the formation of the half-

sandwich compound when a solution of 1,1'-dibenzoylferrocene is irradiated as it flowed through an electrospray tip.

As mentioned previously, the data presented in this manuscript indicate that ruthenocene is a better photoinitiator than ferrocene for the anionic polymerization of ethyl 2-cyanoacrylate. One possible reason for this is that ruthenocene is easier to oxidize than ferrocene. The electrochemical data available on the oxidation of ruthenocene is varied, and the interpretation of electrochemical data on ruthenocene can be difficult to interpret.[85] In one reference[35] it is clearly stated that ruthenocene is easier to oxidize than ferrocene, but the author then goes on to cite the reduction potentials +0.11 V and +0.55 V for ferrocene and ruthenocene, respectively. This general trend for the ordering of the one-electron reduction potential is generally agreed upon in the literature.[85,86] The only way these two seemingly contradictory statements make sense is if you consider the entire electrochemical process. Ruthenocene undergoes a net two electron oxidation in most media whereas ferrocene only undergoes a one electron oxidation process, even at extremely high potentials.[35] Perhaps this is the reason why ruthenocene is a better photoinitiator than ferrocene for the anionic polymerization mechanism described in this text.

This project also determined that the benzoyl-substituted ruthenocenes do not undergo efficient photo-induced ring loss analogous to the benzoyl-substituted ferrocenes. The most likely reason for this is that the metal-ring bond is stronger in ruthenocene than it is in ferrocene.[35,39,87] Therefore, even though the low-energy electronic transitions of the benzoyl-substituted ruthenocenes do

exhibit metal-to-ligand charge transfer character, the bond holding the ring to the metal is inherently stronger, making dissociation of the ring a less favorable process; therefore there is no duality of mechanism for the benzoyl-substituted ruthenocenes. After it is understood that photoinduced ring loss is not an option, it is much easier to understand why addition of benzoyl-groups to ruthenocene results in a less efficient photoinitiator for the anionic polymerization of ethyl 2-cyanoacrylate. It is well understood that the addition of electron withdrawing groups to one or more of the cyclopentadienyl rings of a metallocene make the reduction potential more positive (i.e. the metallocene becomes more difficult to oxidize).[86,88] The reason for this can be evaluated in terms of either the shielding of the metal atom by the carbonyl group, or by the electron-withdrawing power of the substituent. Adding electron-withdrawing groups to the cyclopentadienyl rings should result in a decrease of electron density around the metal atom, thereby making the metal more difficult to oxidize, and rendering an intermolecular charge-transfer-to-solvent initiation pathway less likely.

4.2 Future Studies

There are a couple of different directions to take this project in the future. One is to look at the detailed mechanism of ring loss upon exciting the low-energy electronic transition of 1,1'-dibenzoylferrocene. There are two different possible situations which would lead to the same result (the photodissociation of a benzoyl-substituted cyclopentadienide anion). One option is that the excited state populated by the absorption of a photon (in the low

energy band) is in and of itself a dissociative state leading to a prompt photochemical reaction. In this case where the photochemical reaction is prompt; one would expect the quantum yield to be wavelength dependent. The other option is that the excited state populated is not a dissociative state, but that the vibrationally excited molecule must relax into the dissocative state leading to a delayed photochemical reaction. In this latter case where the photochemical reaction is delayed, one would expect the quantum yield to be wavelength independent.

Another direction to take this project would be to attempt on-line ESI studies (akin to those described for 1,1'-dibenzoylferrocene) using the ruthenium compounds. This would require a different laser (one that provides higher energy light), and one must also check that the electron-accepting solvents needed (most likely carbon tetrachloride rather than CA) can be sprayed from the ESI source. These experiments might be used to identify the ruthenium photoproducts in the precipitate, before they crash out of solution.

CHAPTER 5

PHOTOINITIATED ANIONIC POLYMERIZATION OF METHYL METHACRYLATE

5.1 Polymerization of Methyl Methacrylate

As mentioned in the introduction of this text (section 1.9), the final goal of this project is to expand the use of Group 8 metallocene photoinitiators to other monomers. Methyl methacrylate (MMA) was chosen since it is one of the most widely used industrial monomers. MMA is used, either by itself or as part of a copolymer, in many everyday objects, including plexiglass®, lighting displays, and floor and wall coatings. Since the MMA monomer is readily polymerized via a radical pathway, most research in the area of MMA polymerization has involved the use of radical initiators. Radical polymerization of MMA results in a high yield of high molecular weight polymer; however, the product obtained from radical polymerizations is usually of a very high molecular weight distribution (MWD), indicating that radical synthesis offers little or no control over the polymer. Since the properties of the polymer product depend on the MWD, much research has been focused on the controlled polymerization of MMA. While some advances have been made in the controlled radical polymerization of MMA, these methods usually involve the addition of chain transfer agents or the use of a co-monomer, both of which can introduce a different functionality to part of the polymer chain, thereby changing the characteristics of the polymer.[89]

The broad molecular weight distribution of poly(MMA) produced via radical mechanisms arises from either the coupling or the disproportionation of the polymer chains. The more polymer chains that exist in solution, the more chances they have of interacting to terminate the polymerization, thus increasing

the molecular weight distribution of the polymers.[90] This is where ionic polymerizations come in to play. Ionic polymerizations are not as susceptible to chain transfer reactions or termination reactions as radical polymerizations are. Because of the ester groups on the MMA molecule, it is not susceptible to cationic attack; however, it is susceptible to anionic attack, and this has led to many attempts at the controlled anionic polymerization of MMA. The types of anionic polymerization of MMA which will be discussed here can be classified in to three categories: ligated anionic polymerization ('classical' anionic polymerization), metal free anionic polymerization, and group transfer polymerization. Because metal-free anionic polymerization and group transfer polymerization are not well-suited to making co-polymers containing non-polar vinyl monomers, there is still much research into the classical anionic polymerization of MMA.

Before discussing the methods mentioned above in detail, it should be noted that while the anionic polymerization of MMA *can* be ideal in terms of control over the polymer formed, it is not perfect by any means. Anionic polymerization of MMA does not necessarily mean that a controlled reaction will result. Anionic polymerization of MMA requires rigorously anhydrous techniques to prevent protonation and consequent termination of the propagating polymer chain. Moreover, MMA is susceptible to other termination events; the most common is called backbiting. Both of these termination events are shown in Figure 5.1. The problem of backbiting can be alleviated to a certain extent by lowering the reaction temperature (to −78 ^{O}C), since at lower temperatures the

backbiting reaction becomes less favorable. However, this technique for alleviating backbiting is not ideal, since in an industrial setting, maintaining the low temperature might not be feasible, owing to heat transfer problems, and if it is feasible, it would likely be cost prohibitive.[91]

Most of the recent advances in classical anionic polymerization of MMA have focused on the development and use of new additives, understanding and controlling the role of the counterion in the anionic polymerization, and to lesser extent solvent effects. It is fairly well understood that aprotic non-polar solvents, such as tetrahydrofuran or acetonitrile, are preferred for anionic polymerizations since they support the formation of ion pairs in solution while not protonating (and therefore terminating) anionic initiators and/or propagating anions.

The propagating end in the anionic polymerization of methyl methacrylate is an ester enolate anion. Ester enolate anions are stabilized by forming aggregates; however, the formation of aggregates in equilibrium with the free anion inhibits the control of the polymerization process by undergoing side reactions which are favored by the formation of aggregates.[92] Of the many side reactions MMA undergoes, many of them are explained by the fact that MMA contains a carbonyl group which is also susceptible to nucleophilic attack, and therefore competes with the carbon-carbon double bond. One way to minimize carbonyl side reactions is to use a sterically hindered, stable anion as the initiator. The initiators of choice for this have been bulky organic compounds such as fluorenyl, t-butyl, biphenyl, and diphenylhexyl anions (with alkali metals as counterions). Since these anions are large, sterically hindered, and less

Figure 5.1: Termination Reactions of Methyl Methacrylate

Shown here are protonation (top) and backbiting (bottom) reactions which lead to premature termination of the growing anionic poly(MMA) chain.

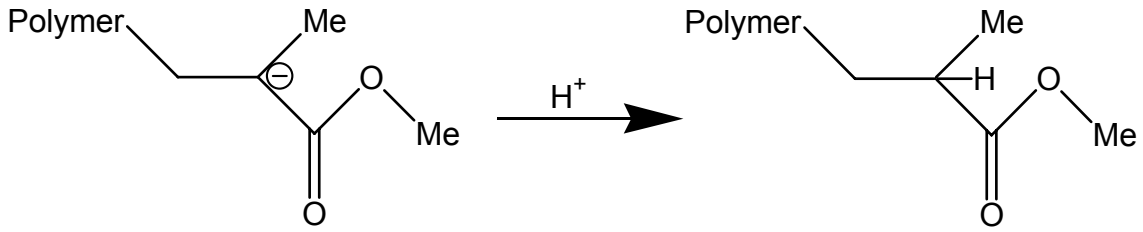
Polymer
Me
O
Me
O
H+
Polymer
Me
H
O
Me
O

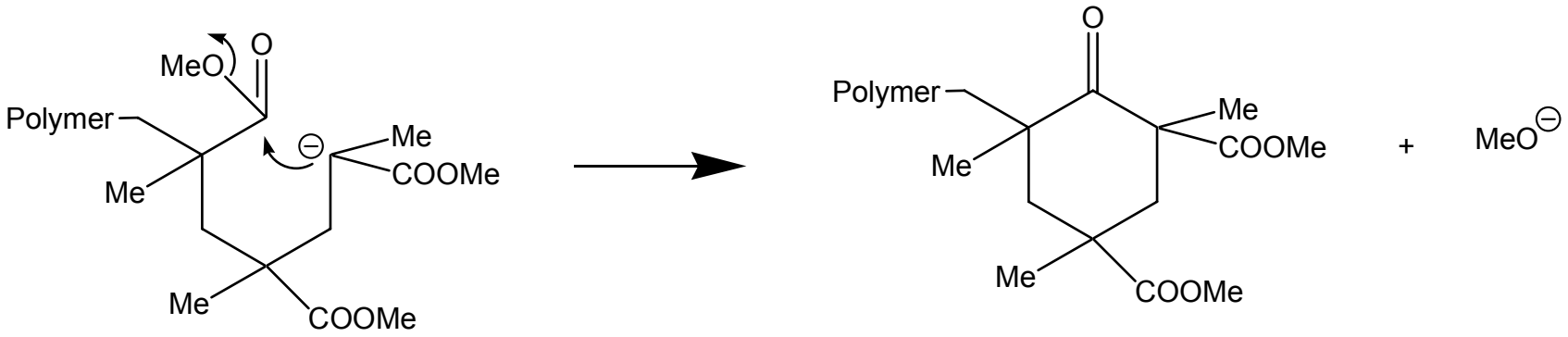
MeO
O
Polymer
Me
Me
COOMe
Me
COOMe
O
Polymer
Me
COOMe
Me
Me
COOMe
+
MeO

reactive that smaller inorganic anions they are less likely to attack the carbonyl group and lead to undesirable side reactions.[92]

More recent advances in anionic polymerization point to the addition of various compounds, which generally also have an alkali metal ion, to help control the reaction; this process is called ligated anionic polymerization. The role of the ligand is multi-faceted: a good ligand must regulate the electron density in one or both parts of the metal-ester enolate ion pair and/or provide a steric barrier by blocking an area around the ion pair to minimize secondary reactions and /or promote a complexation equilibrium between different ion pairs or aggregates which lead to a unique active species.[93] Owing to the promising nature of ligated anionic polymerization, it has been an active area of interest, mainly focusing on the use of various additives; most commonly alkali metal *tert*-alkoxides and alkali metal halides.[93,94]

Alkali metal *t*-alkoxides (most commonly *t*-BuOLi) give quantitative polymerization in non-polar solvents such as toluene; however, the reaction is slow (compared to other initiators) and the initiator efficiency is low. It has been proposed that the role of the added alkali metal *t*-alkoxide is to protect the propagating end of the polymer by complexing with it. Exactly how the *t*-alkoxide performs this task has been the subject of debate. There are several structures that accurately depict how this might happen, but definitive evidence for one structure over the others is not available. It is generally agreed that the alkali metal *t*-alkoxides complex the propagating end and coordinate to the incoming monomer.[89,92-94] Lochmann initially proposed, and Jerome later concurred,

that the dimers shown in Figure 5.2a exist in equilibrium with a tetrameric structure;[93,95] this assertion was based on using a small model compound. Other groups have discounted this based on steric hindrance from the polymer chain which would pose a barrier to the formation of a tetrameric structure;[89,92,94,96] thus the dimeric structures shown in Figure 5.2a are currently accepted as accurate.

As far as using alkali metal halides to help control the anionic polymerization of MMA, the compound of choice is almost exclusively LiCl;[89,93,94] though Baskaran and co-workers have shown that addition of $LiClO_4$ has a similar effect to that seen when using LiCl (and it is presumed to act in the same manner).[97,98] In contrast to the alkali metal *t*-alkoxides, how the alkali metal halides promote the control of the polymerization is much better understood. For simplicity we will consider the most studied system, that of LiCl and assume, as per the literature, that other alkali metal halides operate in the same way. Addition of LiCl to the reaction mixture has the effect of lowering the molecular weight distribution (indicating an increased amount of control over the reaction) only until a mole ratio of 1:1 is reached.[89,94] After this critical ratio, addition of excess LiCl has no further effect. This indicates that LiCl acts by forming a 1:1 adduct with the propagating end (Figure 5.2b) [89,94] and by doing so, prevents side reactions which could result in premature termination. Muller and co-workers showed the effect of LiCl on the kinetics of propagation and the molecular weight distribution are controlled by multiple equilibria. A simplified set of these equilibria are shown in equation 5.1.[89]

$$R^-.....Li^+ \rightleftharpoons R^- / S / Li^+ \rightleftharpoons R^-Li^+ \qquad (5.1)$$

Free Solvent Separated Contact

Acrylic monomers, such as methyl methacrylate, are capable of undergoing Claisen condensation reactions (an example is backbiting) which results in the expulsion of an alkoxide and termination of the polymerization. Furthermore, it has been proposed that the presence of alkali metal cations can promote the Claisen condensation by coordinating to the enolate anion as shown in Figure5.3.[91] Metal-free anionic polymerization (MFAP) was designed by Reetz to avoid this reaction since there is no metal cation present.[91] The most common cation used is tetraalkylammonium, though other groups indicate the use of polyiminophosphphazene or tetraphenylphosphonium as the cation.[25,91,99-105] Regardless of which cation is used, it has been proposed that none of these cations are able to coordinate closely with the ester group, and subsequently promote alkoxide elimination.[91,104] The exact role of the cation in the MFAP systems is not yet fully understood, and it should be pointed out that LiCl and $LiClO_4$ are common additives that promote the ligated anionic polymerization of methyl methacrylate.[89,92] If the Li^+ ions promoted alkoxide elimination as proposed, it seems that lithium salts would *not* be useful promoters for the ligated anionic polymerization of MMA.

The initial reports on MFAP involved the use of alkylthiolates or arylthiolates to initiate the anionic polymerization of relatively reactive monomers such as n-butylacrylate. These alkyl (or aryl) thiolates gave near quantitative

Figure 5.2: Structures Between the Propagating Anion of MMA and Alkali Metal Ligands

Shown here are the proposed dimeric structures which indicate how an alkali metal *t*-alkoxide coordinates to MMA (a), and the adduct formed between LiCl and the propagating anion of MMA (b).

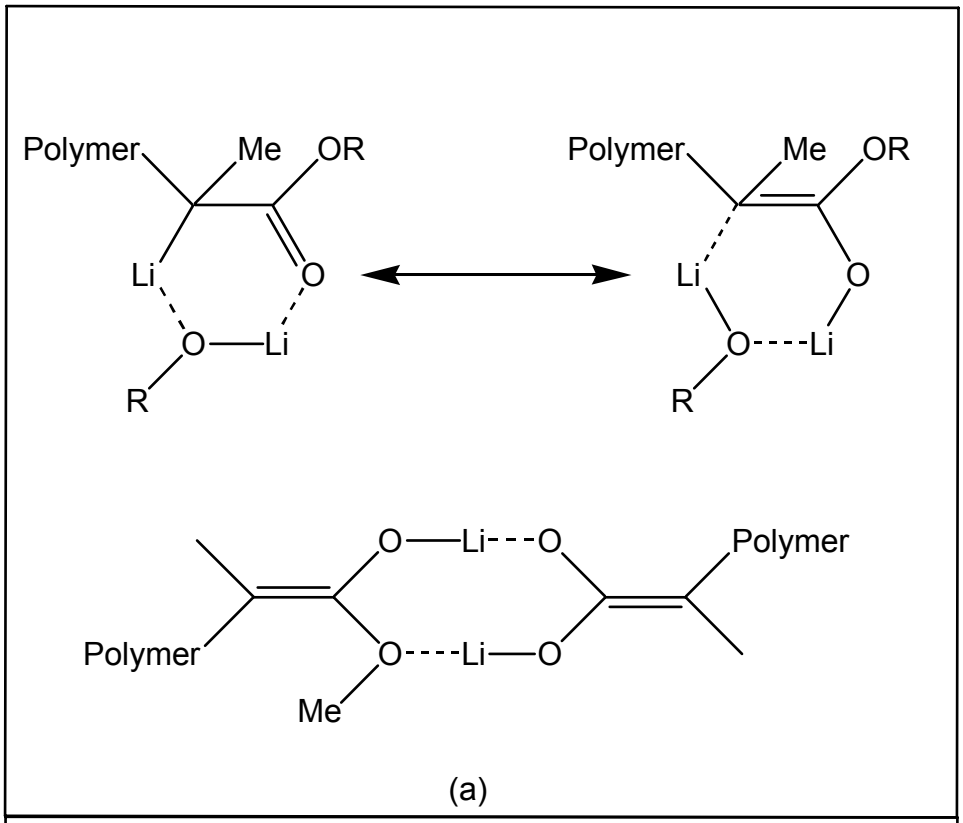
Polymer
Me
OR
Li
O
O
Li
R
Polymer
Me
OR
Li
O
O
Li
R
O
Li
O
Polymer
Polymer
O
Li
O
Me

(a)

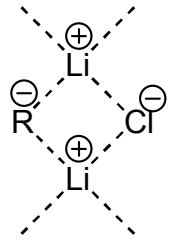
Li
R
Cl
Li

(b)

polymer yields; but they were relatively unstable compounds (decomposing via dealkylation), gave lower than expected molecular weights for the polymer, and the polymer product had a high molecular weight distribution (indicating a lack of control).[100] Reetz proposed that a side reaction occurred which resulted in the elimination of the thiol from the end of the polymer chain. This has two important consequences. Firstly, elimination of the thiol caused termination of the polymerization, and secondly, the newly released thiol could then begin a new polymer chain; these two consequences taken together account for the low molecular weight and the high molecular weight distribution of the polymer product, despite the high yield. MFAP was later expanded to use anions such as carbazole in addition to malonates and other resonance stabilized carbanions to polymerize a variety of acrylic monomers, including methyl methacrylate, and oxiranes..[91,99,101,102,106] Figure 5.4 shows the structures of some of these anions.

Group transfer polymerization (GTP) is another method for the controlled polymerization of acrylic monomers, specifically methyl methacrylate. Originally developed by Webster et. al. from Du Pont in 1983, GTP uses a silyl ketene acetal as an initiator for the polymerization of acrylic monomers with a base or Lewis acid as a co-initiator at room temperature.[107] We shall focus on the nucleophile-assisted GTP, since the focus of this work is anionic polymerization. GTP is a sequential Mukiyama-Michael addition reaction between the silyl ketene acetal and an alkyl methacrylate. The job of the nucleophile is to activate

Figure 5.3: Alkali Metal Promoted Claisen Condensation in MMA

It has been proposed that the presence of alkali metal cations in solution promotes a Claisen condensation reaction (i.e., backbiting) as shown here for Li^+.

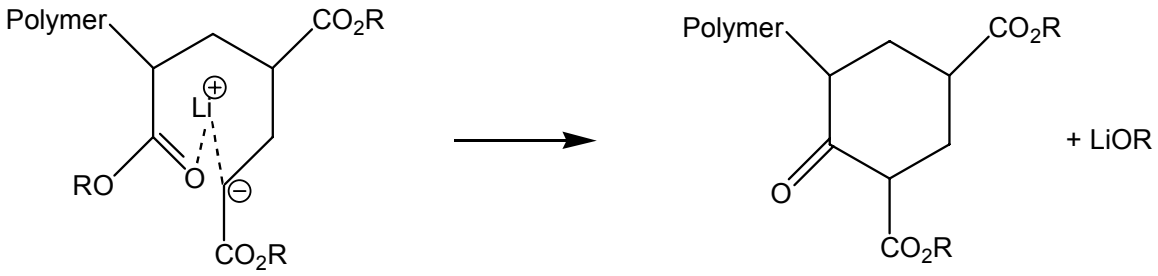
Polymer
CO2R
Li
RO
O
CO2R
Polymer
CO2R
O
CO2R
+ LiOR

Figure 5.4: Examples of Some Anions used in Metal-Free Anionic Polymerization

Shown here are the structures of two ester-enolate anions, as well as the carbazole and fluorenyl anions used in MFAP.

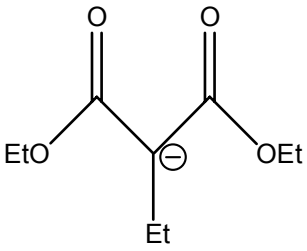
O
O
EtO
OEt
Et

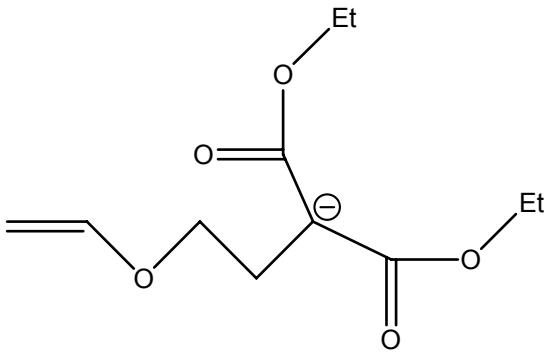
Et
O
O
Et
O
O
O

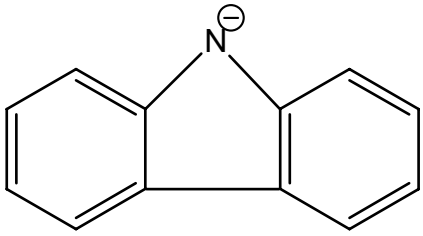
N

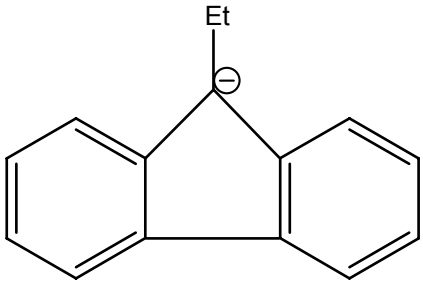
Et

the silyl ketene acetal to form a pentacoordinate siliconate anion. This anion then acts to protect the propagating end from premature termination by coordinating incoming monomer molecules.

The mechanism of group transfer polymerization has been the subject of much discussion in the literature. Webster and co-workers originally proposed,[107] and several groups later agreed,[92,108,109] that polymerization proceeded through an associative mechanism. Figure 5.5 shows this mechanism for the polymerization of methyl methacrylate using 1-methoxy-2-methyl-1-trimethylsiloxypropene (MTS) as the initiator and a generic nucleophile (Nu^-) as the co-initiator. In this mechanism, the nucleophile attacks the silicon atom in MTS to form the pentacoordinate siliconate anion. The siliconate anion then coordinates to the carbonyl oxygen atom of the incoming monomer unit, thereby protecting it from side reactions resulting from undesirable carbonyl chemistry.

Since Webster's initial report, several groups have built upon, expanded, and lent their insight into the mechanism of this process. The original silicon reagents used for GTP were trimethylsilyl ketene acetals (of which MTS is the most common); however, many silicon reagents such as trimethysilylcyanide and other C-silyl comounds, as well as some germanium and tin analogs, have been used as GTP initiators since then.[107,110,111] As far as the co-initiators used, there have been reports of using various anions such as fluoride, bifluoride, trimethyldifluorosiliconate, azide, cyanide, carboxylate, phenolates, and ester enolate anions;[112-115] some of these anions are shown in Figure 5.6

Fig 5.5: Associative Mechanism for Nucleuophile-Assisted Group Transfer Polymerization

Shown here is the associative mechanism for the Group Transfer Polymerization of MMA using a generic nucleophile, Nu^-, as the co-initiator and 1-methoxy-2-methyl-1-trimethylsiloxypropene (MTS) as the initiator.

R
R
R
Si
O
MeO
+ Nu⊖
Nu
R
Si
R
R
O
MeO
MeO
O
Nu
R
R
Si
R
OMe
O
O
MeO
⊖
R
R
R
Si
O
OMe
O
MeO
+ Nu⊖
Nu
R
Si
R
R
O
OMe
O
MeO

Figure 5.6: Examples of Some Anions Used in Group Transfer Polymerization

Shown here are the structures of trimethyldifluorosiliconate, carboxylate, phenolate, and an ester enolate anion. All of these anions have been used as nucleuophilic co-initiators for group transfer polymerization.

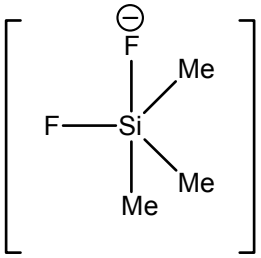
F
Me
F
Si
Me
Me

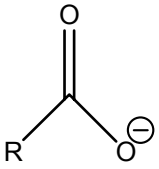
O
R
O

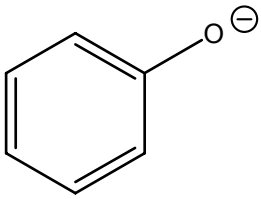
O

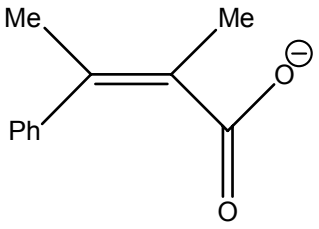
Me
Me
O
Ph
O

The classical anionic polymerization, metal-free anionic polymerization, and group transfer polymerization methods described were of particular interest to our group since they all indicate the use of a resonance stabilized ester enolate carbanion as an initiator (or co-initiator) for the anionic polymerization of MMA. Since the anion of cyanoacrylate is a resonance stabilized ester enolate carbanion, it should be able to initiate the anionic polymerization of MMA. Further, since we can generate this anion photochemically (c.f. Section 1.3), it was our goal to develop photochemical analogs of these methods for the anionic polymerization of MMA as outlined in Figure 5.7.

5.2 Experimental Methods

Purification of Reagents:

Tetrahydrofuran, THF, was dried by refluxing over a sodium-potassium alloy with benzophenone. THF was collected from the still immediately prior to each use. Methyl methacrylate, MMA, was purified by stirring overnight with calcium hydride until no more bubbles (which indicate the presence of water) formed. MMA was then distilled from the calcium hydride; the first and last ~20% were discarded. Triisobutylaluminum was added to the distillate until a persistent pale yellow color developed. MMA was then distilled from triisobutylaluminum, again discarding the first and last ~20%. The MMA was then sealed under Ar with a rubber septum, and stored in a freezer (−20 ^{o}C) until use (within a few days). Ethyl 2-cyanoacrylate (high purity, from Loctite), 1-methoxy-2-methyl-1-trimethylsiloxypropene (MTS) (99%, Aldrich), and tetrabutylammonium

Figure 5.7: Scheme for the Anionic Polymerization of Methyl Methacrylate. Shown here is an anion (X^-) which attacks the carbon-carbon double bond of ethyl 2-cyanoacrylate (CA). The resulting resonance stabilized carbanion then attacks the carbon-carbon double bond of the methyl methacrylate monomer to initiate polymerization, possibly with MTS as a mediator (not shown).

X
CA
N
C
O
O
X
N
C
O
O
CH3
MMA
O
CH3
N
C
X
O
CH3
O
CH3
O
O

thiocyanate (99%, Fluka), TBASCN, (except where indicated) were used as received.

Preparation of Reinecke's Salt ($K[Cr(NH_3)_2(NCS)_4]$ or K^+R^-):

Reinecke's salt is commercially available as the ammonium salt and was converted to the potassium salt as per literature procedure.[31] Under red light, 100 g (one bottle) of the ammonium salt was dissolved in 600 mL of warm (~50°C) water and stirred for 5 minutes. The warm solution was then filtered through qualitative filter paper (Whatman 54) to remove insoluble residues, and 45 g of solid KNO_3 was added to the filtrate. The mixture was stirred for 3 minutes while in a warm (~50°C) water bath and then placed in an ice bath saturated with NaCl. After 10 to 15 minutes the solution was filtered and the crystals were collected. This procedure was repeated for a second time using 360 mL of water and 24 g of KNO_3. After the crystals were collected a second time, they were recrystallized a third time using 180 mL of water and 1.5 g KNO_3. The crystals were collected this time on a glass frit, washed with ice cold water, and then dried in a vacuum dessicator over P_2O_5. The purity of the final product was judged based on the extinction coefficients and tested for free thiocyanate using an Fe^{3+} assay[31] (an acceptable product had less than 1% free NCS^-).

Thermal Anionic Polymerization:

All glassware was dried at 120-125°C for 24 h, flamed upon removal from the oven, fitted with rubber septa, and purged with argon. In a glove box (using standard syringe techniques) were added to a 100 mL round bottom flask 30 mL of THF, 25.6 mL (240 mmole) of MMA, and 0.03 mL (0.27 mmole) of CA; this

solution was stirred for 10 minutes. Then a solution of 0.07 g (0.23 mmole) of TBASCN dissolved in ~1 mL of THF was added dropwise over 90 seconds. After the solution was stirred for 48 hours, 1 mL of methanol (MeOH) was added to quench the reaction. The resulting polymer was precipitated from solution by adding 150 mL of n-hexanes. The polymer was filtered, washed with n-hexanes, and then washed with water. The polymer was dried overnight at room temperature in a vacuum dessicator.

Thermal Group Transfer Polymerization:

All glassware was dried at 120-125°C for 24 h, flamed upon removal from the oven, and then filled with argon and fitted with rubber septa. In a glove box (using standard syringe techniques) were added to a 100 mL round bottom flask 30 mL of THF, 25.6 mL (240 mmole) of MMA, 2.4 mL (12 mmole) of MTS and 0.03 mL (0.27 mmole) of CA. This solution was allowed to stir for 10 minutes. Then a solution of 0.07 g (0.233 mmole) of TBASCN dissolved in 1 mL THF was added dropwise over 90 seconds. After the solution was stirred for 48 hours, 1 mL of MeOH was added to quench the reaction. The resulting polymer was precipitated from solution by adding 150 mL of n-hexanes. The polymer was filtered, washed with n-hexanes, and then washed with water. The polymer was dried overnight at room temperature in a vacuum dessicator.

Photochemical Anionic Polymerization:

All glassware was dried at 120-125°C for 24 h, flamed upon removal from the oven, fitted with rubber septa, and purged with argon. In a glove box (using standard syringe techniques) were added to a 100 mL round bottom flask 30 mL

of THF, 25.6 mL (240 mmole) of MMA, and 0.06 mL (0.54 mmole) of CA; this solution was stirred for 10 minutes. Then a solution of 0.35 g (0.98 mmole) of K^+R^- dissolved in ~1 mL of THF was added dropwise over 90 seconds. The solution was irradiated with 546-nm light for 13 hours, stirred for 48 hours, and then 1 mL of MeOH was added to quench the reaction. The resulting polymer was precipitated from solution by adding 150 mL of n-hexanes. The polymer was dissolved in chloroform and metal containing ionic species were removed by extraction with water one time past when the organic layer looked white. The polymer was re-precipitated in n-hexanes, washed as described above and dried overnight at room temperature in a vacuum dessicator.

Photochemical Group Transfer Polymerization:

All glassware was dried at 120-125°C for 24 h, flamed upon removal from the oven, and then filled with argon and fitted with rubber septa. In a glove box (using standard syringe techniques) were added to a 100 mL round bottom flask 30 mL of THF, 25.6 mL (240 mmole) of MMA, 2.4 mL (12 mmole) of MTS and 0.06 mL (0.54 mmole) of CA. This solution was allowed to stir for 10 minutes. Then a solution of 0.35 g (0.98 mmole) of Reinecke's Salt (K^+R^-) (or an equivalent molar amount of 1,1'-dibenzoylferrocene) dissolved in ~2 mL of THF was added. The solution was irradiated with 546-nm light for 13 hours, stirred for 48 hours, and then 1 mL of MeOH was added to quench the reaction. The resulting polymer was precipitated from solution by adding 150 mL of n-hexanes. The polymer was dissolved in chloroform and metal containing ionic species were removed by extraction with water one time past when the organic layer looked white. The

polymer was re-precipitated in n-hexanes, washed as described above and dried overnight at room temperature in a vacuum dessicator.

There are some variations to this procedure, and they will be discussed later on in this chapter.

5.3 Classical Anionic Polymerization of Methyl Methacrylate

Initial results obtained by Dr. X. Li in our group were promising, though the polymer yield was low (~30%). An attempt (by me) was made to polymerize MMA anionically using a thermal source of NCS^-. The chosen mole ratio of reagents was 80:7:1 (MMA:CA:NCS^-). Forty eight hours later, after working up the product, about 1 g (15% yield) of polymer was isolated. Unfortunately, this was shown by elemental analysis to be mostly poly(ethyl 2-cyanoacrylate). In hindsight this should have been anticipated since approximately 0.6 g of CA was added to the mixture, and CA is a more reactive monomer towards anionic attack. A second attempt at making poly(methyl methacrylate) was performed using a mole ratio of 1000:1:1 (MMA:CA:NCS^-). This ratio was chosen to minimize the production of poly(CA) since only 0.03 mL of CA was added. After forty seven hours, the product was worked up and 3.3 g (13%) of polymer was recovered. Elemental analysis of the product was consistent with pure MMA monomer (%C 59.9 theoretical, 59.4 actual; %H 8.07 theoretical, 8.02 actual; %N 0.0 theoretical, 0.0% actual).

The ultimate goal of this project was to photoinitiate the anionic polymerization of MMA. Since it was shown that the unsubstituted metallocenes

and the benzoyl-substituted ruthenocenes photoinitiate the anionic polymerization of ethyl 2-cyanoacrylate via a charge-transfer-to-solvent mechanism, these compounds were not seen as viable photoinitiators for the methyl methacrylate polymerizations. It seems that these compounds would probably photoinitiate the polymerization reaction, but the likely course would be via a radical pathway. In order to avoid the possibility of forming polymer through a radical pathway, the chosen photoinitiators were 1,1'-dibenzoylferrocene and Reinecke's Salt (K^+R^-) since they both exhibit efficient photochemical release of an anion.[31,57]

A solution containing a 1000:2:4 (MMA:CA:K^+R^-) mole ratio was photolyzed (with 546 nm light) for 13 hours, and then left to stir in the dark. After forty-eight hours, the product was worked up, ionic metal containing species were removed from the sample by extraction with water, and ~3 g (13% yield) of a rock hard mass of a plastic-like material, which was mostly white with a slight purple-tint to it, was isolated. A second photochemical polymerization was performed using 1,1'- dibenzoylferrocene (DFc) as the photoinitiator. The mole ratio was 1000:2:4 (MMA:CA:DFc), and after irradiating for 13 hours with 546 nm light, stirring in the dark for 48 hours, and working the polymer up, very little (~1 g) polymer was obtained.

5.4 Group Transfer Polymerization of Methyl Methacrylate

Since the classical anionic polymerization reactions mentioned previously gave a low yield, attempts were made to increase the percent polymerization

using MTS as a mediator in the group transfer polymerization of MMA. Before attempting the photochemical analog, a solution was prepared containing a mole ratio of 1000:50:1:1 (MMA:MTS:CA:NCS^-). The solution was left to stir for 48 hours, and then worked up. When isolated, there was just over 12 g (48%) of polymer which had an elemental analysis consistent with pure MMA monomer (%C 59.9 theoretical, 59.4 actual; %H 8.07 theoretical, 7.97 actual; %N 0.0 theoretical, 0.0 actual).

The next step was the photochemical group transfer polymerization. This was accomplished by preparing a solution containing a mole ratio of 1000:50:2:4 (MMA:MTS:CA:K^+R^-). This solution was irradiated for 13 hours with 546 nm light and then left to stir in the dark for 48 hours. After working up the product, soluble metal containing ionic species were extracted by dissolving the product in methylene chloride and stirring with several portions of water one time past when the organic layer looked colorless. After reprecipitating the polymer, about 12 grams (46%) of polymer was obtained. Elemental analysis of the polymer was consistent with pure methyl methacrylate (%C 59.9 theoretical, 59.8 actual; %H 8.07 theoretical, 8.11 actual; %N 0.0 theoretical, 0.0 actual). A second attempt was made at this same procedure, except this time, a more intense light source was used (the 514 nm line from a Nd:YAG laser). After the final work up almost 12 g of polymer was recovered (44%). Elemental analysis of the polymer was consistent with pure methyl methacrylate (%C 59.9 theoretical, 59.9 actual; %H 8.07 theoretical, 8.2 actual; %N 0.0 theoretical, 0.0 actual).

After performing the photochemical polymerization using Reinecke's salt, the same procedure was attempted using 1,1'-dibenzoylferrocene (DFc) as the photoinitiator. This procedure produced roughly 12 g of polymer, however the DFc proved difficult to extract due to its insolubility in water; therefore no further data are provided on this polymer.

5.5 Problems that Arose in the Polymerization of Methyl Methacrylate

The preceding polymerizations were run before May of 2002. In May of 2002, there was an accident which caused the gloves on the glove box to break. After replacing the gloves, and cleaning out the glove box, some difficulties in producing polymer were encountered. Whether the glove box breaking and subsequently having a leak was the problem or not, the fact remains that with the exception of a two week period in September of 2002, neither the anionic nor the group transfer polymerization reactions were reproduced. Possible reasons for this irreproducibility can be summarized by two general thoughts. The first is that water had crept into the system somewhere along the line, thereby killing any anion that was produced before polymerization could take place. The second thought was that one of the reagents had been contaminated, or was of insufficient purity. Based on these ideas, we undertook a detailed, systematic study in hopes of identifying the cause of the problem.

In order to make sure that the problem was not the glove box itself, we tried a couple of things. First, a set of polymer runs were performed using a glove box which had oxygen and water sensors indicating the presence of less that 0.1

ppm of these impurities. On the same day, using the same reagents, a similar set of runs was performed using the glove box in our lab. In neither of these runs was polymer obtained in more than 10 % yield, thus indicating that the glove box was not the sole source of the problem. The standard polymerization procedure involved the use of syringes to transfer reagents from one container to the other while in the glove box. In order to again rule out the glove box as the source of the problem, a cannula was used to transfer the reagents from one container to another with an Ar/vacuum line (thus avoiding the use of the glove box). This did not result in polymer formation either. Had the glove box been the problem, either using a different glove box or a cannula would have fixed the problem since in both cases the reagents are never exposed to the atmosphere inside the glove box. The next thought was that since the glove box was not the problem, then one (or more) of the reagents must be.

The next thing attempted was to replace all of the reagents. New bottles of MMA, MTS, and CA were used to avoid any contaminants which may have been in the opened bottles. When using fresh reagents had no effect, the tetrabutylammonium thiocyanate (TBASCN) was recrystallized from benzene. Since TBASCN is very hygroscopic, it was stored under rigorously anhydrous conditions (in a closed bottle inside a second bottle which had Drierite® and calcium hydride as drying agents which was inside the glove box). Using new bottles of reagents and drying the TBASCN did not result in polymer formation.

The next thought was that the solvent, THF, was wet even though the THF still was the purple color which indicates that the benzophenone ketyl is present

(usually the sign of a healthy still). A new still was made using the same materials and glassware. When this had no effect on the polymerizations, several other glassware setups were attempted: In one setup, the one neck round bottom flask which held the refluxing solvent was replaced with a three neck round bottom flask which allowed for flushing the entire system with argon before each use. The thought was that maybe the THF had very minute traces of water in it so that the indicator did not change color, but there was still enough water present to inhibit anionic polymerization. In a second setup, the standard refluxing still (equivalent to ACE Glass Part 6617-35) was replaced with a distilling head assembly (equivalent to ACE Glass Part 5150) with a 3-neck round bottom flask which facilitated the transfer of THF using a cannula rather than a syringe. When neither of these new distillation setups showed any promise, we moved onto thinking that the MMA was contaminated.

Dr. Li had done some tests and discovered that certain suppliers of MMA were better than others. He advised me that Aldrich (99%) MMA was sufficiently pure that the entire purification procedure need not be done. In case Aldrich had changed their synthesis procedure and were now selling less pure MMA, the monomer was purified using what was referred to as the 'rigorous procedure' which was adapted by Dr. Li from the literature.[116] The rigorous procedure consisted of washing MMA three times with an equal volume of 10% NaOH and then washing the MMA five times with water. To remove traces of water, the MMA was initially dried over $MgSO_4$ and then (under argon protection) passed through a column containing 12 cm of activated basic alumina and 12 cm of 4Å

molecular sieves. The MMA was then distilled (under argon) twice, once from calcium hydride and then from triisobutylaluminum. Despite the new purification procedure, polymer was still not obtained.

In a final effort to discover the problem with the polymer synthesis, a polymer run was performed with a small amount of added triisobutylaluminum. This was done since it is known that this type of aluminum compound may facilitate the polymerization of MMA.[89,92,94] In this experiment, 1 mL of triisobutylaluminum was dissolved in 25 mL of THF, and then 1 mL of this solution was added to a standard polymer run of mole ratio 1000:1:1 (MMA:CA:NCS^-) (for a concentration of roughly 600 ppm triisobutylaluminum). In this polymer run, the yield was roughly 48%. This was very disheartening, since this may indicate that the reactions where polymer was produced were due to the presence of residual drying agent, and therefore not authentic results. However, it was pointed out that it was unlikely that the successful polymer runs were due to trace amounts of this particular contaminant for several reasons; one reason this is unlikely is that at least four different batches of purified monomer were used in successful polymer runs. The chances of getting the same amount of the same contaminant in the monomer on four different occasions were slim. Also, successful runs were performed by different chemists in the lab, and even if my distillation technique was *that* bad, the chances of two chemists in the same group having horrible technique (and still getting polymer) were extremely slim. Finally, one more reason we do not believe the polymer successes were a fluke is that many groups have reported group transfer polymerization using a myriad

of drying techniques for their monomer (including some which do not use triisobutylaluminum at all) along with a plethora of catalysts.

5.6 Final Thoughts on the Photoinitiated Anionic Polymerization of Methyl Methacrylate

Since the problem with the polymer project could not be sorted out by trying different permutations of my system, I went back to the literature and attempted to recreate some of the data other groups have reported. In particular work by Bandermann et. al.[114,115] was interesting owing to the good description of the experimental technique which was given, as well as the catalyst used (cyanide) which was readily available in our lab. Despite my best efforts, I was unable to reproduce these results.

In light of this, my final comments are as follows: I do not believe that this project is a failure. I believe that the anionic polymerization of MMA is just a difficult thing to do. Anionic polymerization in general, and group transfer polymerization in particular, require an extremely rigid anhydrous technique, extremely pure reagents, and the chemist to have the patience of a saint. I spent much time thinking about what I had done differently in the runs where polymer was obtained; however, I was unable to come up with a satisfactory answer. I thought about my glassware and began cleaning it using a different method. I thought about whether or not reusing rubber septa could be causing a leak which led to water contamination, so I began using them only once. I thought about whether my needles were the wrong gauge and whether or not using non-coring

needles would make a difference, changing both of these did not help. I thought about the order of addition of my reagents, I tried altering this and ‘pre-forming’ the catalyst before adding the monomer. None of these adjustments to my procedure helped. At this point, I knew that something in my technique changed, and I simply got so frustrated that I was unable to see what this small change was. And then after spending months trying to figure out what changed, I was too frustrated to look at the project objectively.

However, I firmly believe that my results were authentic. I believe that I was able to convert the group transfer polymerization of methyl methacrylate from a thermal process to a photochemical process. I was simply unable to reproduce my original results, and the results of others.

REFERENCES

1. Andrzejewska, E.; *Prog. Polym. Sci.* **2001**, 26, 605-665.
2. Decker, C.; *Prog. Polym. Sci.* **1996**, *21*, 593-650.
3. Odian, G. *Principles of Polymerization*; 3rd Edition ed.; Wiley and Sons: New York, 1991.
4. Pepper, D. C.; *J. Polym. Sci C* **1978**, 62, 65-77.
5. Park, I. J. *Cyanoacrylate Resins-The Instant Adhesives*; Pasadena Technology Press: Los Angeles, 1981.
6. Trozzi, T. A.; Schwartz, R. L.; Hollars, M. L. *Processing Guide for Developing Latent Prints*; U. S. Department of Justice Federal Bureau of Investigation: Washington D. C., 2000, pp 18-19.
7. Eastman, D. P.; Robicsek, F.; *J. Heart Valve Dis.* **1998**, *7*, 72-74.
8. Gonzalez, E.; Orta, J.; Nieminshik, L.; Galera, R.; Onay, D.; Rojas, O.; *Surg. Neurol.* **2000**, *53*, 288-289.
9. Samson, D.; Ditmore, Q. M.; Beyer, C. W.; *Neurosurgery* **1981**, *8*, 43-51.
10. Van Holder, R.; Misotten, A.; Roels, H.; Matton, G.; *Biomaterials* **1993**, *14*, 737-742.
11. Vauthier, C.; Dubernet, C.; Fattal, E.; Pinto-Alphandary, H.; Couvreur, P.; *Adv. Drug Deliv. Rev.* **2003**, *55*, 519-548.
12. DeJesus, O.; Hernandez, V.; *Surg. Neurol.* **1997**, *48*, 482-487.
13. Lijoi, A.; Scarano, F.; Parodi, E.; Dottori, V.; Secchi, G. L.; Delfino, R.; Tallone, M.; Venere, G.; *J. Cardiovasc. Surg.* **1996**, *37*, 627-630.
14. Robello, D. R.; Eldridge, T. D.; Swanson, M. T.; *J. Polym. Sci. A* **1999**, *37*, 4570-4581.

15. Ryan, B.; McCann, G.; *Macromol. Rapid Comm.* **1996**, *17*, 217-227.
16. Guthrie, J.; Otterburn, M. S.; Rooney, J. M.; Tsang, C. N.; *J. Appl. Polym. Sci.* **1985**, *30*, 2861-2867.
17. Pepper, D. C.; *J. Polym. Sci. C* **1978**, *62*, 65-77.
18. Kutal, C.; Grutsch, P. A.; Yang, D. B.; *Macromolecules* **1991**, *24*, 6872-6873.
19. Paul, R.; Kelly, J.; Pepper, D.; Long, C.; *Polymer* **1997**, *38*, 2011-2014.
20. Donnelly, E. F.; Johnston, D. S.; Pepper, D. C.; *J. Polym. Sci. Polym. Lett.* **1977**, *15*, 399-405.
21. Johnston, D. S.; Pepper, D. C.; *Macromol. Chem. Phys.* **1981**, *182*, 393-406.
22. Pepper, D. C.; *Eur. Polym. J.* **1980**, *16*, 407-411.
23. Johnston, D. S.; Pepper, D. C.; *Macrom. Chem. Phys.* **1981**, *182*, 406-420.
24. Johnston, D. S.; Pepper, D. C.; *Macrom. Chem. Phys.* **1981**, *182*, 421-435.
25. Reetz, M. T.; Hutte, S.; Goddard, R.; *J. Phys, Org. Chem.* **1995**, *8*, 231-241.
26. Irie, M.; Tomimoto, S.; Hayashi, K.; *J. Polym. Sci. Polym. Lett.* **1972**, *10*, 669-701.
27. Irie, M.; Yamamoto, Y.; Hayashi, K.; *Pure Appl. Chem.* **1977**, *49*, 455-461.
28. Arsu, N.; Onen, A.; Yagci, Y.; *Macromolecules* **1996**, *29*, 8973-8974.

29. Onen, A.; Arso, N.; Yagci, Y.; *Angew. Makromol. Chem.* **1999**, *264*, 59-59.

30. Jarikov, V.; Neckers, D. C.; *Macromolecules* **2000**, *33*, 7761-7764.

31. Wegner, E. E.; Adamson, A. W.; *J. Am. Chem. Soc.* **1966**, *88*, 394-403.

32. Lavallee, R. J.; Palmer, B. J.; Billing, R.; Hennig, H.; Ferraudi, G.; Kutal, C.; *Inorg. Chem.* **1997**, *36*, 5552-5558.

33. Wilkinson, G.; Rosenblum, M.; Whiting, M. C.; Woodward, R. B.; *J. Am. Chem. Soc.* **1952**, *74*, 2125-2126.

34. Nakamoto, K. *Infrared and Raman Spectra of Inorganic and Coordination Compounds*; 5 ed.; John Wiley and Sons: New York, 1997.

35. Long, N. *Metallocenes: An Introduction to Sandwich Complexes*; Blackwell Science: Oxford, UK, 1998.

36. Geoffroy, G. L.; Wrighton, M. S. *Organometallic Photochemistry*; Academic Press, Inc.: New York, 1979.

37. Clack, D. W.; Warren, K. D. *Structure and Bonding* Berlin, 1980; Vol. 39.

38. Warren, K. D. *Structure and Bonding*; Springer-Verlag: Berlin, 1976; Vol. 27.

39. Sohn, Y. S.; Hendrickson, D. N.; Gray, H. B.; *J. Am. Chem. Soc.* **1971**, *93*, 3603-3612.

40. Daul, C.; Gudel, H. U.; Weber, J.; *J. Chem. Phys.* **1993**, *98*, 4023-4029.

41. Boulet, P.; Chermette, H.; Daul, C.; Gilardoni, F.; Rogemond, F.; Weber, J.; Zuber, G.; *J. Phys. Chem. A* **2001**, *105*, 885-894.

42. Akiyama, T.; Hoshi, Y.; Goto, S.; Sugimori, A.; *B. Chem. Soc. Jpn* **1973**, *46*, 1851-1854.

43. Traverso, O.; Scandola, F.; *Inorg. Chim. Acta* **1970**, *4*, 493-498.

44. Traverso, O.; Sostero, S.; Mazzocch, Ga; *Inorg. Chim. Acta* **1974**, *11*, 237-241.

45. Borrell, P.; Henderson, E.; *J. Chem. Soc. Dalton* **1975**, 432-438.

46. Bergamini, P.; Dimartino, S.; Maldotti, A.; Sostero, S.; Traverso, O.; *J. Organomet. Chem.* **1989**, *365*, 341-346.

47. Granifo, J.; Ferraudi, G.; *Inorg. Chem.* **1984**, *23*, 2210-2212.

48. Tsubakiy, K.; Fujisake, S.; *J. Polym. Sci. B* **1972**, *10*, 341.

49. Woo, H. G.; Park, J. Y.; Ham, H. S.; Park, H. R.; Cho, S. D.; Ko, Y. H. K., W. G.; *B. Kor. Chem. Soc.* **1997**, *18*, 444-447.

50. Woo, H. G.; Hong, L. Y.; Yang, S. Y.; Kim, B. H.; Kang, H. G.; Chae, H. N.; Choi, J. Y.; Park, J. H.; Ham, H. S.; *B. Kor. Chem. Soc.* **1998**, *19*, 580-584.

51. Woo, H. G.; Kim, B. H.; Cho, M. S.; Kim, M. S.; Chung, Y. G.; Ham, H. S.; Paek, C. S.; Hwang, T. S.; Jun, M. J.; Li, H.; *B. Kor. Chem. Soc.* **2002**, *23*, 1343-1346.

52. Kunkely, H.; Vogler, A.; *J. Organomet. Chem.* **1998**, *559*, 215-217.

53. Tarr, A. M.; Wiles, D. M.; *Can. J. Chemistry* **1968**, *46*, 2725-2731.

54. Ali, L. H.; Cox, A.; Kemp, T. J.; *J. Chem. Soc. Dalton* **1973**, *14*, 1468-1475.

55. Bozak, R. E.; Javaheri, H.; *Chem. Ind.* **1973**, *14*, 696-697.

56. Traverso, O.; Rossi, R.; Sostero, S.; *Mol. Photochem.* **1973**, *5*, 457-469.

57. Yamaguchi, Y.; Kutal, C.; *Inorg. Chem.* **1999**, *38*, 4861-4867.

58. Carey, P. R. *Biochemical Applications of Raman Spectroscopy*; Academic Press: New York, 1982.

59. Long, D. A. *The Raman Effect: A Unified Treatment of the Theory of Raman Scattering by Molecules*; Wiley: New York, 2002.

60. Spiro, T. G. *Resonance Raman Spectra of Polyenes and Aromatics*; Wiley and Sons: New York, 1987; Vol. 2, pp 367.

61. Kebarle, P.; Peschke, M.; *Anal. Chim. Acta* **2000**, *406*, 11.

62. Kebarle, P.; *J. Mass Spectrom.* **2000**, *35*, 804-817.

63. Montado, G.; Lattimer, R. *Mass Spectrometry of Polymers*; 1 ed.; CRC Press: New York, 2002, pp 584.

64. Hunsucker, D. *Time-of-Flight Mass Spectrometry to Characterize Inorganic Coordination Complexes and Cyanobacteria*; Virginia Polytechnic Institute and State University: Blacksburg, 2001, pp 139.

65. Kane-Maguire, L. A. P.; Kanitz, R.; Sheil, M. M.; *J. Organomet. Chem.* **1995**, *486*, 243-248.

66. Henderson, W.; Nicholson, B. K.; McCaffrey, L. J.; *Polyhedron* **1998**, *17*, 4291-4313.

67. Traeger, J. C.; *Int. J. Mass Spectrom.* **2000**, *200*, 387-401.

68. Ding, W.; Johnson, K. A.; Amster, I. J.; Kutal, C.; *Inorg. Chem.* **2001**, *40*, 6865-686.

69. Ding, W.; Johnson, K. A.; Kutal, C.; Amster, I. J.; *Anal. Chem.* **2003**, *75*, 4624-4630.

70. Turner, C. A.; Ding, W.; Amster, I. J.; Kutal, C.; *Coord. Chem. Rev.* **2002**, *229*, 9-16.

71. Harrick, N. J. *Internal Reflection Spectroscopy*; Interscience Publishers: New York, 1967.

72. Hatchard, C. G.; Parker, C. A.; *Proc. R. Soc. Lon. Ser. A* **1956**, *253*, 518-536.

73. Rausch, M. D.; Fischer, E. O.; Grubert, H.; *J. Am. Chem. Soc.* **1960**, *82*, 76-82.

74. LeMay, G.; Kaliaguine, S.; Adnot, A.; Nahar, S.; Cozak, D.; Monnier, J.; *Can. J. Chem.* **1986**, *64*, 1943-1948.

75. Cameron, D. G.; Kauppinen, J. K.; Moffatt, D. J.; Mantsch, H. H.; *Appl. Spectrosc.* **1982**, *36*, 245-250.

76. Brinkmann, N. R.; Schaefer, H. F.; Sanderson, C. T.; Kutal, C.; *J. Phys. Chem. A* **2002**, *106*, 847-853.

77. Koch, W.; Holthausen, M. C. *A Chemist's Guide to Density Functional Theory*; Wiley and Sons: New York, 2000.

78. Drozdzewski, P. M.; Johnson, M. K.; *Appl. Specrosc.* **1988**, *42*, 1575-1577.

79. Sanderson, C. T.; Palmer, B. J.; Morgan, A.; Murphy, M.; Dluhy, R. A.; Mize, T.; Amster, I. J.; Kutal, C.; *Macromolecules* **2002**, *35*, 9648-9652.

80. Rienstra-Kiracofe, J. C.; Tschumper, G. S.; Schaefer, H. F.; Nandi, S.; Ellison, G. B.; *Chem. Rev.* **2002**, *102*, 231-282.

81. Welmer, W. *Magnetic Atoms and Molecules*; Van Nostrand Reinhold: New York, 1983.

82. Brinkmann, N. R.; Rienstra-Kiracofe, J. C.; Schaefer, H. F.; *Mol. Phys.* **2001**, *99*, 663-675.

83. Yamaguchi, Y.; Palmer, B. J.; Kutal, C.; Wakamatsu, T.; Yang, D. B.; *Macromolecules* **1998**, *31*, 5155-5157.

84. Yamaguchi, Y.; Kutal, C.; *Macromolecules* **2000**, *33*, 1152-1156.

85. Hill, M. G.; Lamanna, W. M.; Mann, K. R.; *Inorg. Chem.* **1991**, *30*, 4687-4690.

86. Kuwana, T.; Bublitz, D.; Hoh, G.; *J. Am. Chem. Soc.* **1960**, *82*, 5811-5817.

87. Mayor-Lopez, M. J.; Weber, J.; *Chem. Phys. Lett.* **1997**, *281*, 226-232.

88. Batterjee, S. M.; Mazourk, M. I.; Aazab, M. E.; El-Hashash, M. A.; *Appl. Organomet. Chem.* **2003**, *17*, 291-297.

89. Davis, T. P.; Haddleton, D. M.; Richards, S. N.; J. *Macromol. Sci. R M C* **1994**, *C34*, 243-324.

90. Szwarc, M.; Van Beylen, M. *Ionic Polymerization and Living Polymers*; Chapman and Hall: New York, 1993.

91. Reetz, M. T.; *Angew. Chem. Int. Edit.* **1988**, *27*, 994-998.

92. Baskaran, D.; *Prog. Polym. Sci.* **2003**, *28*, 521-581.

93. Zune, C.; Jerome, R.; *Prog. Polym. Sci.* **1999**, *24*, 631-64.

94. Vlcek, P.; Lochmann, L.; *Prog. Polym. Sci.* **1999**, *24*, 793-873.

95. Halaska, V.; Lochmann, L.; *Collection Czech. Chem. C.* **1973**, *38*, 1780-1782.

96. Kriz, J.; Dybal, J.; Janata, M.; Lochmann, L.; Vlcek, P.; *Macromol. Chem. Phys.* **1996**, *197*, 1889-1907.

97. Dhara, M. G.; Baskaran, D.; Sivaram, S.; *Macromol. Chem. Phys.* **2003**, *204*, 1567-1575.

98. Baskaran, D.; Muller, A. H. E.; Sivaram, S.; *Macromolecules* **1999**, *32*, 1356-1361.

99. Reetz, M. T.; Knauf, T.; Minet, U.; Bingel, C.; *Angew. Chem. Int. Edit.* **1988**, *27*, 1373-1374.

100. Reetz, M. T.; OStarek, R.; *J. Chem. Soc. Chem. Comm.* **1988**, *3*, 213-215.

101. Reetz, M. T.; Hutte, S.; Goddard, R.; *Z. Naturfurschung B* **1995**, *50*, 415-422.

102. Reetz, M. T.; Hutte, S.; Goddard, R.; Minet, U.; *J. Chem. Soc. Chem. Comm.* **1995**, *2*, 275-277.

103. Esswein, B.; Steidl, N. M.; Moller, M.; *Macromol. Rapid Comm.* **1996**, *17*, 143-148.

104. Pietzonka, T.; Seebach, D.; *Angew. Chem. Int. Edit.* **1993**, *32*, 716-717.

105. Baskaran, D.; Muller, A. H. E.; Zagala, A. P.; Hogen--Esch, T. E.; *Macromolecules* **1997**, *30*, 6695-6697.

106. Reetz, M. T.; Herzog, H. M.; Konen, W.; *Macromol. Rapid Comm.* **1996**, *17*, 383-388.

107. Webster, O. W.; Hertler, W. R.; Sogah, D. Y.; Farnham, W. B.; Rajanbabu, T. V.; *J. Am. Chem. Soc.* **1983**, *105*, 5706-5708.

108. Haddleton, D. M.; Crossman, M. C.; Hunt, K. H.; Topping, C.; Waterson, C.; Suddaby, K. G.; *Macromolecules* **1997**, *30*, 3992-3998.

109. Mai, P.; Muller, A. H. E.; *Makromol. Chem.-Rapid* **1987**, *8*, 99-107.

110. Bandermann, F.; Speikamp, H. D.; *Makromol. Chem.-Rapid* **1985**, *6*, 335-339.

111. Sogah, D. Y.; Hertler, W. R.; Webster, O. W.; Cohen, G. M.; *Macromolecules* **1987**, *20*, 1473-1488.

112. Bywater, S.; *Makromol. Chem.-M. Symp.* **1993**, *67*, 339-350.

113. Quirk, R. P.; Kim, J. S.; *J. Phys. Org. Chem.* **1995**, *8*, 242-248.

114. Schmalbrock, U.; Sitz, H. D.; Bandermann, F.; *Macromol. Chem. Phys.* **1989**, *190*, 2713-2719.

115. Schubert, W.; Bandermann, F.; *Macromol. Chem. Phys.***1989**, *190*, 2161-2171.

116. Armarego, W. L. F.; Perrin, D. D. *Purification of Laboratory Chemicals*; 5 ed.; Elsevier: Burlington, MA, 2003.